Entanglement and Quantum Gate Processes in the One-Dimensional Quantum Harmonic Oscillator

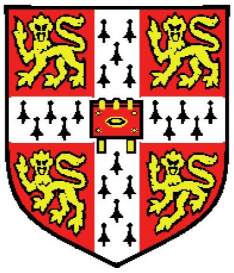

Edmund Thomas Owen

Girton College

University of Cambridge

A thesis submitted for the degree of

Doctor of Philosophy

June 2013

To Granny and D'Dad

Acknowledgements

I would like to start by thanking Crispin Barnes for being my supervisor during my PhD. This work would not have been possible without his continuous supply of encouragement, advice and ideas. I would also like to thank Matthew Dean for countless informative discussions on physics and computing. I thank Adam Thorn for guiding me at the start of my PhD and for the many useful conversations we have had since then. The discussions and feedback I have had from Friday's SAW meetings have also been incredibly useful. I am also grateful to all the members of SP for their support and friendship — Matthew Pooley, Zoë Penfold-Fitch, Marc Fletcher, Matthew Benesh, Simon Chorley, Aleksandar Nikolic, Melanie Tribble, Aquila Mavalankar, James Frake and everyone else.

I acknowledge funding from the Engineering and Physical Sciences Research Council and I would like to thank the Dyke Family Trust for their continuing financial support.

My time at Cambridge would not have been nearly as fun without the many friends I have made at Girton College. In particular, I would like to thank the members of the MCR committee of 2010/11 for making my time as vice-president so enjoyable. I would also like to thank the members of Cambridge University Taekwondo and Cambridge University Bowmen for their friendship and advice.

I would also like to thank Jessica for her love and support over the past two years. Thanks also go to Angel Rubio at the Nano-bio Spectroscopy Group, San Sebastian, Nicole Helbig at the Forschungszentrum, Jülich and Heiko Appel at the Fritz Haber Institute, Berlin for

providing me with the facilities to continue my work whilst being with her.

Most of all, I would like to thank my family for their unending support, love, care and attention. You have made me who I am today: None of this would have been possible without you.

Declaration

The work presented in this thesis was carried out at the Semiconductor Physics Group in the Cavendish Laboratory, University of Cambridge between October 2009 and April 2013.

This dissertation is the result of my own work and includes nothing which is the outcome of work done in collaboration except where specifically indicated in the text. It has not been submitted in whole or in part for any degree at this or any other university, and is less than sixty thousand words long.

Abstract

Quantum states can contain correlations which are stronger than is possible in classical systems. Quantum information technologies use these correlations, which are known as entanglement, as a resource for implementing novel protocols in a diverse range of fields such as cryptography, teleportation and computing. However, current methods for generating the required entangled states are not necessarily robust against perturbations in the proposed systems. In this thesis, techniques will be developed for robustly generating the entangled states needed for these exciting new technologies.

The thesis starts by presenting some basic concepts in quantum information proccessing. In Ch. 2, the numerical methods which will be used to generate solutions for the dynamic systems in this thesis are presented. It is argued that using a GPU-accelerated staggered leapfrog technique provides a very efficient method for propagating the wave function.

In Ch. 3, a new method for generating maximally entangled two-qubit states using a pair of interacting particles in a one-dimensional harmonic oscillator is proposed. The robustness of this technique is demonstrated both analytically and numerically for a variety of interaction potentials. When the two qubits are initially in the same state, no entanglement is generated as there is no direct qubit-qubit interaction. Therefore, for an arbitrary initial state, this process implements a root-of-SWAP entangling quantum gate. Some possible physical implementations of this proposal for low-dimensional semiconductor systems are suggested.

One of the most commonly used qubits is the spin of an electron. However, in semiconductors, the spin-orbit interaction can couple this qubit to the electron's momentum. In order to incorporate this effect into our numerical simulations, a new discretisation of this interaction is presented in Ch. 4 which is significantly more accurate than traditional methods. This technique is shown to be similar to the standard discretisation for magnetic fields.

In Ch. 5, a simple spin-precession model is presented to predict the effect of the spin-orbit interaction on the entangling scheme of Ch. 3. It is shown that the root-of-SWAP quantum gate can be restored by introducing an additional constraint on the system. The robustness of the gate to perturbations in this constraint is demonstrated by presenting numerical solutions using the methods of Ch. 4.

Contents

Contents xii

1 Entanglement and Quantum Information Technology 1
- 1.1 Introduction . . . 1
  - 1.1.1 Bell's Inequality and Non-Classical Correlations . . . 3
  - 1.1.2 Representing Qubits . . . 6
  - 1.1.3 Entanglement as a Resource . . . 10
- 1.2 Quantum Computing . . . 13
  - 1.2.1 Making a Quantum Computer . . . 14
  - 1.2.2 The Two-Qubit Quantum Gate . . . 15
  - 1.2.3 Implementation using the Exchange Interaction . . . 17
- 1.3 Low-Dimensional Semiconductor Devices . . . 18
  - 1.3.1 Semiconductor-Based Quantum Computers . . . 20
- 1.4 Outline of Work . . . 21

2 Numerical Methods for Efficiently Simulating Quantum Systems 25
- 2.1 Introduction . . . 25
- 2.2 Temporal Discretisation and Stability . . . 26
  - 2.2.1 Euler Method . . . 27
  - 2.2.2 Crank-Nicolson Method . . . 29
  - 2.2.3 Staggered Leapfrog Method . . . 30
- 2.3 Spatial Discretisation . . . 31
  - 2.3.1 Magnetic Fields and Harper's Equation . . . 33
- 2.4 Alternative Methods for Solving the TDSE . . . 34

2.5 Accelerating the Staggered Leapfrog Method using the Graphical Processing Unit (GPU) . . . 36
2.5.1 Massive Parallel Processing on the GPU using CUDA . . . 37
2.5.2 Why is GPU acceleration better for the Staggered Leapfrog Method? . . . 39

3 Entangling Qubits in a One-dimensional Harmonic Oscillator 41
3.1 Introduction . . . 41
3.2 Proposal . . . 42
3.3 Parity-Dependent Harmonic Approximation (PDHA) . . . 43
3.3.1 A Limit in which the Approximation is Exact . . . 47
3.3.2 Robustness of Results to Deviations from the PDHA . . . 51
3.4 Numerical Simulations for Various Interaction Potentials . . . 53
3.4.1 Contact Interaction . . . 53
3.4.2 Gaussian Interaction . . . 61
3.4.3 Softened-Coulomb Interaction . . . 63
3.4.4 General Interaction Potentials . . . 65
3.5 Possible physical systems . . . 66
3.6 Discussion . . . 69

4 Discretising the Spin-Orbit Interaction 71
4.1 Introduction . . . 71
4.2 Derivation of the Spin-Orbit Interaction . . . 72
4.2.1 The Breit Equation and Spin-Orbit Interaction for Two-Particle Systems . . . 76
4.3 Discretising the Spin-Orbit Interaction . . . 77
4.3.1 An Explicit Derivation for One-Dimension . . . 78
4.3.2 Comparison of the Grima-Newman Substitution with Harper's Equation . . . 80
4.4 Simulations . . . 82
4.4.1 The Moroz-Barnes Wire . . . 83
4.4.2 Ground State of a Harmonic Oscillator with Spin-Orbit Interaction . . . 86

5 Implementing a $\sqrt{\text{SWAP}}$ Quantum Gate in a One-Dimensional Harmonic Oscillator with Spin-Orbit Coupling **91**

5.1 Introduction 91

5.2 Spin-Orbit Coupling and Qubit Precession 93

5.3 Simulations 99

5.3.1 SOI Coherent States 99

5.3.2 Two-Qubit Gate Implementation with SOI 100

5.3.3 Coulomb interaction 104

6 Conclusions **107**

6.1 Summary 107

6.2 Further Work 111

References **115**

Chapter 1

Entanglement and Quantum Information Technology

1.1 Introduction

Entanglement is one of the fundamental properties of quantum mechanics which differentiates it from classical theory. It is a manifestation of the principle of superposition which states that a quantum system can simultaneously be in a combination of possible measurable states. If there is only one particle, when its state is measured the wave function collapses onto the measured state. However, when we have a system consisting of two or more particles, the states of the combined system can also be in a superposition. If we measure the state of a single particle in this system, the wave function of the *entire system* collapses. It is possible to generate states where this can lead to situations where measuring one part of a system directly determines the state of another part without any explicit interaction between them. This property is refered to as *entanglement*. The correlations between parts of a quantum system which can be generated in such an entangled superposition can exceed what is possible in classical theory.

When quantum mechanics was developed at the beginning of the 20th century, entanglement was a curiousity with which to challenge the validity of the new theory. The best example of this is the seminal paper by Einstein, Podolsky and Rosen (EPR) [1] which considered a pair of entangled, non-interacting particles.

They showed that quantum mechanics allows correlations between particles which seem to violate Heisenberg's uncertainty principle. EPR envisaged creating a pair of particles which are entangled such that their position and momentum are correlated. The particles would then be separated so that they cannot interact. Measuring the first particle leads to collapse of the wave function which specifies which state the second particle is in. By measuring the position or momentum of the first particle, the second particle collapses into two different sets of states – one with definite momentum and one with definite position. As the particles cannot interact, the authors concluded that the two sets of states which the second particle can collapse into must simultaneously have some "element of reality". However, this would mean that the momentum and position of the second particle is in some respect already determined which would violate the uncertainty principle. EPR believed that this implied that quantum mechanics was an incomplete theory but they admitted that the thought experiment also allowed for the process of measurement on one system to affect the state of another system without interacting with it. Whilst they considered this to be an unreasonable description of reality, we will see in Sec. 1.1.1 that experiments have demonstrated that this is not the case and entanglement is a real, non-classical phenomenon.

As quantum theory became widely accepted, the emphasis shifted from entanglement being a physical curiosity to considering how it could be used for new technologies. Quantum information theory has shown that entanglement can be used as a resource. Under certain protocols, entangled systems can make it possible to improve upon classical methods in such diverse fields as cryptography [2, 3], computing [4–7] and data transfer [8]. New technologies which are impossible classically, such as teleportation [9], have also been developed.

In this chapter, we will begin by demonstrating that there is no way in which the effects of entanglement can be reproduced using classical correlations. This necessitates a quantum description of information and the entanglement between composite quantum systems. Entangled systems can be used as a resource for a variety of quantum information protocols which will be discussed, with an emphasis on the development of quantum computation. We will present some of the advantages quantum computers have over their classical counterparts and

we will discuss the DiVincenzo criteria [10] which are required of a system in order to implement quantum computational protocols. Specifically, we will study the two-qubit quantum gate in detail and explain how this gate is traditionally generated using the exchange interaction. We conclude the chapter by describing why this approach is difficult to realise experimentally.

1.1.1 Bell's Inequality and Non-Classical Correlations

In classical mechanics, a system is entirely described by a set of locally defined variables, e.g. the position and momentum of all constituent particles. The correlations in such a system can be represented as a function of these variables and therefore the results of measurements of these correlations can only be influenced locally. We will see below that quantum mechanics seems to provide stronger correlations than this. The EPR experiment demonstrates that measurement of one particle instantaneously influences the state of the other particle. Einstein [11] and others proposed that quantum mechanics was an incomplete theory and that there are "hidden variables" which account for these – seemingly superluminal – correlations classically. However, an experimental test was devised by Bell [12] to show that no system of hidden variables governed by a local, deterministic theory can be compatible with quantum mechanics. Here, we give an overview of Bell's theorem which shows that entanglement provides stronger correlations than are possible with classical mechanics.

Let us assume the existence of some local, deterministic theory governing the evolution of a set of hidden variables, $\boldsymbol{\lambda} = \{\lambda_i\}$. We will assume that the theory is local in the sense that a measurement of one particle cannot influence a concurrent measurement of another particle which is spatially separated from it. Also, we assume that the results of a measurement are completely determined by the hidden variables $\boldsymbol{\lambda}$. Bell's theorem shows that any theory which satisfies these assumptions is incompatible with quantum mechanics.

Let us consider an experiment where a spinless particle decays into two spin-1/2 particles which, therefore, must share the same set of hidden variables. They are then separated and their spins are measured separately along two different measurement axes. If the spin of particle A is measured in the direction $\vec{a}$ and

the spin of particle B is measured in a different direction $\vec{b}$ then the assumption of locality requires that the measurement of A does not affect the result of the measurement of B and vice versa. The possible results of a measurement of the spin of particle A and particle B respectively are

$$A(\vec{a}, \boldsymbol{\lambda}) = \pm 1, \qquad B(\vec{b}, \boldsymbol{\lambda}) = \pm 1. \tag{1.1}$$

We will assume that there is a normalised probability distribution $p(\boldsymbol{\lambda})$ such that

$$\int p(\boldsymbol{\lambda})\, \mathrm{d}\boldsymbol{\lambda} = 1. \tag{1.2}$$

If the theory is deterministic, the correlation function between the spins of A and B for a given set of measurement axes $\vec{a}, \vec{b}$ is

$$P(\vec{a}, \vec{b}) = \int A(\vec{a}, \boldsymbol{\lambda}) B(\vec{b}, \boldsymbol{\lambda}) p(\boldsymbol{\lambda})\, \mathrm{d}\boldsymbol{\lambda}. \tag{1.3}$$

If, instead, particle B is measured along a third axis $\vec{c}$, we have a similar correlation function $P(\vec{a}, \vec{c})$. As the initial particle was spinless, measurement of the two particles along the same axis must be anti-correlated such that

$$A(\vec{a}, \boldsymbol{\lambda}) = -B(\vec{a}, \boldsymbol{\lambda}). \tag{1.4}$$

From this, we note that, as $A(\vec{a}, \boldsymbol{\lambda})^2 = B(\vec{b}, \boldsymbol{\lambda})^2 = 1$,

$$\begin{aligned} P(\vec{a}, \vec{b}) - P(\vec{a}, \vec{c}) &= -\int \Big(A(\vec{a}, \boldsymbol{\lambda}) A(\vec{b}, \boldsymbol{\lambda}) - A(\vec{a}, \boldsymbol{\lambda}) A(\vec{c}, \boldsymbol{\lambda}) \Big)\, p(\boldsymbol{\lambda})\, \mathrm{d}\boldsymbol{\lambda} \qquad (1.5) \\ &= -\int A(\vec{a}, \boldsymbol{\lambda}) A(\vec{b}, \boldsymbol{\lambda}) \Big(1 - A(\vec{b}, \boldsymbol{\lambda}) A(\vec{c}, \boldsymbol{\lambda}) \Big)\, p(\boldsymbol{\lambda})\, \mathrm{d}\boldsymbol{\lambda}. \qquad (1.6) \end{aligned}$$

The absolute value of an integral is less than or equal to the integral of the modulus of the integrand so

$$\Big| P(\vec{a}, \vec{b}) - P(\vec{a}, \vec{c}) \Big| \leq \int \Big| A(\vec{a}, \boldsymbol{\lambda}) A(\vec{b}, \boldsymbol{\lambda}) \Big(1 - A(\vec{b}, \boldsymbol{\lambda}) A(\vec{c}, \boldsymbol{\lambda}) \Big)\, p(\boldsymbol{\lambda}) \Big|\, \mathrm{d}\boldsymbol{\lambda}. \tag{1.7}$$

Also, note that $|x.y.z| \leq |x| \,.\, |y| \,.\, |z|$ and

$$\begin{aligned} \left|A(\vec{a},\boldsymbol{\lambda})A(\vec{b},\boldsymbol{\lambda})\right| &= 1, \\ \left|1 - A(\vec{b},\boldsymbol{\lambda})A(\vec{c},\boldsymbol{\lambda})\right| &\geq 0, \\ p(\boldsymbol{\lambda}) &\geq 0 \end{aligned}$$

so

$$\begin{aligned} \left|P(\vec{a},\vec{b}) - P(\vec{a},\vec{c})\right| &\leq \int \left(1 - A(\vec{b},\boldsymbol{\lambda})A(\vec{c},\boldsymbol{\lambda})\right) p(\boldsymbol{\lambda})\,\mathrm{d}\boldsymbol{\lambda} \qquad (1.8) \\ &\leq 1 + \int A(\vec{b},\boldsymbol{\lambda})B(\vec{c},\boldsymbol{\lambda})p(\boldsymbol{\lambda})\,\mathrm{d}\boldsymbol{\lambda} \qquad (1.9) \end{aligned}$$

or equivalently,

$$\left|P(\vec{a},\vec{b}) - P(\vec{a},\vec{c})\right| - P(\vec{b},\vec{c}) \leq 1. \qquad (1.10)$$

This is the inequality derived by Bell which must be satisfied by all [1] local, deterministic, hidden variables theories. In comparison, the quantum mechanical decay of a spinless particle would produce the singlet state which has the correlation function

$$P(\vec{a},\vec{b}) = -\vec{a}\cdot\vec{b}. \qquad (1.11)$$

If we insert this into Eq. 1.10 and consider the case where the angle between $\vec{a}$ and $\vec{b}$ is $\pi/3$ and the angle $\vec{a}$ and $\vec{c}$ is $2\pi/3$, we get

$$\left|P(\vec{a},\vec{b}) - P(\vec{a},\vec{c})\right| - P(\vec{b},\vec{c}) = 1.5 \not\leq 1. \qquad (1.12)$$

This produces an experimentally testable contradiction between quantum mechanics and any local, deterministic hidden variables theorem. Violation of a generalized form of Bell's inequality was observed by Aspect [14] using pairs of linearly polarized photons in 1981 thus ruling out most local, deterministic hidden variables theories. Since then, many other experimental setups [15–17] have

[1] Naturally, there are still some ways of violating the inequality whilst retaining the possibility of having local, hidden variables but these scenarios require extremely unlikely coincidences and are often considered as "conspiracy" theories due to their "ad hoc" nature and are often discarded by physicists as having no place in empirical science [13].

shown a similar violation of Eq. 1.10 and associated inequalities.

The essential difference between classical and quantum correlations demonstrated here is that a pair of entangled quantum particles are correlated in whichever basis one chooses. For example, consider two spin-1/2 particles which have been produced in the entangled state

$$|\Psi\rangle = \frac{|\uparrow\rangle_A |\downarrow\rangle_B - |\downarrow\rangle_A |\uparrow\rangle_B}{\sqrt{2}} \tag{1.13}$$

where the subscripts correspond to labels for the individual particles. The particles are sent to two observers, Alice and Bob, such that the particles are distinguishable by their space-like separation. If Alice measures the spin of her particle in the basis $\{|\uparrow\rangle, |\downarrow\rangle\}$ and finds it to be in the state $|\uparrow\rangle$, she immediately knows that the other particle must be in the state $|\downarrow\rangle$ without having to communicate with Bob. The entanglement is an intrinsic property of the state and is independent of any measurement basis. If we consider the state $|\Psi\rangle$ in an alternate basis, $\{|\rightarrow\rangle = (|\uparrow\rangle - |\downarrow\rangle)/\sqrt{2}, |\leftarrow\rangle = (|\uparrow\rangle + |\downarrow\rangle)/\sqrt{2}\}$, say, then

$$|\Psi\rangle = \frac{|\rightarrow\rangle_A |\leftarrow\rangle_B - |\leftarrow\rangle_A |\rightarrow\rangle_B}{\sqrt{2}}. \tag{1.14}$$

Basis-independent entanglement allows particles to be more correlated than is possible in classical mechanics and it is these correlations which provide the resource for quantum information technologies.

1.1.2 Representing Qubits

In Sec. 1.1.1, we used the spin-1/2 particle as the archetype with which to understand entanglement. In order to discuss quantum information more generally, we will introduce a more information theoretic language by describing two-level systems, such as the spin-1/2 particle, in terms of qubits. For classical information theory, data is stored as an array of ones and zeros. Each element of the array is called a "bit" and takes one of these two values. For quantum information, the data is stored on a two-level system with states $\{|0\rangle, |1\rangle\}$ but, due to the

superposition principle, the system can be in a continuous set of possible states

$$|\psi\rangle = \alpha\,|0\rangle + \beta\,|1\rangle\,, \tag{1.15}$$

$$|\alpha|^2 + |\beta|^2 = 1. \tag{1.16}$$

The state $|\psi\rangle$ is called a "qubit" and is the fundamental building block of quantum information technologies. It will be useful to consider a geometric representation of the qubit $|\psi\rangle$ which can be done by reparametrising Eq. 1.15 as

$$|\psi\rangle = \cos(\theta/2)\,|0\rangle + e^{i\phi}\sin(\theta/2)\,|1\rangle \tag{1.17}$$

which obeys the constraint given by Eq. 1.16. The angles θ and ϕ correspond to the polar and azimuthal angles describing the surface of a unit sphere where the states $|0\rangle$ and $|1\rangle$ are on the north and south poles respectively. This is the Bloch sphere representation of a qubit, shown in Fig. 1.1, which provides an easy visualisation for qubit dynamics. The unitary operations on a two level system are described by the group $SU(2)$ which is generated by the Pauli matrices

$$\sigma_x = \begin{pmatrix} 0 & 1 \\ 1 & 0 \end{pmatrix}, \qquad \sigma_y = \begin{pmatrix} 0 & -i \\ i & 0 \end{pmatrix}, \qquad \sigma_z = \begin{pmatrix} 1 & 0 \\ 0 & -1 \end{pmatrix}. \tag{1.18}$$

Therefore, any rotation of the qubit can be described by

$$R^{\vec{n}}(\theta) = e^{i\theta\vec{\sigma}\cdot\vec{n}/2} \tag{1.19}$$

$$= \mathbb{1}\cos(\theta/2) + i\vec{\sigma}\cdot\vec{n}\sin(\theta/2) \tag{1.20}$$

where $\vec{n}$ is an arbitrary unit vector and $\vec{\sigma} = (\sigma_x, \sigma_y, \sigma_z)^T$ is the vector of Pauli matrices. The operator $R^{\vec{n}}$ rotates the state by an angle θ around $\vec{n}$.

Unlike for classical information, when we combine a set of qubits, the resulting state is not necessarily a linear combination of the individual qubits. The composite particle postulate of quantum mechanics states that the state space of a composite system is the tensor product of the state spaces of the individual

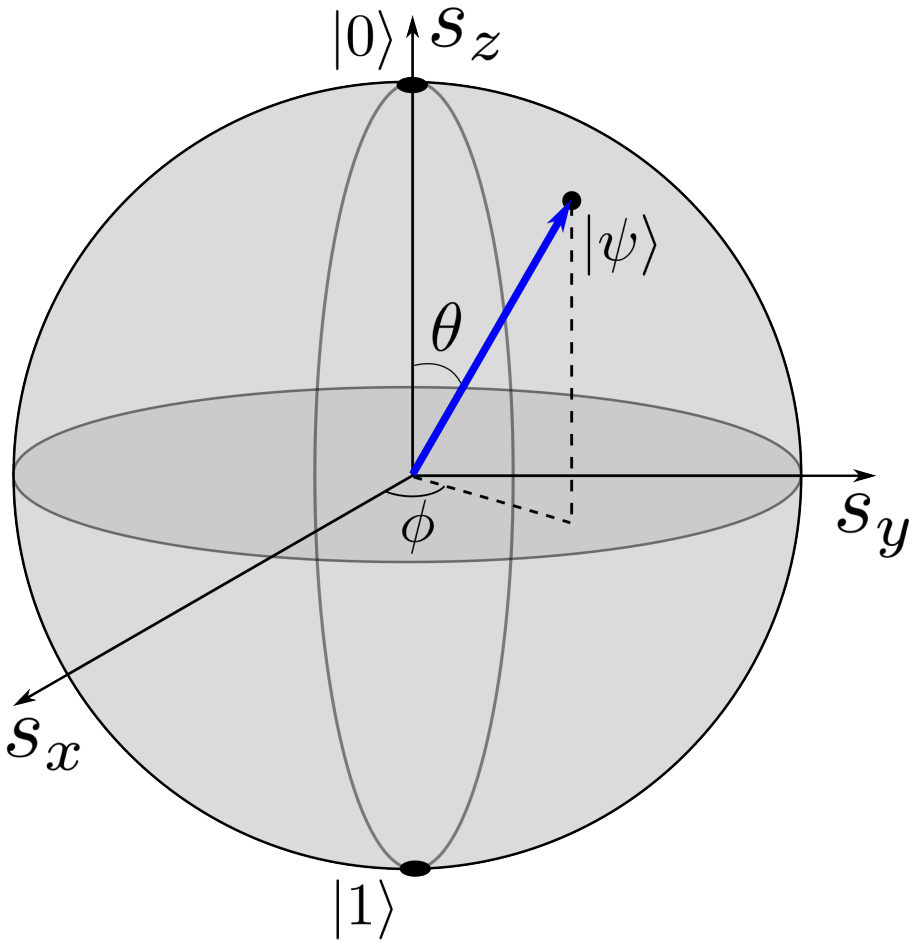

Figure 1.1: Bloch sphere representation of the qubit from Eq. 1.17.

system so, for a pair of qubits, the state's most general form is

$$|\phi\rangle = \alpha\,|00\rangle + \beta\,|01\rangle + \gamma\,|10\rangle + \delta\,|11\rangle \tag{1.21}$$

with the constraint that $|\alpha|^2+|\beta|^2+|\gamma|^2+|\delta|^2 = 1$. A useful representation of the state $|\phi\rangle$ is the Schmidt decomposition [18]. For any two particle system, we can express the state as $|\phi\rangle = \sum a_{jk}\,|j\rangle\,|k\rangle$. a is a matrix of complex numbers which can be expressed in terms of its singular value decomposition $a_{jk} = \sum_i v_{ji} d_{ii} u_{ik}$ where d is a diagonal matrix with eigenvalues λ_i and u, v are unitary matrices [19]. By defining a new set of states $|i_A\rangle = \sum_j v_{ji}\,|j\rangle$ and $|i_B\rangle = \sum_k u_{ik}\,|k\rangle$ we can write any two particle state as a Schmidt decomposition

$$|\phi\rangle = \sum \lambda_i\,|i_A\rangle\,|i_B\rangle\,. \tag{1.22}$$

This is the closest that one can get to expressing the state $|\phi\rangle$ a tensor product state. The number of terms in Eq. 1.22 gives a measure of the entanglement between the two particles.

Another useful description of a quantum system is its density matrix $\rho = |\phi\rangle\,\langle\phi|$. For a two particle system, we can define a reduced density matrix for one of the components by performing a partial trace over one of the particles, $\rho_A = \mathrm{Tr}_B \rho$. The Schmidt decomposition is unique so the reduced density matrix is the same for both particles: $\rho_A = \rho_B$. A common measure for the entanglement between a pair of qubits is given by the von Neumann entropy of the reduced density matrix [20]

$$S_{\mathrm{vN}}(\rho_A) = -\mathrm{Tr}(\rho_A \log_2 \rho_A). \tag{1.23}$$

Due to the cyclicity of the trace, Eq. 1.23 is independent under basis transformations so, by using the Schmidt decomposition of $|\phi\rangle$, we see that $S_{\mathrm{vN}}(\rho_A) = -\sum_i \lambda_i^2 \log_2 \lambda_i^2$. Normalisation of the wave function requires that $\lambda_1^2 + \lambda_2^2 = 1$. If the particles are in a separable tensor product state only one of the $\lambda_i \neq 0$, so $S_{\mathrm{vN}} = 0$ and there are no quantum correlations whilst S_{vN} is maximal when $\lambda_1^2 = \lambda_2^2 = \frac{1}{2}$. These maximally entangled states are of particular interest in quantum information processing. One of the main themes of this thesis will be developing methods for reliably generating these states. The most common

representation of maximally entangled states is the Bell basis:

$$\left|\Psi^{\pm}\right\rangle = (|00\rangle \pm |11\rangle)/\sqrt{2}, \tag{1.24}$$
$$\left|\Phi^{\pm}\right\rangle = (|01\rangle \pm |10\rangle)/\sqrt{2}. \tag{1.25}$$

$|\Phi^{-}\rangle$ was the state used in Sec. 1.1.1 to demonstrate maximum violation of the Bell inequality. In this thesis, it will be useful to generalise this basis to

$$\left|\Psi^{\pm\mu}\right\rangle = (|00\rangle \pm \mu\,|11\rangle)/\sqrt{2}, \tag{1.26}$$
$$\left|\Phi^{\pm\nu}\right\rangle = (|01\rangle \pm \nu\,|10\rangle)/\sqrt{2} \tag{1.27}$$

where μ and ν are complex numbers which must have modulus one, $|\mu| = |\nu| = 1$. These states are also maximally entangled and form an orthonormal basis set spanning the two qubit Hilbert space.

Finally, having defined the type of states we will be interested in, we need a measure to determine the distance between two states $|\alpha\rangle$ and $|\beta\rangle$. This will allow us to define a measure of the accuracy with which we can produce a desired state. A common measure of this distance is the fidelity

$$\mathcal{F} = |\langle\alpha|\beta\rangle|\,. \tag{1.28}$$

If the states are the same – up to a phase factor – then $\mathcal{F} = 1$, whilst the fidelity between two orthogonal states is $\mathcal{F} = 0$. Of more interest is the fidelity between a maximally entangled state and a classical, tensor product state. For example, the fidelity between the product state $|\gamma\rangle = |00\rangle$ and the Bell state $|\Psi^{+}\rangle$ is $\mathcal{F} = 1/\sqrt{2}$. This is the classical limit and if the fidelity of an arbitrary state $|\delta\rangle$ with a Bell state is greater than $1/\sqrt{2}$ then $|\delta\rangle$ must contain quantum correlations.

1.1.3 Entanglement as a Resource

As our physical understanding of entanglement has increased, a number of different techniques have been developed which require entangled states. There are two main directions in which quantum technologies have sought to use entanglement: quantum computation, which we will discuss in the next section, and quantum

communication, which we will focus on here.

Quantum communication typically involves transmitting information using entangled states. This takes a significantly different character in quantum mechanics due to the "no-cloning" theorem of Wootters and Zurek [21], which states that it is impossible for a unitary process to faithfully replicate an arbitrary quantum state. Taking the qubit basis $\{|0\rangle, |1\rangle\}$ for simplicity, suppose that there is a unitary process $\hat{U}$ which copies this information onto an ancilla state $|\phi\rangle$ then

$$|0\rangle |\phi\rangle \xrightarrow{\hat{U}} |0\rangle |0\rangle , \qquad |1\rangle |\phi\rangle \xrightarrow{\hat{U}} |1\rangle |1\rangle . \tag{1.29}$$

However, if we try to clone an arbitrary state, then

$$|\psi\rangle |\phi\rangle = (a |0\rangle + b |1\rangle) |\phi\rangle \xrightarrow{\hat{U}} a |0\rangle |0\rangle + b |1\rangle |1\rangle \neq |\psi\rangle |\psi\rangle \tag{1.30}$$

due to the linearity of the unitary operator. Whilst states can be approximately cloned [22, 23], the inability to replicate quantum states is the key to quantum communication protocols.

Cryptography involves transmitting a shared messages between two remote parties, conventionally named Alice and Bob, without another party, Eve, intercepting the message. All classical messages can be encoded in a single bit string M which can be encoded using a "one-time pad". This unbreakable cipher involves a random bit string K of the same length as the message which is shared between Alice and Bob. By adding the two strings, modulo 2, the ciphertext $C = M \oplus K$ can be publicly relayed from Alice to Bob as it contains no information about M without the key K. Bob decodes the message by adding K to the ciphertext as $C \oplus K = M \oplus K \oplus K = M$.

The challenge in this cryptographic scheme involves generating a secret random key K which is shared between Alice and Bob. The Bennett [2] and Ekert [3] proposals use entangled qubits to generate a shared key. As described in Sec. 1.1.1, entanglement is basis independent. Therefore, taking a pair of qubits in the singlet state in the $\{|\uparrow\rangle, |\downarrow\rangle\}$ basis given by Eq. 1.13, which is equivalent to the singlet state in the $\{|\leftarrow\rangle, |\rightarrow\rangle\}$ basis in Eq. 1.14, Alice and Bob measure a stream of entangled pairs randomly in either of these bases. They can then

communicate classically which bases they used and when they coincide they keep the result of their measurement as a single bit of a shared one-time pad. The no-cloning ensures that Eve cannot copy the transmitted qubit. If she tries to intercept the key, then she will collapse the entangled state which can be detected by Alice and Bob. Therefore, using entangled states it is possible to create a shared random key which Alice and Bob can use to encrypt a message with complete security.

Teleportation protocols allow an arbitrary quantum state to be transfered from one qubit to another [9]. Alice starts with three qubits which we will label with subscripts on their ket vectors. Qubit 1 is in an arbitrary state $|\psi\rangle_1 = a|0\rangle_1 + b|1\rangle_1$ which she wants to transmit to Bob without transferring the qubit to him directly. The no-cloning theorem forbids her from copying this state onto either qubit 2 or 3 and sending one of these to Bob but Alice can transmit $|\psi\rangle_1$ using entanglement. If she creates the Bell state $|\Psi^+\rangle_{23}$ and gives qubit 3 to Bob, then the total state of the three qubits $|\Phi\rangle_{123}$ is given by

$$|\Phi\rangle_{123} = |\psi\rangle_1 |\Psi^+\rangle_{23} = (a|0\rangle_1 + b|1\rangle_1) \cdot \frac{1}{\sqrt{2}} (|00\rangle_{23} + |11\rangle_{23}) \tag{1.31}$$

which can be written in terms of the Bell states of qubits 1 and 2 as

$$\begin{aligned} |\Phi\rangle_{123} \quad \propto \quad & |\Psi^+\rangle_{12} (b|0\rangle_3 - a|1\rangle_3) \\ & + |\Psi^-\rangle_{12} (b|0\rangle_3 - a|1\rangle_3) \\ & + |\Phi^+\rangle_{12} (a|0\rangle_3 + b|1\rangle_3) \\ & + |\Phi^-\rangle_{12} (a|0\rangle_3 - b|1\rangle_3). \end{aligned} \tag{1.32}$$

Alice can measure which of the states her qubits are in as the Bell states form a complete basis. This collapses the total state $|\Phi\rangle_{123}$ in such a way that Alice knows which state Bob's qubit is in. When Alice tells Bob which of the Bell states she measured, Bob can correct his state using local unitary operations such that he replicates the initial state. The protocol does not violate the no-cloning theorem as the original state is destroyed.

Both quantum key distribution and teleportation use the entangled state as a resource which is consumed during the protocol. In order to perform the protocols

accurately, it is important to use states which have high fidelity to the Bell states. Experimental methods for generating Bell states will always have some imperfections but there are methods of "distilling" the entanglement [24] which produce maximally entangled states from an ensemble of partially entangled states.

1.2 Quantum Computing

Quantum computing is one of the most powerful, but also one of the most difficult, quantum information technologies to implement. The principle is to utilise the massive amount of information contained within a composite quantum system. To describe the state of a classical computer consisting of n bits requires an array of length n. However, to describe a quantum computer with n qubits requires an array of length 2^n. This exponential scaling means that the number of bits required to store the state of a quantum computer containing 300 qubits classically is comparable to the number of atoms in the known universe.

Not only is the amount of information contained within composite quantum systems truly staggering, by operating on these qubits, we can explore all possibilities at once. Classically, we must run the program for each input state we want to test, whilst, by transforming into the correct state, a quantum computer can test all input states at once. However, it is not possible to obtain complete information about this superposition and, instead, algorithms must be developed which measure properties of the state, such as its period, or which contain an oracle which increases the probability that the correct answer will be measured [25]. The most powerful example of this is Shor's algorithm [5] which uses the quantum Fourier transform [7] to find the prime factors of large numbers. A classical computer would search through all the possible prime factor combinations, which takes a very long period of time, $\mathcal{O}(10^{23}\text{s})$, but a quantum computer can search through all combinations instantaneously. For this, and many other reasons, creating a general-purpose quantum computer is an important research goal in quantum information.

1.2.1 Making a Quantum Computer

Many systems can be described quantum mechanically so the question is; what does a system need in order to perform quantum computation? Five requirements for physical implementation of a quantum computer have been identified by DiVincenzo [10]:

1. Scalability — The system must contain a set of scalable, well characterised qubits. They must be well characterised in the sense that they are quantum two-level systems with well understood dynamics and the qubits' coupling to other degrees of freedom should be known. Scalability requires that multiple qubits can be combined and that, by combining qubits, the full Hilbert space of the combined system must be accessible, eg. for the two particle system, any state of the form Eq. 1.21 must be possible.

2. Initialisation — It must be possible to set all of the qubits in a simple initial state such as $|000\ldots\rangle$.

3. Long coherence times — The quantum coherences times of the qubits must be longer than the time required for the computational gates to operate on them. More specifically, the interference effects of quantum superpositions must remain such that a state initially of the form $a|0\rangle + b|1\rangle$ does not transform into the mixed state $\rho = |a|^2 |0\rangle\langle 0| + |b|^2 |1\rangle\langle 1|$ through contact with the environment [26, 27]. Decoherence can be mitigated against using "error correcting codes" but these methods still require a minimum decoherence rate [28].

4. Universal quantum gates — The system should be able to implement a quantum algorithm by operating on the qubits in a controllable, reliable way. Quantum algorithms can be specified as a series of unitary operations individually acting on a small subset of the qubits. It has been shown that a single qubit gate which can perform any unitary transformation on the Bloch sphere, along with two qubit gates which can, at least sequentially, operate on any pair of qubits [29] is sufficient.

5. Measurement — It must be possible to measure the state of each of the

qubits. The measurement can have an efficiency of less than 100%, in which case multiple computations can be performed to increase the reliability of the answer. Furthermore, for some error-correcting codes, it is necessary to perform measurements during the calculation.

The task of designing a quantum computer is complicated by the fact that each individual physical implementation involves a trade-off between these requirements. For example, photons have long coherence times and are easy to measure but they only interact weakly with each other, making two-qubit gates difficult to engineer.

In this thesis, we will focus on DiVincenzo's fourth requirement which, as he put it, is "at the heart of quantum computing" [10]. We will try to develop general physical methods to generate high-fidelity two-qubit quantum gates which are robust against initialisation errors and inaccuracies in the system parameters.

1.2.2 The Two-Qubit Quantum Gate

For universal quantum computation, we want to be able to perform any unitary transformation on the n qubit system with a finite number of gates. Barenco *et al.* showed that it is possible to perform any unitary transformation on a set of n qubits using only arbitrary single qubit rotations and two-qubit entangling gates between any pair of qubits [29]. This result was extended by Boykin *et al.* who showed that only a finite number of single qubit gates were necessary if the unitary transformation only needed to be performed with an arbitrary, pre-defined accuracy [7, 30]. The simplest gate set is given by the single qubit rotations

$$H = \frac{1}{\sqrt{2}} \begin{pmatrix} 1 & 1 \\ 1 & -1 \end{pmatrix}, \tag{1.33}$$

$$T = \begin{pmatrix} 1 & 0 \\ 0 & \exp(i\pi/4) \end{pmatrix} \tag{1.34}$$

operating on the one-qubit basis $(|0\rangle, |1\rangle)^T$ and the two-qubit CNOT gate

$$U_{CNOT} = \begin{pmatrix} 1 & 0 & 0 & 0 \\ 0 & 1 & 0 & 0 \\ 0 & 0 & 0 & 1 \\ 0 & 0 & 1 & 0 \end{pmatrix} \tag{1.35}$$

operating on the two-qubit basis $(|00\rangle, |01\rangle, |10\rangle, |11\rangle)^T$. Whilst performing the single qubit rotations can be a difficult task in its own right, the real essensce of quantum computation is generated by the entangling operation of the U_{CNOT} gate. This gate generates entanglement if we pass a qubit superposition into the CNOT gate

$$\frac{1}{\sqrt{2}}(|0\rangle + |1\rangle)\,|0\rangle \overset{U_{CNOT}}{\longrightarrow} \frac{1}{\sqrt{2}}(|00\rangle + |11\rangle)\,. \tag{1.36}$$

Sometimes it is more useful to use a gate which conditionally creates entanglement automatically without requiring an initial superpositional state. This can be done with the "root-of-SWAP" gate

$$U_{SWAP}^{\frac{1}{2}} = \begin{pmatrix} 1 & 0 & 0 & 0 \\ 0 & \frac{1+i}{2\sqrt{2}} & \frac{1-i}{2\sqrt{2}} & 0 \\ 0 & \frac{1-i}{2\sqrt{2}} & \frac{1+i}{2\sqrt{2}} & 0 \\ 0 & 0 & 0 & 1 \end{pmatrix}. \tag{1.37}$$

It was demonstrated by Loss and DiVincenzo [31] that, along with single qubit rotations, the root-of-SWAP gate can perform the same operation as a CNOT gate

$$U_{CNOT} = R_1^{\vec{z}}(\theta/2) R_2^{\vec{z}}(\theta/2) U_{SWAP}^{\frac{1}{2}} R_1^{\vec{z}}(\theta) U_{SWAP}^{\frac{1}{2}} \tag{1.38}$$

where $R_i^{\vec{z}}(\theta)$ are rotations around the z axis of the Bloch sphere by an angle θ for qubit i, as described in Sec. 1.1.2. It is the robust experimental realisation of the root-of-SWAP gate which will be one of the major focuses of this thesis.

1.2.3 Implementation using the Exchange Interaction

In order to implement the two-qubit quantum gate, the most common method, originally proposed by Loss and DiVincenzo [31], is to use the exchange interaction between a pair of spin qubits in a double well potential. Using the Hund-Mulliken approximation [32], we can approximate the Hamiltonian as a two-site Hubbard model

$$\hat{H}_{\text{Hubb}} = -t \sum_{\sigma=\uparrow,\downarrow} (c^{\dagger}_{1,\sigma} c_{2,\sigma} + c^{\dagger}_{2,\sigma} c_{1,\sigma}) + U \sum_{i=1,2} n_{i,\uparrow} n_{i,\downarrow} \tag{1.39}$$

where $c^{\dagger}_{1,\uparrow}$ and $c_{1,\uparrow}$ are the creation and annihilation operators for a spin-up particle on one of the sites and with similar operators for the other site and spin combinations. t is the hopping energy between the dots, U is the contact energy for two particles on the same site, typically due to Coulomb repulsion, and $n = c^{\dagger}c$ is the number operator. The tunnel coupling mixes $c^{\dagger}_{1,\uparrow}c^{\dagger}_{2,\downarrow}|0\rangle$ and $c^{\dagger}_{1,\downarrow}c^{\dagger}_{2,\uparrow}|0\rangle$ through the virtual states $c^{\dagger}_{1,\downarrow}c^{\dagger}_{1,\uparrow}|0\rangle$ and $c^{\dagger}_{2,\uparrow}c^{\dagger}_{2,\downarrow}|0\rangle$ to produce an exchange interaction. We can calculate the eigenstates of the Hamiltonian in this basis [33]

$$H = \begin{pmatrix} 0 & 0 & -t & -t \\ 0 & 0 & t & t \\ -t & t & U & 0 \\ -t & t & 0 & U \end{pmatrix} \begin{matrix} |\uparrow,\downarrow\rangle \\ |\downarrow,\uparrow\rangle \\ |\uparrow\downarrow,\cdot\rangle \\ |\cdot,\uparrow\downarrow\rangle \end{matrix} . \tag{1.40}$$

If we assume that U is large, then the states $|\uparrow\downarrow,\cdot\rangle$ and $|\cdot,\uparrow\downarrow\rangle$ are virtual and the accessible states are

$$|\Psi_T\rangle = \frac{1}{\sqrt{2}}(|\uparrow,\downarrow\rangle + |\downarrow,\uparrow\rangle) \qquad |\Psi_S\rangle = \frac{1}{\sqrt{2}}(|\uparrow,\downarrow\rangle - |\downarrow,\uparrow\rangle) \tag{1.41}$$

which are separated in energy by $\Delta E = E_S - E_T = 4t^2/U$. These are the same eigenstates of the Heisenberg Hamiltonian

$$\hat{H}_{\text{Heis}} = -J\,\vec{S}_1 \cdot \vec{S}_2 \tag{1.42}$$

where $\vec{S}_i$ are the spin operators on the ith site and the coupling $J = 4t^2/U$. Therefore, the exchange interaction in the Hubbard Hamiltonian, Eq. 1.39, can

be described using $\hat{H}_{\text{Heis}}$.

To implement a two-qubit gate using the exchange interaction, we must make the coupling time-dependent by modulating the potential of the double well. The coupling between the states is quantified by the integrated coupling $J_{\text{tot}} = J_0\tau'/\hbar = \int_0^{\tau'} J(\tau)/\hbar \ \mathrm{d}\tau$ which determines the two-qubit gate implemented: for $J_{\text{tot}} = n\pi$, we have a "SWAP" gate if n is even and a "root-of-SWAP" gate if n is odd. These gates are conditional as $c^\dagger_{1,\uparrow}c^\dagger_{2,\uparrow}|0\rangle$ and $c^\dagger_{1,\downarrow}c^\dagger_{2,\downarrow}|0\rangle$ are eigenstates of the Hamiltonian in Eq. 1.42.

1.3 Low-Dimensional Semiconductor Devices

In this section, we will describe how electrons constrained within low dimensional structures of a semiconducting substrate can be used to create a quantum computer. There are many proposals for experimental implementations for quantum computation but we will focus on developments in solid-state quantum computing. There are proposals for performing quantum computations by manipulating individual quantum systems, such as cavity QED [34], linear optics [35], optical lattices [36] and nuclear magnetic resonance [37]. However, the technology required to control these systems can be exceedingly complex and there are questions as to whether these proposals are scalable with respect to the first DiVincenzo criterion in Sec. 1.2.1.

Solid state quantum computers, on the other hand, are naturally scalable as they can be developed using standard fabrication techniques and addressing individual qubits mostly requires only electrical control. Proposals using phosphorous donors in silicon [38–40] and, more recently, superconducting resonators [41–45] have been developed and significant experimental progress has been made. However, in this section, we will focus on electon spin qubits in low-dimensional semiconducting devices.

In order to control the electrons which we want to use as qubits, we need to confine them in lower dimensional structures. It is possible to grow heterostructures of GaAs and AlGaAs with atomically smooth interfaces using molecular beam epitaxy (MBE), an example of which is given in Fig. 1.2. If the heterostructure is doped with Si, electrons will dissociate from the dopant layer.

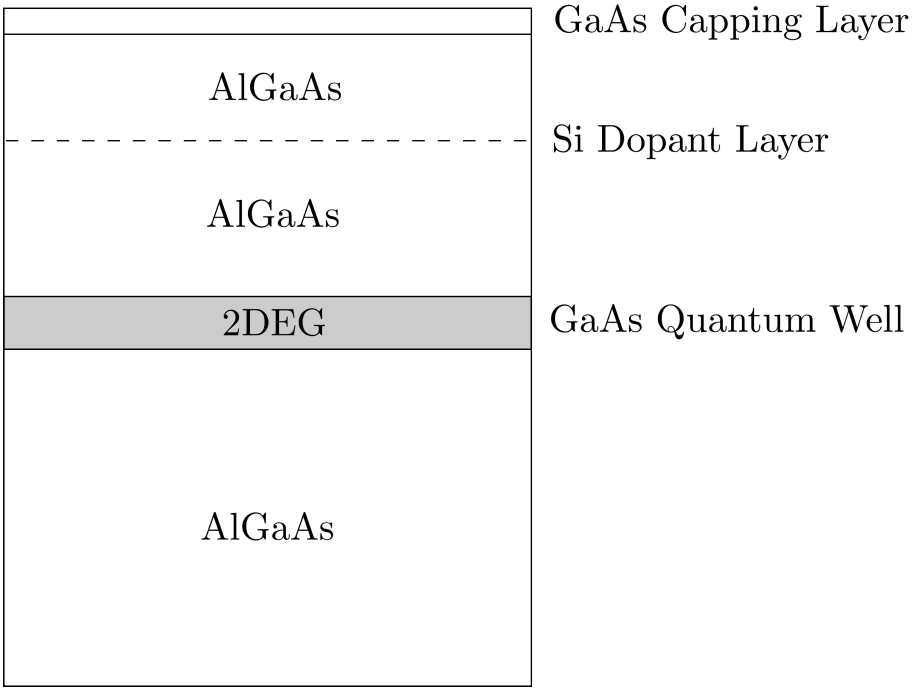

Figure 1.2: A typical semiconductor quantum well heterostructure. The AlGaAs/GaAs/AlGaAs interface provides a confining quantum well potential which fills with dissociated electrons from the Si dopants to create a two-dimensional electron gas (2DEG).

The difference in the band gaps of GaAs and AlGaAs means that these electrons will be confined to form a two-dimensional electron gas (2DEG) in the GaAs layer. Lateral confinement can be acheived either by etching away the material or by depositing metal gates on the surface of the heterostructure and electrostatically depleting the regions underneath these gates. Using these methods, we can confine individual electrons into one-dimensional quantum wires or zero-dimensional quantum dots.

1.3.1 Semiconductor-Based Quantum Computers

Loss and DiVincenzo [31] first proposed creating a quantum computer using a linear array of quantum dots each containing a single electron with the spin acting as the qubit. Individual spins can be manipulated by applying local magnetic fields and the qubits could be entangled using the method of Sec. 1.2.3. However, whilst conceptually simple, this technique is difficult to realise experimentally. Petta *et al.* [46] have demonstrated entanglement generation for a double quantum dot system but widespread adoption of this technique for quantum information architectures has been hampered by experimental challenges. The primary problem is that the integrated coupling J_{tot} is strongly dependent on the coupling between the two quantum dots of the double well potential. As shown in Sec. 1.2.3, $J_{\text{tot}} \sim t^2$ but the tunneling rate t is exponentially dependent on the width and height of the barrier separating the two sites, which can be characterised by a parameter a. Therefore, the integrated coupling is $J_{\text{tot}} \sim \int_0^{\tau'} e^{2a(\tau)}\,\mathrm{d}\tau$. Small variations in a due to electrical noise or from the resolution of the controlling voltage sources can significantly change J_{tot}, thereby reducing the gate fidelity.

As well as requiring a high degree of control over the form of the potential, both spatially and temporally, the dynamics of a typical system entangles the spins in around 180 ps [46]. Even when this is possible, as GaAs is a piezoelectric matrial, phonons will be generated which could affect the control of remote qubits [47, 48]. High frequency control over the confining potential can be avoided by drawing the qubits through a set of static gates. This was proposed by Barnes *et al.* [49] using surface acoustic waves (SAWs) to drag electrons through a pre-defined gate pattern on the surface of the heterostructure. However, these

proposals are still subject to the exponential dependence of the coupling on the tunnel barrier and must be highly calibrated in order to produce the desired gate operations with high fidelity.

1.4 Outline of Work

In this chapter, we have provided a motivation for studying methods to entangle qubits and for developing techniques for implementing two-qubit quantum gates. The correlations present in entangled systems are greater than is possible classically. The field of quantum information processing has provided numerous algorithms which use entangled states as a resource to improve upon classical limits in fields as diverse as cryptography, teleportation and computing. Whilst entanglement is useful on its own, if we have a process which generates it conditionally depending on the initial state, then we can use this process to implement a two-qubit quantum gate which is one of the required elements for building a quantum computer. We described how the exchange interaction for a pair of qubits confined in a double well within a semiconductor heterostructure can be used as a two-qubit quantum gate but we noted that this technique has some disadvantages which leaves open the possibility to develop superior entangling processes.

The majority of the techiques used in quantum information processing are dynamical in that they involve evolving qubits from one state into another. This is typically done using the time-dependent Schrödinger equation (TDSE). However, most systems are too complex to solve analytically so in Ch. 2 we will study methods for finding numerical solutions to the TDSE. We will focus on methods where the temporal dimension is discretised and an initial wave function is propagated over a large number of time steps. We will also consider how to discretise real-space Hamiltonians with and without magnetic fields. Furthermore, we would like to be able to solve the TDSE efficiently. In recent years, massively-parallel computing has become readily available through advances in graphics processing (GPU) technology. We finish the chapter by showing that one of the propagation techniques we have described, namely the staggered leapfrog method, is ideal for GPU acceleration.

In Ch. 3, we will propose a technique for implementing the root-of-SWAP two-qubit quantum gate using a pair of interacting particles in a one-dimensional harmonic potential. We use the energy spectrum of the system to show that it is should be possible to generate maximally entangled states with arbitrarily high fidelity. We provide a limit where the approximations we make to get this result are exact and we demonstrate that the proposal is robust against deviations from these approximations. We generate numerical solutions for a range of possible potentials and show that the proposal does generate high-fidelity maximally entangled states. We describe some physical systems where this method could be implemented and we finish the chapter by discussing how the proposed system differs from the exchange interaction scheme of Sec. 1.2.3.

In Ch. 4, we will consider the spin-orbit interaction (SOI). The SOI couples the spin and momentum variables of the electron so, for spin qubits, this will significantly affect the dynamics of the qubit states. As a tool for developing components for quantum computation, we would like to be able to include SOI in the numerical methods from Ch. 2. However, unlike for magnetic fields, there is no generally accepted form for discretising the SOI Hamiltonian. We start by deriving this Hamiltonian using a low energy expansion of the Dirac equation. We then provide a new discretisation for SOI using an adapted form of an exponential substitution originally developed for fluid dynamics. Having discretised the Hamiltonian we see that the effects of the SOI are similar to those from magnetic fields. We finish the chapter by using analytically soluable Hamiltonians with SOI to show that this technique provides higher fidelity solutions than the most obvious discretisation method.

In Ch. 5, we investigate how the SOI effects the entangling proposal of Ch. 3. We start by developing a simple point-particle model of the system and show how the SOI affects the precession of the qubits. In order to generate a root-of-SWAP gate, we demonstrate that an additional constraint on the initial displacement of the particles is needed. We use the SOI discretisation from Ch. 4 to simulate the system for particles which are spatially extended states and show that the gate error is negligible when this constraint is obeyed. We also show that the error is robust against perturbations of the constraint on the initial displacement of the particles.

In Ch. 6, we summarise the work and provide some possible avenues for future research.

Chapter 2

Numerical Methods for Efficiently Simulating Quantum Systems

2.1 Introduction

The quantum information processes described in Ch. 1 are dynamical, in that they take a state and evolve it into a new quantum state. The relevant equation of motion for non-relativistic quantum dynamics is the time-dependent Schrödinger equation (TDSE):

$$i\hbar\frac{\partial\Psi(t)}{\partial t} = \hat{H}\Psi(t) \tag{2.1}$$

where $\Psi(t)$ is the – potentially many-body – time-dependent wave function and $\hat{H}$ is the Hamiltonian for the system. The formal solution to Eq. 2.1, for an initial wave function $\Psi(t')$, is given by $\Psi(t'') = \hat{U}(t'', t')\Psi(t')$ where

$$\hat{U}(t'', t') = \mathcal{T}\exp\left[-\frac{i}{\hbar}\int_{t'}^{t''}\hat{H}(\tau)\,\mathrm{d}\tau\right] \tag{2.2}$$

is the time-evolution operator and $\mathcal{T}$ indicates time-ordering. Analytic solutions to Eq. 2.2 are only available for simple systems and if one wants to study more complex quantum dynamics, numerical solutions to Eq. 2.1 must be found.

In this chapter, we will discuss methods to efficiently, stably and accurately find solutions to the TDSE. As numerical solutions are generated on computers, we must discretise the system in space and time which means that we no longer describe the system exactly. It is possible that solutions to the TDSE are no longer stable, that is, there is no guarantee that the time evolution $U(t'', t')$ is unitary so the norm of the wave function is not necessarily conserved. This can lead to solutions which have exponentially growing probability. We will show that for the simplest temporal discretisation, this always occurs. Therefore, more sophisticated methods are needed so we will introduce two more methods and investigate their stability criteria. Spatial discretisation is easier as there exist physical systems, such as the Hubbard model, which we can use as an approximation for a continuous system. We will demonstrate how this relates to both kinetic and magnetic terms in standard Hamiltonians. We will also briefly outline some alternative methods for solving the TDSE.

When generating numerical solutions to the TDSE, the propagation method must be efficient as well as being stable. As we described in Sec. 1.2, the curse of dimensionality means that even simple quantum systems may require a huge amount of information to store the state of the system. Processing large amounts of information takes a long time so we also need efficient algorithms. Parallel processing, and especially massive parallel processing using graphics cards (GPUs), can significantly increase the performance of certain types of algorithms. We will show that one of the iteration schemes described earlier in the chapter has the ideal form for GPU acceleration.

2.2 Temporal Discretisation and Stability

We can discretise the time-evolution operator, Eq. 2.2, onto a set of N_t equally spaced time steps separated by an interval, $\Delta t = (t'' - t')/N_t$ by repeated use of the semi-group property of the time-evolution operator $\hat{U}(t'', t) = \hat{U}(t'', t')\hat{U}(t', t)$.

Explicitly, the discretisation takes the form

$$\Psi(t') = \prod_{j=1}^{N_t} U_j \Psi(t) \tag{2.3}$$

where the U_j propagate the wave function from step j to step $j+1$. This temporally discretised approximation of $\hat{U}(t'', t)$ is called the Trotter expansion [50]. We will assume that the time step is sufficiently small that the Hamiltonian is quasi-static and we can make the approximation, $\hat{H}(t + \Delta t) \approx \hat{H}(t)$. This allows us to write the propagator as

$$\hat{U}(t, t + \Delta t) = \exp\left[-\frac{i\hat{H}(t)\Delta t}{\hbar}\right]. \tag{2.4}$$

However, the matrix operator $\hat{H}(t)$ is potentially large and finding an accurate expression for the exponentiated matrix in Eq. 2.4 is non-trivial [51]. In this section, we will present three techniques for approximating Eq. 2.4; the Euler, Crank-Nicolson and staggered leapfrog methods. All of these methods are based on the assumption that the propagation step length Δt is small. We will introduce these methods and investigate whether and in what regime these propagation methods are stable.

2.2.1 Euler Method

The argument of the exponential in $\hat{U}(t, t + \Delta t)$ is small so a first approximation to Eq. 2.4 would be a Taylor expansion. Ignoring terms at $\mathcal{O}(\Delta t^2)$, the propagator becomes

$$\hat{U}_{\mathrm{E}}(t, t + \Delta t) \approx 1 - \frac{i\hat{H}(t)\Delta t}{\hbar}. \tag{2.5}$$

We instantly see that Eq. 2.5 is not a good propagator as it is not unitary, $U^{\dagger}(t, t + \Delta t) \neq U^{-1}(t + \Delta t, t)$, and therefore is not norm preserving. This cannot

be corrected for by increasing the order of the Taylor expansion as the non-unitarity contributions from higher order terms will not cancel the non-unitarity at lower orders of Δt. Numerically, the non-unitary part of $\hat{U}_{\mathrm{E}}$ will become insignificant if Eq. 2.5 is continued to higher orders but this would require higher powers of $\hat{H}$ to be calculated. This may be computationally inefficient and we will see in Sec. 2.2.3 that there are better explicit methods for propagating the wave function.

Although the probability is not conserved, this iteration scheme, known as the Euler method, may still be stable. To demonstrate the stability of a given propagation method, we will use von Neumann stability analysis [52, 53]. Consider the computational error $\epsilon(t) = \Psi(t) - \overline{\Psi(t)}$ where $\overline{\Psi(t)}$ is the exact solution to the Trotter expansion in Eq. 2.3 and $\Psi(t)$ is the computed value. Therefore, the numerical error has an amplification factor $\xi = \frac{\epsilon(t+\Delta t)}{\epsilon(t)}$ such that the iteration scheme is unstable if $|\xi| > 1$. We can also define a spectral decomposition of the error $\epsilon(t) = \sum_m \epsilon_m(t)\psi_m$ where ψ_m are the instantaneous energy eigenfunctions satisfying $\hat{H}(t)\psi_m = E_m\psi_m$, such that we have amplification factors for each of the eigenfunctions in the decomposition ξ_m. In general, if $|\xi_m| > 1$, then $|\xi| > 1$. This is strictly true when the Hamiltonian is time-independent. For the Euler propagator, $\Psi(t + \Delta t) = \hat{U}_{\mathrm{E}}(t + \Delta t, t)\Psi(t)$, so

$$\epsilon_m(t + \Delta t) = \left(1 + \frac{iE_m\Delta t}{\hbar}\right)\epsilon_m(t). \tag{2.6}$$

Therefore, we have $|\xi_m| = \sqrt{1 + (E_m\Delta t/\hbar)^2} > 1$ so the Euler method is unconditionally unstable. If we were to use this propagator, the error in the final solution will be of the order $(\frac{E_m\Delta t}{\hbar})^{N_t}$. As with all propagation techniques, the error can be reduced by increasing the number of time steps, therefore decreasing Δt, as this makes the temporal discretisation approach the continuum limit. However, increasing N_t is not an efficient solution and there are better propagation techniques which are not unstable.

2.2.2 Crank-Nicolson Method

We have concluded that the Euler method will not provide us with satisfactory solutions to the TDSE so we must use a more sophisticated expansion of the matrix exponential in the propagator $\hat{U}(t, t+\Delta t)$. A stable, norm-preserving approximation can be obtained by using Cayley's form of the propagator, which is the (1, 1) Padé approximation for the matrix exponential [51]

$$\hat{U}(t+\Delta t, t) \approx \left(1+\frac{i\Delta t}{2\hbar}\hat{H}(t)\right)^{-1}\left(1-\frac{i\Delta t}{2\hbar}\hat{H}(t)\right), \quad (2.7)$$

$$\left(1+\frac{i\Delta t}{2\hbar}\hat{H}(t)\right)\Psi(t+\Delta t) \approx \left(1-\frac{i\Delta t}{2\hbar}\hat{H}(t)\right)\Psi(t). \quad (2.8)$$

Known as the Crank-Nicolson method [53, 54], Eq. 2.8 has the matrix form $\mathbf{A}\vec{y} = \mathbf{B}\vec{x}$, where $\mathbf{A}$ and $\mathbf{B}$ are matrices, $\vec{x}$ is a known vector and we need to solve for the vector $\vec{y}$.

Probability is conserved as the Crank-Nicolson propagator in Eq. 2.7 is unitary. Using the von Neumann analysis described in Sec. 2.2.1 for Eq. 2.8, the eigenfunction amplification factors are

$$|\xi_m| = \left|\frac{1-\frac{i\Delta t E_m}{2\hbar}}{1+\frac{i\Delta t E_m}{2\hbar}}\right| = 1. \quad (2.9)$$

Therefore, $|\xi| = 1$, the error is bounded and the method is unconditionally stable. It is worth noting that the stability of a propagation algorithm does not guarantee its accuracy. The temporal discretisation of the Trotter expansion is only an approximation to the real dynamics of the system so errors will occur when the time step is too large. To test whether a numerical solution to the TDSE is accurate involves running a set of simulations with differing time step Δt and observing when the solutions converge. This also applies for the spatial discretisation we will describe in Sec. 2.3.

Eq. 2.8 can be broken up into an explicit and an implicit calculation. For the right-hand side of Eq 2.8, $\vec{z} = \mathbf{B}\vec{x}$ is calculated explicitly through matrix multiplication, whilst in order to calculate the wave function at the next time step, we must implicitly solve the coupled set of equations on the left-hand side,

$\mathbf{A}\vec{y} = \vec{z}$. This can be done by calculating the inverse such that $\vec{y} = \mathbf{A}^{-1}\vec{z}$, however, computing $\mathbf{A}^{-1}$ is excessive and the implicit solve can be acheived using standard matrix methods, such as LU decomposition of $\mathbf{A}$. This is often the slowest step in the calculation, which can, in general, take up to $\mathcal{O}(n^3)$ operations when $\hat{H}$ is a matrix of order n although better algorithms are available [53]. For time-independent problems, the decomposition only needs to be calculated once and stored in memory for subsequent iterations but for time-dependent problems, performing the decomposition every time step is impractical.

2.2.3 Staggered Leapfrog Method

We would like to find an approximation to the propagator in Eq. 2.4 which conserves probability, is stable and does not involve an implicit matrix solve. The staggered leapfrog method of Askar and Cakmak [55] provides us with an explicit method which is conditionally stable. This method involves combining a pair of Taylor expansions of Euler form, one propagating forward and one propagating backwards from time t and subtracting them such that

$$\Psi(t+\Delta t) = \Psi(t-\Delta t) + \left(e^{-i\hat{H}\Delta t} - e^{i\hat{H}\Delta t}\right)\Psi(t) \tag{2.10}$$

$$\approx \Psi(t-\Delta t) - \frac{2i\Delta t}{\hbar}\hat{H}\Psi(t) + \mathcal{O}(\Delta t^3). \tag{2.11}$$

Von Neumann stability analysis can be used by recognising that $\xi^2 = \frac{\epsilon(t+2\Delta t)}{\epsilon(t)}$. Inserting the spectral decomposition of the error into Eq. 2.11 gives

$$\xi_m^2 = 1 - \frac{2iE_m\Delta t}{\hbar}\xi_m \tag{2.12}$$

which has solutions

$$\xi_m^{\pm} = -\frac{iE_m\Delta t}{\hbar} \pm \sqrt{1 - \left(\frac{E_m\Delta t}{\hbar}\right)^2}. \tag{2.13}$$

For $E_m\Delta t/\hbar \leq 1$, the term in the square root is real and $|\xi_m^{\pm}| = 1$ whilst for $E_m\Delta t/\hbar > 1$, the root term becomes imaginary and the error becomes un-

bounded. Therefore, the stability criterion for the staggered leapfrog method is

$$\Delta t \leq \frac{\hbar}{E_{\max}} \tag{2.14}$$

where $E_{\max}$ is the largest eigenvalue of the discretised Hamiltonian $\hat{H}$. Finally, although the scheme is not strictly norm preserving, the propagation step is unitary up to $\mathcal{O}(\Delta t^4)$. For this thesis, the norm was monitored during the simulations and its value was never observed to drift far from unity. For further discussions on the accuracy of this method, see Ref. [56].

Given that the staggered leapfrog method is a nearly unitary and explicit propagation algorithm, we will sacrifice the unconditional stability of the Crank-Nicolson method and use Eq. 2.11 as the propagator for this thesis. Typically, the stability criterion, Eq. 2.14, constrains the time step Δt to around a half of the time step required for the Crank-Nicolson method to generate accurate solutions. In Secs. 2.5, we will show that having to propagate the wave function for double the number of time steps is irrelevant compared to the speed up through parallelisation using GPU acceleration.

2.3 Spatial Discretisation

The temporal discretisation of Sec. 2.2 is general for the Hamiltonian of any closed system $\hat{H}$. If the system has a finite dimensional Hilbert space, then no further approximations are necessary. However, often we want to simulate systems described by continuous variables which requires the Hamiltonian to be spatially discretised in order to make the propagation computationally tractable. The most common discretisation – and the only one that we will consider in this thesis – is when the wave function is limited to an ordered, real space lattice.

The canonical Hamiltonian for a single, spinless particle in one dimension is given by

$$\hat{H}\Psi(x) = \left(\frac{\hat{p}^2}{2m} + \hat{V}\right)\Psi(x) \tag{2.15}$$

$$= -\frac{\hbar^2}{2m}\frac{\partial^2\Psi(x)}{\partial x^2} + V(x)\Psi(x) \tag{2.16}$$

where m is the mass of the particle, $\hat{p} = -i\hbar\partial_x$ is the momentum operator and $\hat{V}$ is some local, external potential. Whilst it is possible to create a non-regular grid using finite element techniques [57], this level of complexity will not be needed for the systems we will be considering. We discretise the wave function onto a set of N_x lattice sites with equal spacing Δx, so to evaluate $\hat{H}\Psi(x)$, we need to find a discretised form of the second derivative. This can be done using the Taylor expansions

$$\Psi(x + \Delta x) = \Psi(x) + \Delta x \frac{\partial \Psi(x)}{\partial x} + \frac{\Delta x^2}{2}\frac{\partial^2 \Psi(x)}{\partial x^2} + \frac{\Delta x^3}{3!}\frac{\partial^3 \Psi(x)}{\partial x^3} + \dots \tag{2.17}$$

$$\Psi(x - \Delta x) = \Psi(x) - \Delta x \frac{\partial \Psi(x)}{\partial x} + \frac{\Delta x^2}{2}\frac{\partial^2 \Psi(x)}{\partial x^2} - \frac{\Delta x^3}{3!}\frac{\partial^3 \Psi(x)}{\partial x^3} + \dots \tag{2.18}$$

By adding these expressions together, we get

$$\frac{\partial^2 \Psi(x)}{\partial x^2} = \frac{\Psi(x + \Delta x) - 2\Psi(x) + \Psi(x - \Delta x)}{\Delta x^2} + \mathcal{O}(\Delta x^2). \tag{2.19}$$

With Eq. 2.19, we have a fully discretised form of Eq. 2.16. Comparing this discretised form of the Hamiltonian, Eq. 2.16, we notice that this is a multi-site version of the Hubbard Hamiltonian in Eq. 1.39, with tunneling energy $t = \hbar^2/2m\Delta x^2$ and on-site energy $U = \hbar^2/m\Delta x^2 + V(x)$. Therefore, we can easily calculate the spectrum of the Hamiltonian using Bloch's theorem [58]. An approximation for the maximum energy eigenfunction can be made by adding the kinetic energy from the highest energy Bloch function to the maximum potential energy. This provides a value for $E_{\max}$ which we can use in the staggered-leapfrog stability criterion, Eq. 2.14:

$$E_{\max} \approx \frac{\hbar^2}{m\Delta x^2}(1 - \cos k\Delta x) + V_{\max} \tag{2.20}$$

where $-\frac{\pi}{\Delta x} \leq k \leq \frac{\pi}{\Delta x}$ are the wave numbers of the eigenstates.

Typically, we will limit our simulation domain to the interval $[x_{\min}, x_{\max}]$ and

impose hard-wall Dirichlet boundary conditions such that $\Psi(x_{\min}) = \Psi(x_{\max}) = 0$. Spurious reflections from the boundaries are avoided by ensuring that the wave function is negligible at the edge of the domain.

We can extend the discretisation to systems with a larger number of spatial dimensions using multi-dimensional Taylor expansions. In this thesis, we will be considering two-dimensional systems: either a single particle moving in two dimensions or two particles confined to one dimension.

2.3.1 Magnetic Fields and Harper's Equation

An important deviation from the canonical Hamiltonian of Eq. 2.15 is when we have a particle with charge q in a magnetic field. For a magnetic vector potential $\vec{A}$, the canonical momentum transforms as $\hat{p} \to (\hat{p} + q\vec{A})$. Magnetic fields have no observable effects on one-dimensional systems so we need only consider their effects in two dimesions. For a perpendicular magnetic field $\vec{B} = (0, 0, B)$, we will use the Landau gauge $\vec{A} = (0, Bx, 0)$. Inserting this into Eq. 2.15 gives

$$\hat{H}\Psi(x) = -\frac{\hbar^2}{2m}\frac{\partial^2\Psi(x,y)}{\partial x^2} - \frac{\hbar^2}{2m}\left(\frac{\partial}{\partial y} + i\frac{qBx}{\hbar}\right)^2 \Psi(x,y) + V(x,y)\Psi(x,y). \quad (2.21)$$

It is possible to discretise this Hamiltonian using the techniques of Sec. 2.3. Expanding the second term gives a first order derivative which can be discretised to $\mathcal{O}(\Delta x^2)$ by subtracting Eq. 2.18 from Eq. 2.17. However, the resulting discretisation does not represent a physical system and so dynamics observed in the discretised system may not relate to real, physical phenomena.

The Hamiltonian in Eq. 2.21 was studied by Hofstadter [59] who noticed that, on a lattice, a perpendicular magnetic field introduces an additional phase to the hopping terms. The momentum operator is the generator for translations, that is $\psi(x+a) = e^{ia\hat{p}}\psi(x)$, so if $\hat{p} \to (\hat{p}+q\vec{A})$, a non-zero magnetic field has the effect of multiplying the hopping term in the Hamiltonian by a position-dependent phase which Hofstadter refered to as a *Peierls substitution*. Using this insight, we can

use an exponential expansion to discretise the terms containing derivatives in Eq. 2.21:

$$\left(\frac{\partial}{\partial y}+i\frac{qBx}{\hbar}\right)^2\Psi(x,y)=\frac{\partial^2\Psi(x,y)}{\partial y^2}+\frac{2iqBx}{\hbar}\frac{\partial\Psi(x,y)}{\partial y}-\left(\frac{qBx}{\hbar}\right)^2\Psi(x,y) \quad (2.22)$$

$$\begin{aligned}\approx\ & \frac{1}{\Delta x^2}\left(1+i\frac{qBx\Delta x}{\hbar}+\frac{1}{2}\left(\frac{iqBx\Delta x}{\hbar}\right)^2+\dots\right)\times \\ & \left(\Psi(x,y)+\Delta x\frac{\partial\Psi(x,y)}{\partial y}+\frac{\Delta x^2}{2}\frac{\partial^2\Psi(x,y)}{\partial y^2}+\dots\right) \\ & +\frac{1}{\Delta x^2}\left(1-i\frac{qBx\Delta x}{\hbar}+\frac{1}{2}\left(\frac{iqBx\Delta x}{\hbar}\right)^2+\dots\right)\times \\ & \left(\Psi(x,y)-\Delta x\frac{\partial\Psi(x,y)}{\partial y}+\frac{\Delta x^2}{2}\frac{\partial^2\Psi(x,y)}{\partial y^2}+\dots\right)-\frac{2}{\Delta x^2}\Psi(x,y) \quad (2.23)\end{aligned}$$

$$=\ \frac{1}{\Delta x^2}\left(e^{\frac{iqBx\Delta x}{\hbar}}\Psi(x,y+\Delta y)-2\Psi(x,y)+e^{-\frac{iqBx\Delta x}{\hbar}}\Psi(x,y-\Delta y)\right) \quad (2.24)$$

This form, known as Harper's equation, provides us with a discretisation of the Hamiltonian in the presence of a magnetic field.

2.4 Alternative Methods for Solving the TDSE

The staggered leapfrog propagator from Sec. 2.2.3 combined with spatial discretisation from Sec. 2.3 will be the iteration scheme we will use throughout this thesis. However, there are various other methods for solving the TDSE which we will briefly review in this section.

The simplest and most general method for systems where the Hamiltonian is time-independent is to perform a spectral decomposition of the wave function [60]:

$$\Psi(x,t)=\sum_m a_m e^{-\frac{iE_m t}{\hbar}}\psi_m(x) \quad (2.25)$$

where $\hat{H}\psi_m = E_m\psi_m$ gives the eigenfunctions and eigenenergies of $\hat{H}$. The

spectral weights a_m depend on the initial wave function and are calculated as

$$a_m = \int \Psi^*(x,0)\psi_m(x)\,\mathrm{d}x. \tag{2.26}$$

The wave function $\Psi(x,t)$ is the complete solution to the TDSE. This method is derived by using separation of variables in x and t to solve the TDSE and is only applicable if $\hat{H}$ does not depend on time. Furthermore, even if $\hat{H}$ is time-independent, this method can prove inaccurate for some continuous systems where ψ_m and E_m, and therefore a_m, are difficult to calculate to a high degree of accuracy.

One can also use an eigenbasis expansion of the matrix exponential, Eq. 2.2. A common method is to expand $\hat{U}(t'',t')$ in terms of Chebyshev polynomials of the Hamiltonian which operate on the initial state $\Psi(t')$ to give the final state $\Psi(t'')$ [56, 61]. This method can be very accurate as the polynomial operator expansion can be extended up to higher orders but it assumes that the Hamiltonian is time-independent. Furthermore, the calculation is a one-step process which does not require the Trotter expansion so there is no information about the wave function at intermediate time steps.

An alternative approximation for the short-time propagator, Eq. 2.4, is the Fourier split-operator method [62]. This technique uses the Baker-Campbell-Hausdorf formula to approximate the propagator as a product of matrix exponentials which are diagonal in either the momentum or position basis

$$\hat{U}(t,t+\Delta t) = \exp\left(-\frac{i\hat{p}^2\Delta t}{4m\hbar}\right)\exp\left(-i\hat{V}\Delta t/\hbar\right)\exp\left(-\frac{i\hat{p}^2\Delta t}{4m\hbar}\right)+\mathcal{O}(\Delta t^3). \tag{2.27}$$

The method relies on the fact that the Fourier transform $\mathcal{F}$ and its inverse commute with both $\hat{p}$ and $\hat{V}$. Therefore, by transforming between momentum and position space, the exponentiated operators can be evaluated simply by multiplying the wave function elements by a phase factor. This method is unconditionally

stable [56] but is not applicable for Hamiltonians with mixed terms of the form $f(x)g(p)$. Therefore, the split-operator method cannot be used for magnetic fields as the Schrödinger equation contains cross terms of the form $\vec{A}(x) \cdot \vec{p}$. Additionally, the computationally expensive steps in this algorithm are the Fourier and inverse Fourier transforms and, although these can be accelerated using graphical processing units (GPUs) [63], the potential performance gains are not as great as for the staggered leapfrog method.

2.5 Accelerating the Staggered Leapfrog Method using the Graphical Processing Unit (GPU)

When simulating quantum systems, choosing a stable, norm-preserving algorithm is important but it is also essential to implement the algorithm in an efficient way. Efficiency is especially important for quantum mechanical systems as the information contained within the wave vector Ψ can be very large. The composite particle postulate of quantum mechanics, which states that the Hilbert space for a composite system is the tensor product of the Hilbert spaces of the individual systems, means that the information in Ψ increases exponentially with the number of particles. To clarify this point, a classical wave, discretised onto a set of N_x lattice sites, is described by a vector of length N_x. For a system of d waves, the composite classical system is described by the sum of the individual waves, which is a vector of length $N_x d$. In quantum mechanics, the wave function for a single particle is still described by a vector of length N_x but, for d particles, the tensor product requires a vector of length N_x^d to describe the composite system. This exponential scaling – known as the "curse of dimensionality" – means that the computer memory required to store many-particle wave functions is very large and therefore a large amount of processing power is needed to iterate it. In this section, we will introduce the concept of parallel programming using Graphical Processing Units (GPUs) and show that this technique greatly speeds up the staggered leapfrog method.

2.5.1 Massive Parallel Processing on the GPU using CUDA

To understand the advantages of parallel processing, we will initially focus on a simple example. A code snippet for adding together two vectors of length N_x is given by[1]

```
for (int i = 0; i < N_x; i++)
    c[i] = a[i] + b[i];
end
```

Using the CPU (central processing unit), this code will be executed serially, that is, each of the terms are calculated sequentially. The loop is effectively unrolling such that the CPU processes this code as

```
c[0] = a[0] + b[0];
c[1] = a[1] + b[1];
c[2] = a[2] + b[2];
.....................
c[N_x - 1] = a[N_x - 1] + b[N_x - 1];
```

However, as there is no co-dependence between any of the elements, each of the terms could be executed in parallel.

General purpose programming for graphics cards provides a cheap, simple and efficient method for executing massively parallel code. GPUs were developed for generating high-performance 3D graphics in real time – a demand well suited to massive parallel processing and which has led to the production of incredibly high performance GPUs, as demonstrated in Fig. 2.1. For GPUs developed by NVIDIA, the CUDA™ general purpose parallel computing architecture [64] provides a means to program code directly for the graphics card. Whilst other non-proprietry programming frameworks, such as OpenCL, are also available, CUDA provided the best performance at the time the programs used in the thesis were written.

The programming model is to define code snippets (known as kernels in CUDA) which are executed by parallel threads. These threads are allocated

[1] For this thesis, all programs were written in C# for the CPU and CUDA C for the GPU.

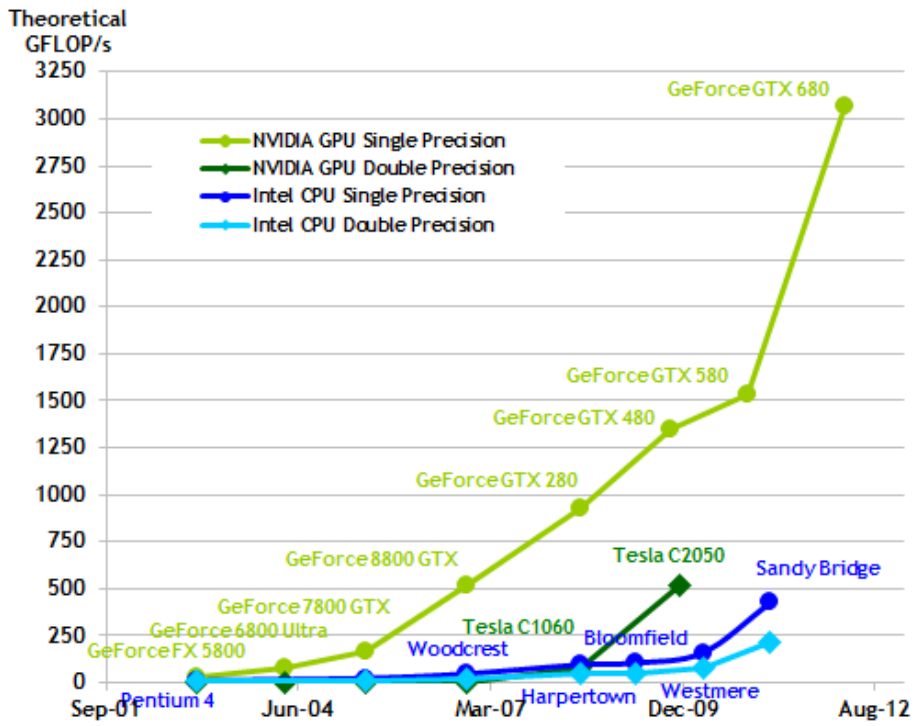

Figure 2.1: Theoretical maximum processing speeds for CPUs and GPUs in floating point operations per second (FLOPS) over time. GPU performance is growing considerably faster than for CPUs demonstrating that for algorithms which can approach this limit, GPU acceleration will lead to dramatic improvements in the time which the algorithms take to run. Figure taken from Ref. [64].

into blocks of a size determined by the type of GPU being used and an arbitrary number of blocks can be queued for execution on the graphics card. For our vector addition example, we would have

```
__global__ void VecAdd(float* A, float* B, float* C)
{
    int i = threadIdx.x;
    int j = blockIdx.x;

    int index = j * blockDim.x + i;
    C[index] = A[index] + B[index];
}
```

The kernel is then launched from the CPU which sends a request to the GPU to execute the method `VecAdd` N_x times. A set of N_x threads are created, each with their own block and thread ID, and the GPU executes the threads of a given block in parallel. It is not guaranteed what order the threads are executed in but this does not matter as there is typically no interaction between the threads. Depending on the GPU, around 10^4 threads can be run in parallel at a clock speed comparable to the CPU. This means that GPU acceleration can generate speed-ups of $\mathcal{O}(10^2 - 10^3)$ for simple tasks.

2.5.2 Why is GPU acceleration better for the Staggered Leapfrog Method?

This leaves us with an important question; do any of the propagation algorithms described in Sec. 2.2 constitute a "simple task"? In this section, we will try to make the argument that explicit schemes are more conducive to GPU acceleration than implicit schemes. This implies that the staggered leapfrog method should be used rather than Crank-Nicolson.

As a comparison of implicit and explicit matrix solves, let us consider an upper-triangular matrix $\mathbf{C}$ with a known vector $\vec{x}$ and an unknown vector $\vec{y}$ such that the implicit and explicit matrix solves are $\mathbf{C}\vec{y} = \vec{x}$ and $\vec{y} = \mathbf{C}\vec{x}$ respectively.

For a two-dimensional system, the equations are explicitly given by

$$\begin{pmatrix} c_{11} & c_{12} \\ 0 & c_{22} \end{pmatrix} \begin{pmatrix} y_1 \\ y_2 \end{pmatrix} = \begin{pmatrix} x_1 \\ x_2 \end{pmatrix}, \tag{2.28}$$

$$\begin{pmatrix} y_1 \\ y_2 \end{pmatrix} = \begin{pmatrix} c_{11} & c_{12} \\ 0 & c_{22} \end{pmatrix} \begin{pmatrix} x_1 \\ x_2 \end{pmatrix}. \tag{2.29}$$

In Eq. 2.28, using Gaussian elimination, we can solve for y_1 only after we have calculated y_2. For Eq. 2.29, we can solve for y_1 and y_2 simultaneously which can be done using parallel processing. Whilst it is possible to parallelise implicit algorithms to some extent, the performance gains are not as great as for explicit algorithms. This is the reason that we chose to solve the TDSE using the staggered leapfrog method in this thesis.

In this chapter, we have introduced methods for solving the time-dependent Schrödinger equation. Quantum information processes are often dynamical so, in order to develop new methods for entangling qubits, we will need to know how these states evolve in time. Analytic solutions to the TDSE are rare, so it is important to develop techniques for obtaining these solutions numerically. Having discussed a number of iterative techniques, we have concluded that the staggered leapfrog method is a good choice for the work in this thesis. Unlike the Crank-Nicolson method, there is a stability criterion which puts a maximum value of the length of our time step. However, this limitation is greatly outweighed by the advantages that GPU acceleration provide. The speed increase will allow us to make more thorough scans of our parameter spaces in the following chapters.

Chapter 3

Entangling Qubits in a One-dimensional Harmonic Oscillator

3.1 Introduction

Entangled qubits are the main resource required for quantum information processing. In this chapter, we will propose a new method for generating maximally entangled states using two interacting particles in a one-dimensional harmonic potential. We will analyse the energy spectrum of the system in order to demonstrate the properties of the interaction necessary to produce entangled states. We introduce the *parity-dependent harmonic approximation* which allows us to explain why maximally entangled states are generated and we show a physically reasonable limit for which these assumptions are exact. We will also demonstrate that the entanglement between the qubits remains high even when the approximation is less accurate. We present numerical solutions for a variety of interaction potentials which demonstrates the robustness of our proposal. The method is simple, requires no time-dependent control and depends only weakly on initialisation errors. This proposal is general, in the sense that it is not restricted to any particular physical system, but we will investigate some possible

implementations in Sec. 3.5. The results of Secs. 3.2, 3.3 and 3.4 were published in Physical Review A [65].

3.2 Proposal

The system is defined as follows: We have two qubits ς_i with $i = 1, 2$ assigned to a pair of particles, each confined within a one-dimensional harmonic oscillator. The particles are initialised in a tensor product state

$$\begin{aligned} |\Psi(t=0)\rangle &= \left(\int \psi_L(x_1) c^\dagger_{\varsigma_1}(x_1)\,\mathrm{d}x_1\right) \times \left(\int \psi_R(x_2) c^\dagger_{\varsigma_2}(x_2)\,\mathrm{d}x_2\right)|0\rangle \quad (3.1)\\ &\equiv \iint \Psi(x_1, x_2; t=0) c^\dagger_{\varsigma_1}(x_1) c^\dagger_{\varsigma_2}(x_2)\,\mathrm{d}x_1\,\mathrm{d}x_2\,|0\rangle \quad (3.2)\\ &\equiv |L_{\varsigma_1} R_{\varsigma_2}\rangle \quad (3.3) \end{aligned}$$

where $\psi_L(x_1)$ and $\psi_R(x_2)$ are the single particle wave functions, $|0\rangle$ is the vacuum state and $c^\dagger_{\varsigma_i}(x_i)$ is the creation operator for a qubit ς_i at coordinate x_i. If the particles are indistinguishable, the operators satisfy the (anti)commutation relations for (fermions) bosons:

$$c^\dagger_{\varsigma_i} c^\dagger_{\varsigma_j} \pm c^\dagger_{\varsigma_j} c^\dagger_{\varsigma_i} = 0. \quad (3.4)$$

The particles obey the time-dependent Schrödinger equation, Eq. 2.1, which conserves the (anti)symmetry of $|\Psi(t)\rangle$ so this method is applicable irrespective of the symmetry of the wave function. The single-particle wave functions are localised on either side of the harmonic potential such that

$$\int_{-\infty}^{0} |\psi_R(x)|^2\,\mathrm{d}x \to 0, \quad (3.5)$$

$$\int_{0}^{\infty} |\psi_L(x)|^2\,\mathrm{d}x \to 0 \quad (3.6)$$

and we will assume that they are the parity inversions of each other — that is, we define $\psi_L(x) = \psi_R(-x)$. This is for convenience and we will investigate deviations from this assumption in Sec. 3.3.2.

Finally, there is an interaction $V_{\text{int}}(x_1 - x_2)$ between the two particles with a functional form which we will not specify at this point. Therefore, the total Hamiltonian for the system is given by:

$$\hat{H} = -\frac{\hbar^2}{2m}\left(\frac{\partial^2}{\partial x_1^2} + \frac{\partial^2}{\partial x_2^2}\right) + \frac{1}{2}m\omega^2\left(x_1^2 + x_2^2\right) + V_{\text{int}}(x_1 - x_2) \tag{3.7}$$

where m is the mass of the particles and ω is the frequency of the oscillator.

In this chapter, we will show that with this system it is possible to generate maximally entangled states with arbitrarily high fidelity. In brief, the particles begin by falling towards the centre of the harmonic oscillator. When they reach the centre of the potential, there are two possible processes: the particles can scatter off each other or they pass through each other. Quantum mechanically, both of these processes occur and a superposition of scattered and transmitted wave packets is generated. By tuning the interaction potential, it is possible to give the two parts of the superposition equal weight. As we have identified each of the wave packets with the qubits ς_i and ς_j, the qubits are therefore in one of the maximally entangled states defined in Sec. 1.1.2.

3.3 Parity-Dependent Harmonic Approximation (PDHA)

To further understand the process described above, and in order to prove its robustness against initialisation errors, we must make some approximations for the system. Firstly, let us transform Eq. 3.7 into the centre-of-mass and relative coordinate basis $R = (x_1 + x_2)/2$ and $r = x_1 - x_2$. In this basis, Eq. 3.7 separates into two independent Hamiltonians for R and r

$$\hat{H}_r = -\frac{\hbar^2}{2m}\frac{\partial^2}{\partial r^2} + \frac{1}{2}m\omega^2 r^2 + V_{\text{int}}(r), \tag{3.8}$$

$$\hat{H}_R = -\frac{\hbar^2}{2m}\frac{\partial^2}{\partial R^2} + \frac{1}{2}m(2\omega)^2 R^2 \tag{3.9}$$

with $\hat{H} = \frac{1}{2}\hat{H}_R + 2\hat{H}_r$ which allows us to separate variables for the two-particle wave function $\Psi(x_1, x_2; t) = \psi(r, t)\zeta(R, t)$. The frequency of the oscillator in Eq. 3.9 is twice the frequency of the original oscillator of Eq. 3.7 so the state $\zeta(R, t)$ will be the same at each half period $t = \nu\pi/\omega$ where $\nu = 1, 2, \ldots$

In order to understand the dynamics of $\psi(r, t)$, we expand the wave function in a spectral decomposition of the eigenstates of the Hamitonian $\hat{H}_r$ and we split the sum into even and odd states

$$\psi(r,t) = \sum_{n=0}^{\infty} a_n \varphi_n e^{-iE_n t/\hbar} \tag{3.10}$$

$$= \sum_{n \text{ odd}} a_n \varphi_n e^{-i\omega\left(n+\frac{1}{2}\right)t} e^{-i\omega\xi_n t} + \sum_{n \text{ even}} a_n \varphi_n e^{-i\omega\left(n+\frac{1}{2}\right)t} e^{-i\omega\phi_n t} \tag{3.11}$$

where φ_n are the eigenstates of Eq. 3.8, E_n are the eigenenergies, which we express in terms of energy shifts due to the interaction potential $V_{\text{int}}(r)$ as fractions of the energy spacing of the unperturbed oscillator ϕ_n and ξ_n for even and odd states respectively;

$$E_n \equiv \begin{cases} \hbar\omega(n + 1/2 + \phi_n), & n \text{ even} \\ \hbar\omega(n + 1/2 + \xi_n), & n \text{ odd} \end{cases} \tag{3.12}$$

and the spectral weights a_n are the overlaps of the initial wave function with the nth eigenstate

$$a_n = \int_{-\infty}^{\infty} \psi^*(r, t = 0)\varphi_n(r)\,\mathrm{d}r \tag{3.13}$$

which are time-independent.

We will now make the *parity-dependent harmonic approximation*. Natural interaction potentials are typically localised, in the sense that the interaction is strongest when both particles are in the same place. This means that we expect the interaction potential $V_{\text{int}}(r)$ to be strongly peaked around $r = 0$. The energy of the eigenstates are defined by $E_n = \langle\varphi_n|\hat{H}_r|\varphi_n\rangle$ so the energy shifts $\hbar\omega\phi_n = \langle\varphi_n|V(r)|\varphi_n\rangle$ and similarly for $\hbar\omega\xi_n$. We expect the values of ϕ_n and ξ_n to be markedly different as the overlap with $V(r)$ depends strongly on the parity of the eigenstate. For odd states, $\varphi_n = 0$ at $r = 0$ and we expect the wave function to remain small around the origin as the wave function is continuous. This suggests that ξ_n is small so we will approximate $\xi_n \to 0$. For even states, the

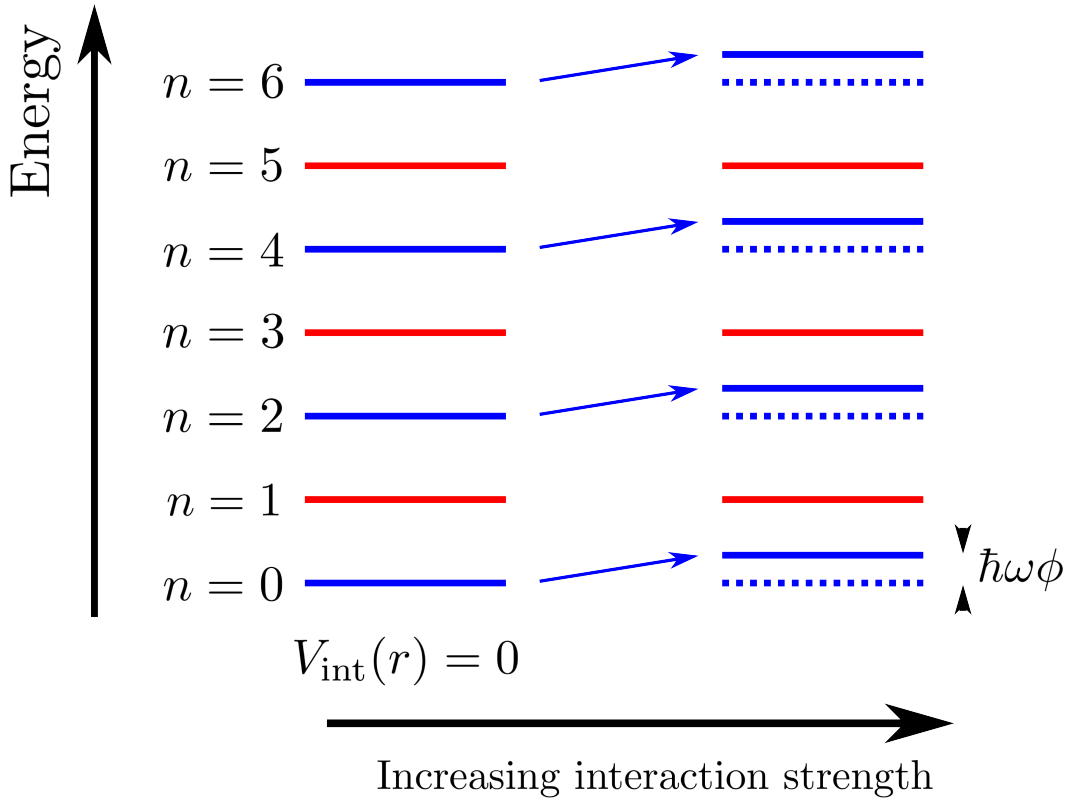

Figure 3.1: An inter-particle potential $V(r)$ perturbs the energy levels of the non-interacting system. The Parity-Dependent Harmonic Approximation (PDHA) assumes that the odd energy levels (red) are not shifted whilst the even energy levels (blue) shift by a fixed amount $\hbar\omega\phi$ independent of n.

overlap with $V(r)$ may be significant but we will make an additional, simplifying assumption which we will justify in Sec. 3.3.1: that all the energy shifts of the even states are the same — i.e. $\phi_n = \phi$ for all n.

This set of assumptions, which we call the *parity-dependent harmonic approximation* (PDHA), leads to a parity-dependent shift in the energies of the harmonic oscillator, as shown in Fig. 3.1. This allows us to simplify the spectral decomposition in Eq. 3.11. We are specifically interested in the wave function at half-integer periods of the oscillator $t = \nu\pi/\omega$:

$$\psi(r, t = \nu\pi/\omega) \approx \sum_{n \text{ odd}} a_n \varphi_n e^{-i\pi\left(n+\frac{1}{2}\right)\nu} + \sum_{n \text{ even}} a_n \varphi_n e^{-i\pi\left(n+\frac{1}{2}\right)\nu} e^{-i\pi\phi\nu} \tag{3.14}$$

$$= e^{-i\pi(\phi+1)\nu/2}\left(\sum_{n\ \text{odd}} a_n\varphi_n e^{i\pi\phi\nu/2}e^{-i\pi\nu} + \sum_{n\ \text{even}} a_n\varphi_n e^{-i\pi\phi\nu/2}\right) \tag{3.15}$$

$$= -e^{-i\pi(\phi+1)\nu/2}\Bigg[\cos(\nu\pi\phi/2)\left(\sum_{n\ \text{even}} a_n\varphi_n \mp \sum_{n\ \text{odd}} a_n\varphi_n\right) -i\sin(\nu\pi\phi/2)\left(\sum_{n\ \text{even}} a_n\varphi_n \pm \sum_{n\ \text{odd}} a_n\varphi_n\right)\Bigg] \tag{3.16}$$

where the sign in Eq. 3.16 depends on whether ν is odd or even and we have simplified the factor $e^{-i\pi n\nu}$ between Eqs. 3.14 and 3.15 by noting that, as ν is an integer, if n is even, $e^{-i\pi n\nu} = 1$ and if n is odd, $e^{-i\pi n\nu} = e^{-i\pi\nu}$. The eigenfunctions φ_n have definite symmetry under reflections, $r \to -r$, due to the symmetry of $\hat{H}_r$ so under parity inversion $\varphi_n(r) = +\varphi_n(-r)$ for n even and $\varphi_n(r) = -\varphi_n(-r)$ for n odd. Remembering that $\psi(r, t = 0) = \sum_n a_n\varphi_n$, we see that the first term in Eq. 3.16 can be written as $\psi(-r, t = 0)$. Therefore, after ν half-periods, we can recombine the separated wave function to give

$$\Psi(x_1, x_2; t = \nu\pi/\omega) \propto \iint \zeta(R, t = 0)\Big(\cos(\nu\pi\phi/2)\psi(-r, t = 0) -i\sin(\nu\pi\phi/2)\psi(r, t = 0)\Big)\,\mathrm{d}r\,\mathrm{d}R. \tag{3.17}$$

where, for simplicity, we have assumed that ν is odd. Furthermore, as $r = x_1 - x_2$, the reflection $r \to -r$ is equivalent to swapping the coordinates, $x_1 \leftrightarrow x_2$ so the state of the system is given by

$$|\Psi(t = \nu\pi/\omega)\rangle \propto \cos(\nu\pi\phi/2)\iint \psi_R(x_1)\psi_L(x_2)c^\dagger_{\varsigma_1}(x_1)c^\dagger_{\varsigma_2}(x_2)\,|0\rangle\ \mathrm{d}x_1\,\mathrm{d}x_2 -i\sin(\nu\pi\phi/2)\iint \psi_L(x_1)\psi_R(x_2)c^\dagger_{\varsigma_1}(x_1)c^\dagger_{\varsigma_2}(x_2)\,|0\rangle\ \mathrm{d}x_1\,\mathrm{d}x_2. \tag{3.18}$$

The integrals in Eq. 3.18 are the same as in the initial wave function, Eq. 3.1, except that the single particle wave functions ψ_L and ψ_R are swapped in the first term. We see that in the first term, qubit ς_1 is on the right side of the well and ς_2 is on the left and vice versa for the second term. Therefore, we can write Eq. 3.18

in terms of the original state in Eq. 3.1

$$|\Psi(t = \nu\pi/\omega)\rangle \propto \cos\theta\,|L_{\varsigma_2}R_{\varsigma_1}\rangle - i\sin\theta\,|L_{\varsigma_1}R_{\varsigma_2}\rangle \tag{3.19}$$

where we have swapped the dummy variables in the second term and commuted the creation operators[1]. The first term of Eq. 3.19 corresponds to the two particles passing through each other whilst the second term is the scattered component where the particles return to their original state. The superposition is characterised by a paramater

$$\theta = \nu\pi\phi/2 \tag{3.20}$$

and, most importantly, we get maximally entangled states when

$$\nu\phi = (2j-1)/2, \qquad j = 1, 2, \ldots \tag{3.21}$$

as this corresponds to an equal superposition of scattered and transmitted components of the wave function from Eq. 3.18. If we define the qubit on the left as "qubit 1" and the qubit on the right as "qubit 2" then for these angles we get maximally entangled, Bell-type states

$$\left|\Psi^{\pm i}\right\rangle \equiv \left(|\varsigma_1\varsigma_2\rangle \pm i\,|\varsigma_2\varsigma_1\rangle\right)/\sqrt{2}. \tag{3.22}$$

This is the main result of this chapter. Note that when $\varsigma_1 = \varsigma_2$, this corresponds to a phase rotation of the initial state and no entanglement is generated. This conditional entanglement generation is equivalent to the root-of-SWAP two-qubit quantum gate described in Sec. 1.2.2.

3.3.1 A Limit in which the Approximation is Exact

Whilst we have justified the PDHA in Sec. 3.3 on physical grounds, we will now provide a limit in which the approximation is exact. For a contact potential, the

[1] This is the only point in this derivation where, for clarity, we have specified the symmetry of the wave function. For fermions, this is an anticommutation and the state in Eq. 3.19 would be $|\Psi(t = \nu\pi/\omega)\rangle \propto \cos\theta\,|L_{\varsigma_1}R_{\varsigma_2}\rangle + i\sin\theta\,|L_{\varsigma_2}R_{\varsigma_1}\rangle$.

interaction is given by

$$V_{\text{Cont}}(x_1 - x_2) = U\delta(x_1 - x_2) \tag{3.23}$$

where U is a measure of the interaction strength. The time-independent Schrödinger equaton for two-particles in a harmonic potential with this interaction was solved by Janke and Cheng [66]. As the δ-function is infinitesimally narrow, the overlap with the odd states is necessarily zero. Therefore, the approximation that $\xi_n \to 0$ for odd states is valid for all odd n. For the even states, the eigenenergies are given by

$$\begin{aligned} E_n &= \hbar\omega(\mu_n + 1/2) && (3.24)\\ &= \hbar\omega(n + 1/2 + \phi_n) && (3.25) \end{aligned}$$

where μ_n satisfies the transcendental equation

$$\frac{\Gamma\left(\frac{1}{2} - \frac{1}{2}\mu_n\right)}{\Gamma\left(-\frac{1}{2}\mu_n\right)} - \tan(\pi\mu_n/2)\frac{\Gamma\left(1 + \frac{1}{2}\mu_n\right)}{\Gamma\left(\frac{1}{2} + \frac{1}{2}\mu_n\right)} = -\left(\frac{m}{\hbar^3\omega}\right)^{\frac{1}{2}}\frac{U}{2} \tag{3.26}$$

where $\Gamma(z)$ is the gamma function. We are interested in the energy shifts $\hbar\omega\phi_n$, so we can rewrite the gamma functions in Eq. 3.26 by iteratively using the recursion relation $\Gamma(1 + z) = z\Gamma(z)$ [67]

$$\begin{aligned} \Gamma(m + x) &= (m - 1 + x)\Gamma(m - 1 + x) && (3.27)\\ &= \prod_{j=1}^{m}(j - 1 + x)\Gamma(x) && (3.28) \end{aligned}$$

and

$$\begin{aligned} \Gamma(-m + x) &= \frac{\Gamma(-m + 1 + x)}{(-m + x)} && (3.29)\\ &= \prod_{j=1}^{m}\frac{\Gamma(x)}{(x - j)}. && (3.30) \end{aligned}$$

We can use these recursion relations, along with the identity $\tan(z+\pi) = \tan(z)$, to rewrite Eq. 3.26 in terms of ϕ_n, where n is even:

$$\left(\prod_{j=1}^{n/2} \frac{2j+\phi_n}{2j-1+\phi_n}\right)\left[\frac{\Gamma\left(\frac{1}{2}-\frac{1}{2}\phi_n\right)}{\Gamma\left(-\frac{1}{2}\phi_n\right)} - \tan(\pi\phi_n/2)\frac{\Gamma\left(1+\frac{1}{2}\phi_n\right)}{\Gamma\left(\frac{1}{2}+\frac{1}{2}\phi_n\right)}\right] = -\left(\frac{m}{\hbar^3\omega}\right)^{\frac{1}{2}}\frac{U}{2}. \tag{3.31}$$

The PDHA requires that all even energy shifts are the same, which is equivalent to requiring that the ϕ_n for adjacent even energy levels are equal. Therefore, we can test this approximation by dividing Eq. 3.31 with $n = p+2$ by the same equation with $n = p$ and, assuming that the shifts are the same, $\phi_{p+2} = \phi_p$, which gives us

$$\frac{p+1+\phi_p}{p+\phi_p} = 1. \tag{3.32}$$

Evidently, the PDHA is never exact for the contact interaction in Eq. 3.23. However, the approximation is valid in the limit $p \gg 1$.

The substitution $\phi_n \to \phi$ made in Eq. 3.14 is weighted by the spectral weights a_n of the initial wave function. Therefore, when $\phi_n = \phi + \Delta\phi_n \neq \phi$, this deviation from the PDHA only affects the form of the final state when this energy level has substantial weight. This allows us to relax the PDHA to only require that the energy shifts are equal over the range of eigenstates where $a_n \not\approx 0$. If the spectrum only obeys the approximation for a given limit, maximally entangled states can still be generated as long as the spectral weight of the initial wave function is predominantly in this part of the spectrum.

For the δ-function interaction, the PDHA is obeyed for large n so we want an initial state which has the majority of its spectral weight in this limit. The ideal candidate is the coherent state of the harmonic oscillator [68, 69]:

$$\psi(x,t) = N\exp\left[-\frac{(x-x_t)^2}{2\sigma^2} + \frac{ip_t}{\hbar} - i\gamma_t\right] \tag{3.33}$$

where

$$x_t = x_0 \cos \omega t, \tag{3.34}$$

$$p_t = -m\omega x_0 \sin \omega t, \tag{3.35}$$

$$\gamma_t = \frac{m\omega x_0^2 \sin 2\omega t}{2} + \frac{\hbar \omega t}{2}, \tag{3.36}$$

$$\sigma = \sqrt{\frac{\hbar}{m\omega}} \tag{3.37}$$

and N is a normalisation constant. Coherent states were originally proposed by Schrödinger as the quantum states which behave similarly to their classical counterparts. In real space, this state is created by displacing the ground state of the harmonic oscillator from the origin by x_0. The state retains its shape but oscillates with frequency ω. The coherent state can also be expressed as a Poissonian distribution of the quanta in the oscillator

$$|\psi(x,t)\rangle = e^{-\frac{|\alpha|^2}{2}} \sum_{n=0}^{\infty} \frac{\left(\alpha(t)a^\dagger\right)^n}{n!} |0\rangle \tag{3.38}$$

where $\alpha(t) = e^{i\omega t}\alpha(0)$ is the mean number of quanta and is related to Eq. 3.33 by $\alpha(0) = \left(\sqrt{m\omega/2\hbar}\right) x_0$. By the central limit theorem, as α becomes large, Eq. 3.38 approaches a Gaussian with mean and variance $|\alpha|$ so the spectral weight becomes concentrated at large n. This limit provides us with a wave function which satisfies the PDHA. In the real space representation, it is equivalent to giving the wave packets a large initial displacement.

From this analysis, we have obtained a limit for which the PDHA is exact. If the initial particles have a large displacement and the interaction potential is infinitesimally narrow, maximally entangled states are generated exactly. These requirements are, in general, equivalent as most interactions have a natural length scale. If the particles are in coherent states, as they are displaced further from the origin we can rescale the coordinates so that the interaction is narrower. The corollary is that if the potential is already extremely narrow, the necessary initial displacement need not be as large.

3.3.2 Robustness of Results to Deviations from the PDHA

The conclusions in Sec. 3.3.1 demonstrated a limit in which the PDHA is exact. However, this limit can never strictly be satisfied for physical systems so it is useful to analyse how deviations from this limit influence how far the final state is from the result given in Eq. 3.18. We will assume that the odd states do satisfy the PDHA as the interaction potentials of interest are always localised around $r = 0$. However, the assumption that the energy shifts of the even levels is constant was not justified outside the limit given in Sec. 3.3.1 so we will loosen this requirement and see how this affects the resultant wave function.

For $\phi_n \neq \phi$, the even terms retain their exponential factors so Eq. 3.16 becomes

$$\begin{aligned}\psi(r, t = \nu\pi/\omega) \quad = \quad & -e^{-i\pi(\phi+1)\nu/2}\Bigg[\cos(\nu\pi\phi/2)\left(\sum_{n\ \text{even}} a_n\varphi_n e^{-i\pi\Delta\phi_n} \mp \sum_{n\ \text{odd}} a_n\varphi_n\right) \\ & -i\sin(\nu\pi\phi/2)\left(\sum_{n\ \text{even}} a_n\varphi_n e^{-i\pi\Delta\phi_n} \pm \sum_{n\ \text{odd}} a_n\varphi_n\right)\Bigg] \quad (3.39)\end{aligned}$$

where $\Delta\phi_n = \phi_n - \phi$ is the deviation from the spectrally weighted average of $\phi = \sum_n |a_n|^2 \phi_n$. Taking the difference between Eq. 3.16 and Eq. 3.39 gives us

$$\Delta\psi = \sum_{n\ \text{even}} a_n \left(1 - e^{-i\pi\Delta\phi_n}\right)\varphi_n. \quad (3.40)$$

For the wave function to remain in the original basis, we require that $\Delta\psi = 0$. As the eigenstates φ_n are linearly independent, Eq. 3.39 only equates to the maximally entangled states $|\Psi^{\pm i}\rangle$ when the PDHA is exact.

However, the relevant measure of how far we are from a desired state is the fidelity $\mathcal{F} = |\langle\alpha|\psi\rangle|$ where $|\alpha\rangle = |\Psi^{\pm i}\rangle$ is the state we want to generate. Taking the overlap between the states in Eq. 3.16 and Eq. 3.39, we get

$$\mathcal{F} = \left|1 - \sum_{n\ \text{even}} |a_n|^2 \left(1 - e^{-i\pi\Delta\phi_n}\right)\right|. \quad (3.41)$$

We can rewrite this in terms of an error defined by $\mathcal{F} = |1 - \epsilon|$ which means that

the loss of fidelity due to deviations from the PDHA is given by

$$\epsilon = \sum_{n \text{ even}} |a_n|^2 \left(1 - e^{-i\pi\Delta\phi_n}\right). \tag{3.42}$$

Assuming that the $\Delta\phi_n$ are indeed small, we can expand the exponential which, to $\mathcal{O}(\Delta\phi_n^2)$, gives us an error measure

$$\epsilon \approx i\pi \sum_{n \text{ even}} |a_n|^2 \Delta\phi_n. \tag{3.43}$$

Eq. 3.43 shows that if the $\Delta\phi_n$ are small when the spectral weight $a_n \not\approx 0$, then the error is small[1]. In Sec. 3.4, we provide numerical solutions for a variety of interactions $V(r)$ which justify this analysis and show that the fidelity to the maximally entangled states is indeed high.

We have shown in Eq. 3.18 that after an integer number of half-periods of the oscillator, we obtain a parity-swapped superposition of the original state. The spatial wave function of the reflected part of the superposition is the same as for the transmitted part due to our first simplifying assumption that the single particle wave functions were parity inversions of each other, i.e. $\psi_L(r) = \psi_R(-r)$. However, initialisation errors might lead to deviations in the shape or displacement of $\psi_L(r)$ and $\psi_R(r)$. This would result in a final state where the values of the qubit could be inferred by measuring their position.

We can ignore these initialisation errors by coarse graining the system such that we only have knowledge of which side of the harmonic oscillator the wave function is on. To apply this coarse graining to Eq. 3.18, we map the states

$$\{c_{\varsigma_1}^\dagger(x_1)c_{\varsigma_2}^\dagger(x_2)\,|0\rangle\} \to |L_{\varsigma_1}R_{\varsigma_2}\rangle\,, \qquad x_1 < 0, x_2 > 0, \tag{3.44}$$

$$\{c_{\varsigma_1}^\dagger(x_1)c_{\varsigma_2}^\dagger(x_2)\,|0\rangle\} \to |R_{\varsigma_1}L_{\varsigma_2}\rangle\,, \qquad x_1 > 0, x_2 < 0. \tag{3.45}$$

We can assume that the wave functions will remain localised on either side of the

[1]It is reasonable to object that ϵ is imaginary and, as we have defined $\mathcal{F} = |1 - \epsilon|$, the fidelity is greater than one. However, this is a consequence of the Taylor expansion of the exponential as $\left|e^{-ix}\right| \approx |1 - ix|$ even though $\left|e^{-ix}\right| = 1$. The reason we choose to approximate the error as Eq. 3.43 is that it provides a first-order measure of the distance between $|\alpha\rangle$ and $|\psi\rangle$.

well so we can pull the qubits apart at half-integer periods to obtain maximally entangled states. As the centre of mass is invariant at these times, we can ignore the possibility that $x_1, x_2 < 0$ or $x_1, x_2 > 0$. Therefore, the coarse grained states are maximally entangled so this scheme is robust against initialisation errors.

3.4 Numerical Simulations for Various Interaction Potentials

In the previous sections, we have shown that, with appropriate constraints on the initial wave function and applying the parity-dependent harmonic approximation to the spectrum of the Hamiltonian in Eq. 3.7, we can generate maximally entangled states with arbitrarily high fidelity. Furthermore, in Sec. 3.3.2, we showed that the fidelity to the maximally entangled states should remain high even under deviations in the approximations made. However, the results so far have been formulated based on idealised interaction potentials and initial wave functions.

In this section, we will present numerical solutions to the time-dependent Schrödinger equation using the propagation methods described in Ch. 2 and show that the proposed method does indeed produce high fidelity, maximally entangled states. The simulations propagate an initial product of coherent states, with the single particle states in Eq. 3.1 given by:

$$\psi_{L/R}(x) = N \exp\left[-\frac{(x \pm x_0)^2}{2\sigma^2}\right] \tag{3.46}$$

where $\sigma = \sqrt{\hbar/m\omega}$ and $x_0 = 2.5\ \sigma$. The requirement that the single particle wave functions are localised on one side of the well can be verified numerically. For this value of x_0, $\int_0^\infty \psi_L(x)\,\mathrm{d}x = 0.0073$ which is sufficiently vanishing for our purposes. The simulations were performed using natural units $\hbar = \omega = m = 1$.

3.4.1 Contact Interaction

The first interaction we will consider is the contact interaction

$$V_{\mathrm{Cont}}(x_1 - x_2) = U\delta(x_1 - x_2). \tag{3.47}$$

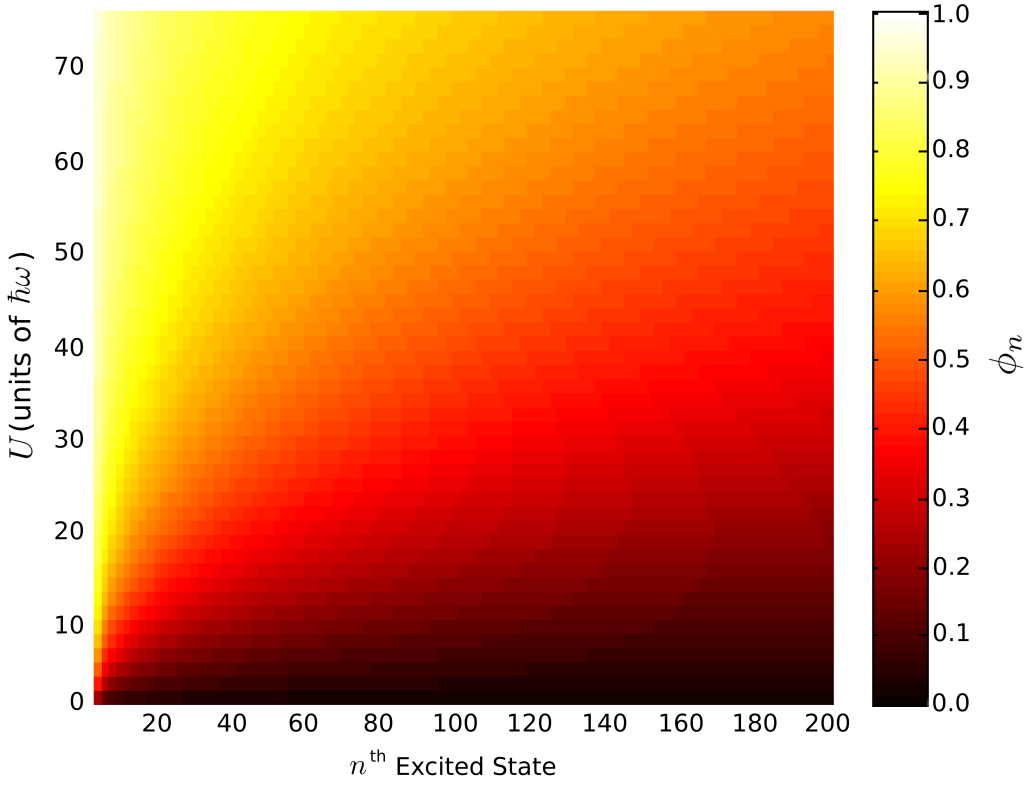

Figure 3.2: Energy shift parameter of the even states of the harmonic oscillator ϕ_n due to a perturbing contact interaction, $V(r) = U\delta(r)$. Contours of constant ϕ_n tend asymptotically towards the horizontal for large n as demonstrated in Sec. 3.3.1.

As we showed in Sec. 3.3.1, in the limit that $x_0 \to \infty$, the spectrum of Eq. 3.23 exactly satisfies the PDHA and therefore creates maximally entangled states with 100% fidelity. However, when x_0 is finite, the spectrum of the Hamiltonian Eq. 3.7 can be calculated exactly by finding solutions to the transcendental equation, Eq. 3.31. Fig. 3.2 shows ϕ_n for the even excited states of Eq. 3.8. As we can see, contours of constant ϕ_n are not horizontal although they become asymptotically so as n gets larger. Fig. 3.2 shows that we expect deviations from the PDHA of $\Delta\phi_n \sim \mathcal{O}(10^{-1})$.

First, let us investigate the dynamics of the system when the qubits are initialised with $\varsigma_1 = 1$ and $\varsigma_2 = 0$ — that is, using the qubit identification discussed at the end of Sec. 3.3, in the $|01\rangle$ state. Figs 3.3 and 3.4 show snapshots of the probability density of the two-particle wave function at $t = 0, \pi/2\omega, \pi/\omega$ for $U = 0$ and $U = 2000\,\hbar\omega$ respectively. In the limit of no interaction, the coherent states pass through each other so $|01\rangle \to |10\rangle$. $U = 2000\,\hbar\omega$ represents the limit where the interaction strength is very large. The particles reflect entirely off each other when they reach the centre of the harmonic oscillator so $|01\rangle \to |01\rangle$. Fig. 3.5 shows the intermediate case where $U = 207\,\hbar\omega$ for $t = 0, 2\pi/5\omega, 3\pi/5\omega, \pi/\omega$. We see a combination of scattering and transmission events at the centre of the well. In the qubit basis, we have $|01\rangle \to (|01\rangle + e^{i\vartheta}\,|10\rangle)/\sqrt{2}$ but we cannot infer the value of ϑ from Fig. 3.5. However, from the PDHA, we expect that $\vartheta = -\pi/2$ such that the final state is $|\Psi^{-i}\rangle$ and we can test this prediction using the fidelity.

Having verified that the dynamics of the wave function is as expected, we will now investigate how accurately we generate maximally entangled states. Fig. 3.6 shows the fidelity to the state

$$\left|\Psi^{-i}\right\rangle = \frac{N^2}{\sqrt{2}} \int\int \Psi^{-i}(x_1, x_2) c^\dagger_{\varsigma_1}(x_1) c^\dagger_{\varsigma_2}(x_2)\,|0\rangle\;\mathrm{d}x_1\,\mathrm{d}x_2, \tag{3.48}$$

$$\Psi^{-i}(x_1, x_2) = \exp\left(-\frac{(x_1+x_0)^2 + (x_2-x_0)^2}{2\sigma^2}\right) - i\exp\left(-\frac{(x_1-x_0)^2 + (x_2+x_0)^2}{2\sigma^2}\right) \tag{3.49}$$

as a function of time t and interaction strength U. $|\Psi^{-i}\rangle$ is a constant state so when the particles are in the centre of the well, there is no overlap and the fidelity

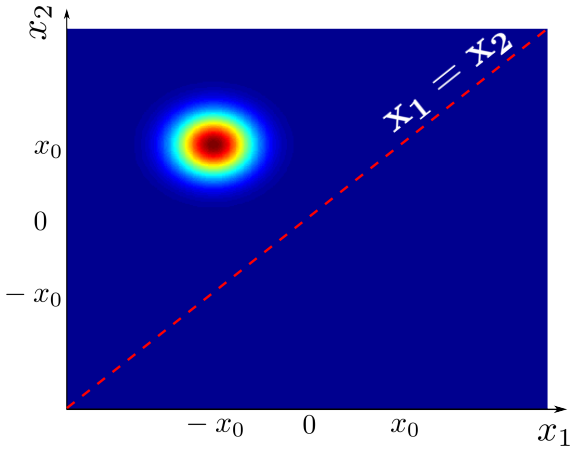

(a) $t = 0$

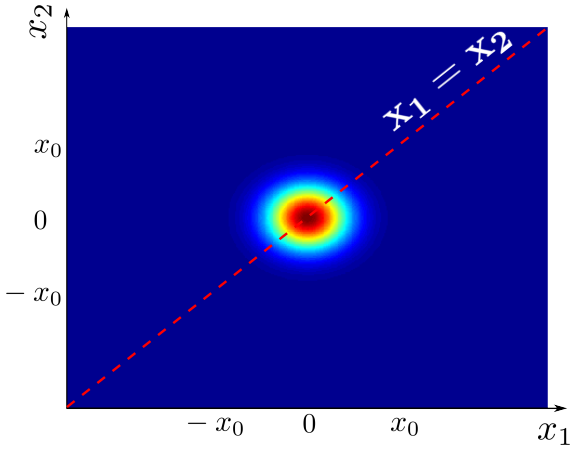

(b) $t = \pi/2\omega$

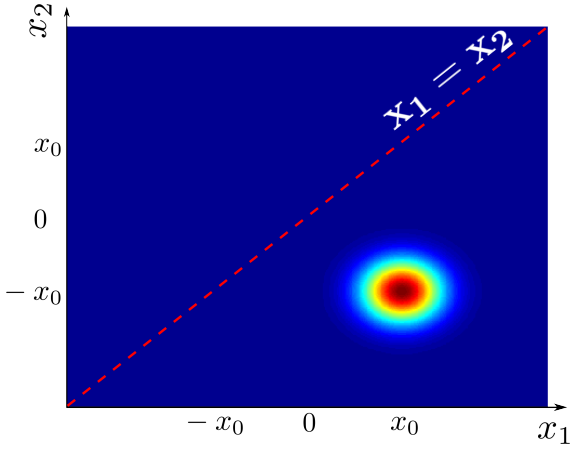

(c) $t = \pi/\omega$

Figure 3.3: Probability density for $U = 0$. The particles pass through each other as there is no interaction. In the qubit basis, $|01\rangle \rightarrow |10\rangle$.

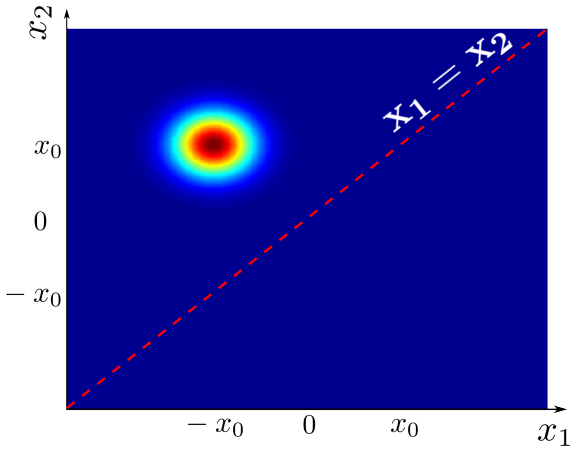

(a) $t = 0$

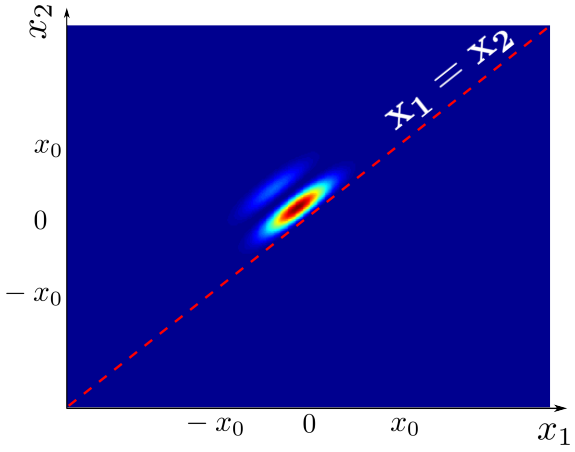

(b) $t = \pi/2\omega$

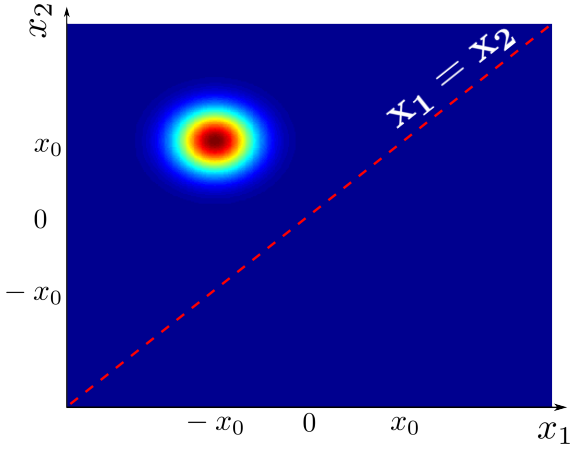

(c) $t = \pi/\omega$

Figure 3.4: Probability density for $U = 2000\,\hbar\omega$ which represents the limit of infinite interaction strength. The particles completely scatter off each other at the centre of the well. In the qubit basis, $|01\rangle \rightarrow |01\rangle$.

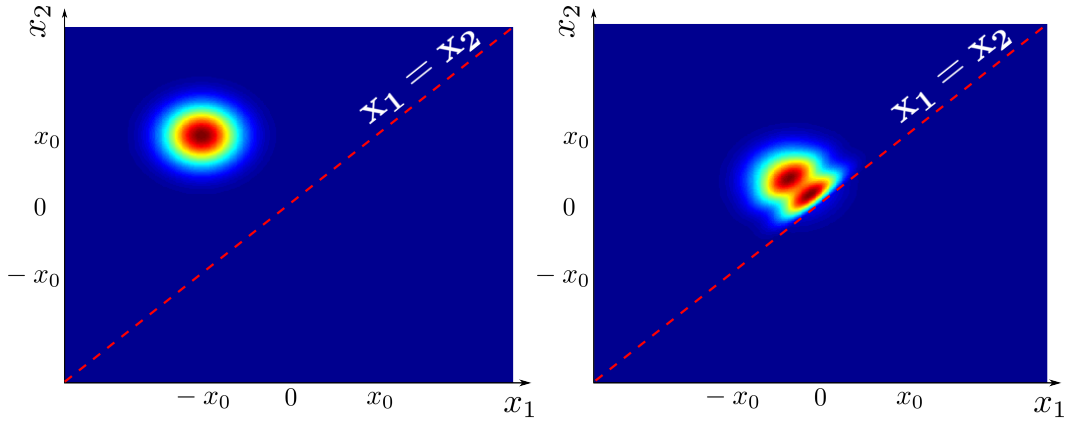

(a) $t = 0$ (b) $t = 2\pi/5\omega$

(c) $t = 3\pi/5\omega$ (d) $t = \pi/\omega$

Figure 3.5: Probability density for $U = 207\,\hbar\omega$ which is the intermediate interaction strength. At the centre of the well, the particles form a superposition of scattered and transmitted states. In the qubit basis, $|01\rangle \to (|01\rangle + e^{i\vartheta}\,|10\rangle)/\sqrt{2}$.

vanishes. At half-integer periods of the oscillator, the overlap of the particles with the initial state wave function $\Psi(x_1, x_2)$ and its parity swapped partner $\Psi(x_2, x_1)$ increases and the fidelity to $|\Psi^{-i}\rangle$ reaches a maximum. For $U = 0$, the fidelity peaks at $\mathcal{F} = 1/\sqrt{2}$, as the wave function only overlaps completely with the first term in Eq. 3.49. Stronger interactions also tend to peak at $\mathcal{F} = 1/\sqrt{2}$ as the wave funcition overlaps with the second term in Eq. 3.49 although this limit is not shown in Fig. 3.6. The periodic behaviour of the fidelity starts to "blur out" at large U after many oscillations as the PDHA becomes less accurate for larger U. Lines of constant ϕ_n are not as horizontal for large U which was the requirement of the PDHA and therefore the wave function scatters out of the coherent states which make up the entangled wave function in Eq. 3.49.

For small U or ν, the wave function has not yet scattered out of the original basis. Well defined lines at half-integer periods show the fidelity oscillating between zero and unity. These lines give the overlap between the general entangled state, Eq. 3.18, and the maximally entangled state, Eq. 3.49. The fidelity depends on the θ given in Eq. 3.20 which is a linear function of ϕ. The PDHA predicts that the energy levels are shifted by the interaction potential so $\phi = \phi(U)$. As the fidelity to $|\Psi^{-i}\rangle$ oscillates sinusoidally as a function of ϕ, $\mathcal{F}$ should be approximately a sinusoidal function of U. Therefore, the "dark spots" in Fig. 3.6 are in fact maximally entangled states with a high fidelity to the orthogonal state $|\Psi^{+i}\rangle$.

From Fig. 3.6, the absolute value of the fidelity is not very clear. Figs. 3.7 and 3.9 show the fidelity to $|\Psi^{-i}\rangle$ after a single half-oscillation $t = \pi/\omega$. We see that for small and large interaction strengths, the fidelity tends asymptotically to $\mathcal{F} = 1/\sqrt{2}$ as the particles either completely scatter off or transmit through each other. For intermediate values of the interaction strength U we create high fidelity, maximally entangled states with $\mathcal{F} > 0.98$. U has been plotted on a logarithmic scale and the fidelity varies smoothly at its maximum. Therefore, the fidelity at this point will be relatively insensitive to variations in U which demonstrates that the generation of maximally entangled states is robust against fluctuations in the interaction potential.

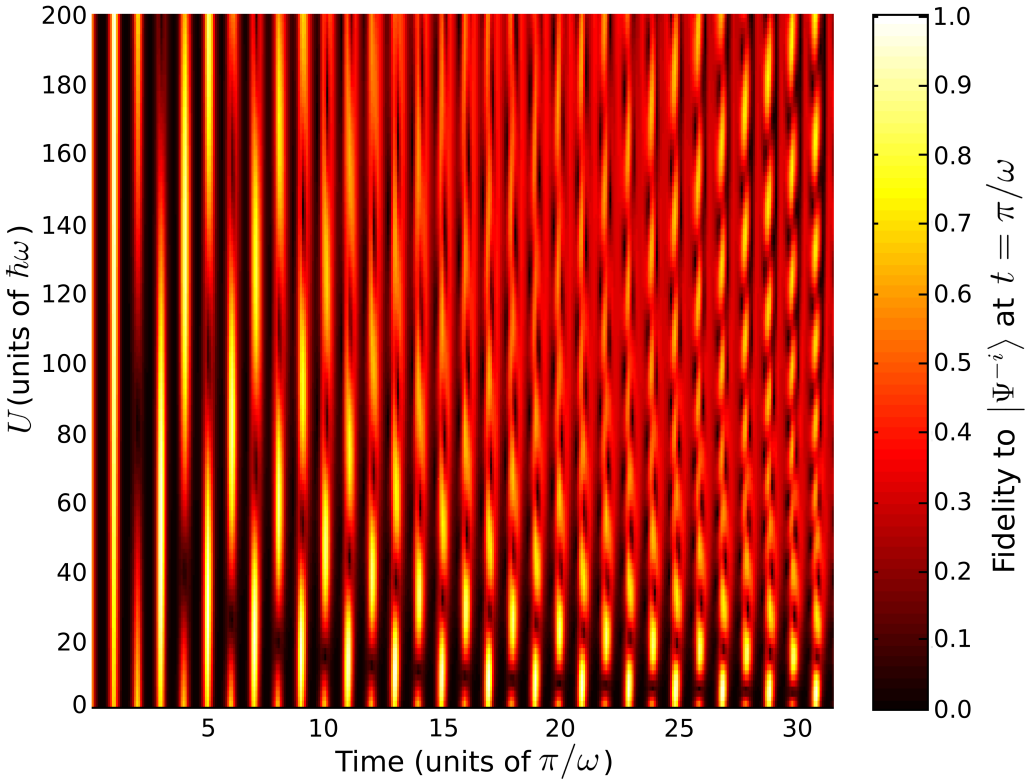

Figure 3.6: Fidelity to the maximally entangled state $\left|\Psi^{-i}\right\rangle$ for a contact interaction $V_{\text{int}} = U\delta(r)$ as a function of time and interaction strength. For half-integer periods, the fidelity is maximal as the wave function's spatial form is the same as at $t = 0$. This property is due to the contact interaction being well approximated by the PDHA. For large U, this approximation is not as good so the strong periodicity of the fidelity decreases at large t. The "dark spots" at half-integer periods for certain values of U also demonstrate a high degree of entanglement but to the orthogonal state $\left|\Psi^{+i}\right\rangle$.

3.4.2 Gaussian Interaction

The contact interaction is not a very realistic interaction due to its divergence at $r = 0$ although there are some systems, such as ultra-cold atomic gases [70], where particles do interact through such a potential. Most interactions have a characteristic length scale γ over which they act. This could have major implications for the PDHA as the shift of the odd energy levels $\hbar\omega\xi_n$ will not necessarily vanish. To study the effects of non-singular interactions, firstly we will look at the Gaussian potential,

$$V_{\text{Gauss}}(r) = \frac{Ue^{-\frac{r^2}{\gamma^2}}}{\sqrt{\pi\gamma^2}} \tag{3.50}$$

where the contact interaction is recovered in the limit $\gamma \to 0$.

Fig. 3.7 shows the fidelity to the maximally entangled state $|\Psi^{-i}\rangle$ after a single half-period of the oscillator as a function of U for different γ. As γ decreases,

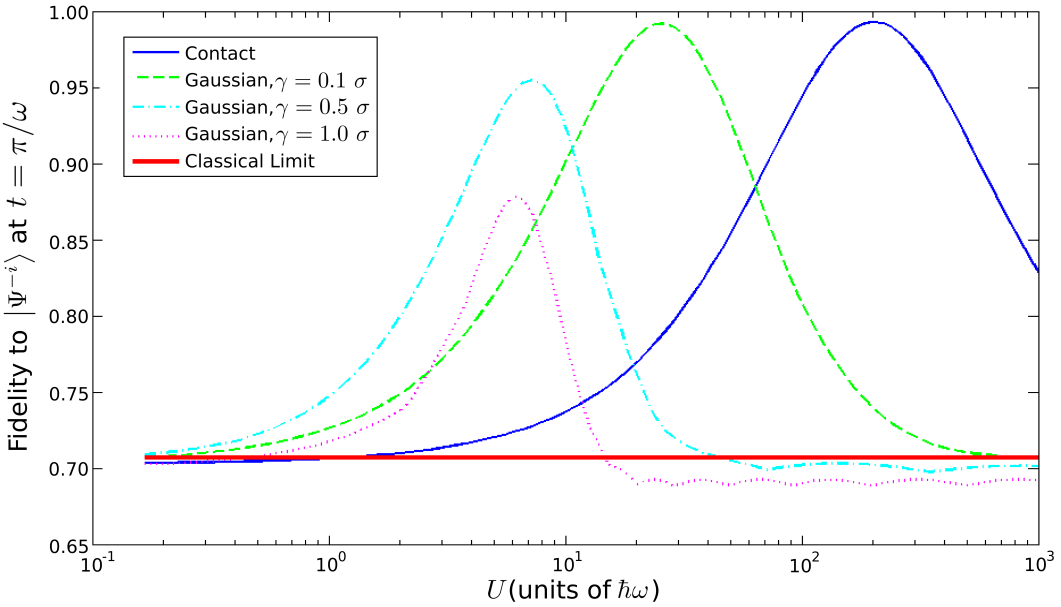

Figure 3.7: Fidelity to the maximally entangled state $|\Psi^{-i}\rangle$ after a single half-oscillation for the Gaussian potentials defined in Eq. 3.50. γ characterises the length scale of the interaction, with a δ-function interaction as the limit that $\gamma \to 0$. The fidelity reaches a maximum at intermediate values of the interaction strength which is smooth and therefore robust against variations in U. The classical limit is equivalent to the initial product state.

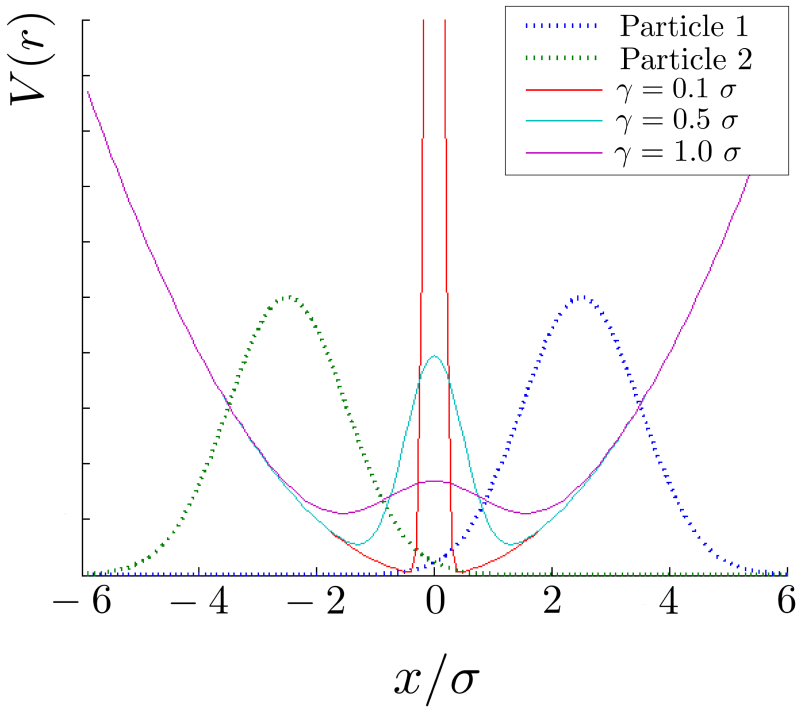

Figure 3.8: The combined interaction and harmonic potentials for the Gaussian interactions from Fig. 3.7 which generate the highest fidelity states. The initial one-particle wave functions ψ_L and ψ_R at $x_0 = 2.5\,\sigma$ are included for reference.

we see that the fidelity to $|\Psi^{-i}\rangle$ increases as we approach the contact interaction limit. The point at which reflection and transmission of the particles is equal, i.e. when we create a maximally entangled state, depends both on the height *and* the width of the interaction. As γ increases, the value of U needed to maximise the fidelity decreases[1]. Also, we see that the maximum fidelity drops as the width of the interaction increases because the PDHA becomes less accurate and the odd energy level shifts $\hbar\omega\xi_n \not\to 0$.

At this point, we emphasise the robustness of the PDHA. Fig. 3.8 shows the total potential, that is $\frac{1}{2}m\omega^2 r^2 + V_{\text{int}}(r)$ from Eq. 3.8, for the value of U which generates the highest fidelity state along with the initial single particle

[1]This is similar to the simple, one-dimensional scattering problem for a plane wave incident on a rectangular barrier which has a potential greater than the energy of the incoming wave [71]. To first order in the width of the barrier, the transmission and reflection coefficients of the wave are functions of the area under the barrier.

wave fuctions. We see that for $\gamma = 0.5\ \sigma$, the interaction looks considerably different from a δ-function, even though we still create states with $\mathcal{F} > 0.95$ to the maximally entangled state $|\Psi^{-i}\rangle$. Additionally, the results presented here are the fidelities to the exact state $|\Psi^{-i}\rangle$. This is a strong constraint as the fidelity measures how similar the wave function is to the target state. For the coarse-grained version of the proposal outlined in Sec. 3.3.2, the expected fidelities would be higher than in Fig. 3.7.

3.4.3 Softened-Coulomb Interaction

The Gaussian interaction is arguably even less realistic than the contact potential so in this section we will focus on probably the most ubiquitous spatial interaction: the Coulomb interaction. The Coulomb interaction diverges at $r = 0$ so we introduce a softening parameter γ in order to make the simulations numerically tractable. The softened Coulomb interaction, sometimes known as the Ohno interaction [72–74], is given by

$$V_{\text{Coul}}(r) = \frac{1}{4\pi\epsilon}\frac{q^2}{\sqrt{r^2+\gamma^2}} \tag{3.51}$$

where q is the charge on the particles and ϵ is the dielectric constant of the medium. The softening parameter can be interpreted geometrically as the perpendicular distance between the two one-dimensional systems. We do not expect our physical systems to be perfectly one dimensional – instead, we imagine constraining the particles using some perpendicular, confining potential. However, this confinement will never be perfect and when the particles encounter a divergent potential, such as the Coulomb interaction, the particles will "slide past" each other by displacing themselves by a small amount in the perpendicular direction. Therefore, there is a good physical basis for using this form of the Coulomb potential. Whilst the γ variable in V_{Gauss} and V_{Coul} is not the same, they both provide a characteristic length scale for the interactions.

The interaction strength of the Coulomb interaction can be effectively changed by varying the frequency of the harmonic oscillator. If we change $\omega \to \alpha^2\omega$ and make the transformation $x \to \alpha x$, the kinetic and harmonic parts of Eq. 3.8

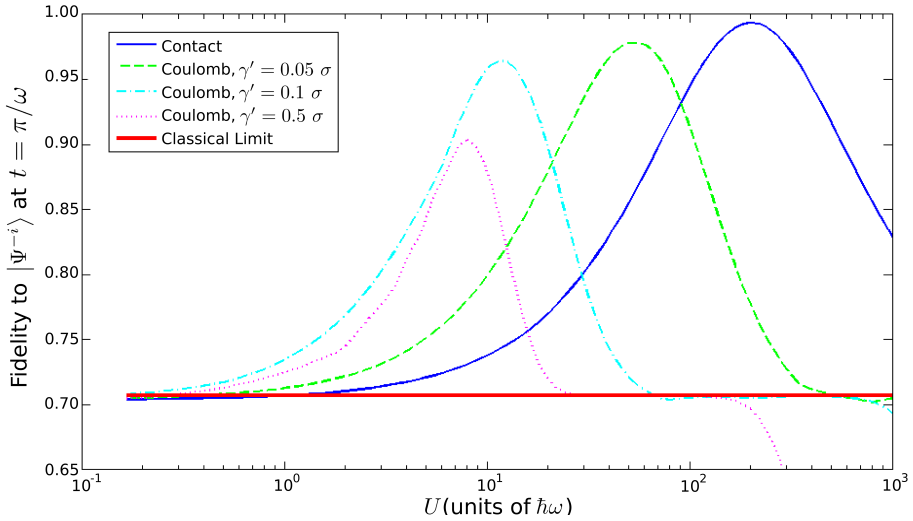

Figure 3.9: Fidelity to the maximally entangled state $\left|\Psi^{-i}\right\rangle$, after a single half-oscillation for the softened Coulomb interaction defined in Eq. 3.52. As with the Gaussian interaction, the fidelity reaches a maximum at intermediate values of the interaction strength which is smooth and therefore robust against variations in U. However, the initial displacement of the particles is fixed at $x_0 = 2.5\,\sigma$ and σ is a function of α, and therefore of the interaction strength U. This varies the width and displacement of the initial state.

remain unchanged whilst the interaction potential transforms as

$$V_{\text{Coul}}(r) \to \frac{1}{4\pi\epsilon\alpha} \frac{q^2}{\sqrt{r^2+\gamma'^2}} \tag{3.52}$$

where $\gamma = \alpha\gamma'$. Using this rescaled version of the potential, we can alter the potential height by defining $U = q^2/4\pi\epsilon\alpha$. In the limit that $\gamma' \to 0$, $V_{\text{Coul}}(r)$ tends towards the contact interaction.

For the numerical simulations, we varied U for a range of γ' values. Note that we have kept $x_0 = 2.5\ \sigma$ whilst varying the width of the harmonic oscillator. Therefore, in the original coordinates x_1, x_2 varying U changes the initial width and position of the single particle wave functions. The fidelities to $|\Psi^{-i}\rangle$ are shown in Fig. 3.9. We see that as we increase γ', the interaction becomes broader and the maximum fidelity drops. However, fidelities of $\mathcal{F} > 0.95$ are still possible for a wide range of parameters. For larger U, the fidelity decreases below $\mathcal{F} = 1/\sqrt{2}$ as the Coulomb interaction between the particles is so strong that it overpowers the confinement potential of the harmonic oscillator. The particles are initially repulsed which prevents the states from returning to the original basis at $t = \pi/\omega$. Therefore, for these large values of U, there is no overlap between the final state and the maximally entangled state $|\Psi^{-i}\rangle$.

3.4.4 General Interaction Potentials

Whilst we have studied some of the most relevant interactions for our proposal, it is useful to have a tool with which to determine whether a general system may obey the PDHA. The Hellman-Feynman theorem [75] allows us to describe how the spectrum of a Hamiltonian varies under a continuously deformed perturbation. If we consider Eq. 3.8 slowly "switching on" the interaction potential $V(r)$ by increasing some parameter which controls the strength of the interaction U, the Hellman-Feynman theorem states that the energy levels change as

$$\frac{dE_n}{dU} = \int_{-\infty}^{\infty} |\varphi_n(U)|^2 \frac{\partial V(r;U)}{\partial U}\, \mathrm{d}r \tag{3.53}$$

where $\varphi_n(U)$ are the eigenstates of Eq. 3.8 when $V(r) = V(r;U)$. The PDHA is equivalent to requiring that $dE_n/dU = 0$ for n odd and $dE_n/dU = f(U)$ for n even, where $f(U)$ is some function independent of n. As the eigenstates $\varphi_n(U)$ will be different depending on the form of the interaction $V(r)$, Eq. 3.53 has to be evaluated on a case by case basis. Finally, note that if $V(r)$ diverges at $r = 0$ and has a non-vanishing length scale[1], i.e. $\gamma \neq 0$, then the particles will always reflect off of each other and the proposal is not applicable.

3.5 Possible physical systems

In this section, we will discuss possible physical systems in which the proposal of Sec. 3.2 could be realised. We have shown that this entangling scheme is relatively insensitive to the form of the inter-particle interaction and, as most particles interact, we will not focus on the physical forms of $V_{\text{int}}(x_1 - x_2)$. One of the major difficulties would be generating and controlling the coherent states. In semiconductor systems, coherent states have been demonstrated using surface acoustic waves (SAWs). By generating surface waves on a GaAs semiconductor heterostructure to drive single electrons in dynamical quantum dots through a bent quantum wire, Katoaka *et al.* [76] were able to demonstrate coherent states with an occupation of 14% in the first excited state. From the number state formulation of the coherent state in Eq. 3.38, one can see that this corresponds to a displacement of $x_0 = 20\text{nm}$ which will be too small for our purposes so we need to consider novel methods for generating coherent states.

A simple method for generating coherent states would be to release an electron from a quantum dot directly into an adjacent harmonic oscillator at a displacement x_0 from the centre of potential. In order to control the system, these structures would need to be defined using electrostatically defined gates. In GaAs, the level spacing of a gate-defined quantum dot is typically of the order of $E_{\text{conf}} \sim 0.1\text{meV}$ [77],which corresponds to a ground state with a width of $\sigma = \sqrt{\hbar^2/m^* E_{\text{conf}}} = 110\text{nm}$, where $m^* = 0.067 m_e$ is the effective mass of the electron. For an electron injected from a quantum dot into a harmonic well to be a coherent state, the width of the ground states of both systems must be the

[1] i.e. It is not a contact interaction, Eq. 3.23

same. This means that the harmonic potential must have an angular frequency of $\omega = E_{\text{conf}}/\hbar = 0.15\text{ps}^{-1}$, which corresponds to a frequency of $f = \omega/2\pi = 24\text{GHz}$. Additionally, for the results in this chapter to apply to semiconductor systems, the band structure must be approximately quadratic as this guarantees that $p^2 \propto \partial_x^2$. For conduction band excitations in GaAs, this is valid if the energy of the particle is less than $E_{\text{band}} \sim 100\text{meV}$ [78]. This limits the initial displacement of the particle to $E_{\text{band}} < \frac{1}{2}m^*\omega^2 x_0^2$ which gives a maximum of $x_0^{(\text{max})} = 4.5\mu\text{m}$ so the requirement that $x_0 \gg \sigma$ can be fulfilled.

Unfortunately, in order to "catch" the electron after the entangling process would require control over the potentials at frequencies of $\mathcal{O}(100\text{GHz})$ which is not possible with current technologies. Additionally, pulsing electrostatic gates at these frequencies generates SAW wave packets which will interfere with other parts of the system [48]. The harmonic potential could be made shallower but this would decrease the confinement of the quantum dot. The electron would have to be cooled further in order to reduce contributions from higher energy eigenstates in the quantum dot's initial state which could strongly affect the dynamics of the system. One method of performing high frequency control on a one-dimensional system is by using surface acoustic waves (SAWs) to draw the electrons through a static gate structure, as described in Sec. 1.3.1. The electrons are confined to a SAW minimum and in their rest frame they experience a dynamical electric potential. The entangling technique of this chapter could be implemented by confining a pair of electrons in a pair of one-dimensional quantum wires. When one wanted to perform the entangling gate operation, the barrier separating the two wires would open up and the particles would oscillate and interact in a single SAW minimum, as shown in Fig. 3.10. By redefining the two wires at a certain point, the electrons will be caught and the qubits will have been entangled. The SAW potential is given by $V_{\text{SAW}} = A\cos(2\pi x/\lambda)$, where $A \sim 10\text{meV}$ is a typical SAW amplitude [79] and $\lambda \sim 1\mu\text{m}$ is a typical wavelength. For an electron in the ground state, V_{SAW} is approximately quadratic with $\frac{1}{2}m^*\omega_{\text{SAW}}^2 = 8A\pi^2/\lambda^2$ which defines the longitudinal width of the electron as $\sigma_{\text{SAW}} = \sqrt{\hbar/m^*\omega_{\text{SAW}}} = 28\text{nm}$. The SAW travels at 2.8nm ps^{-1} so the definition of the two wires will be removed in 10ps. For the system described above, the period of the harmonic oscillator potential is $T = 42\text{ps}$ so this could be sufficient. This transience time would be

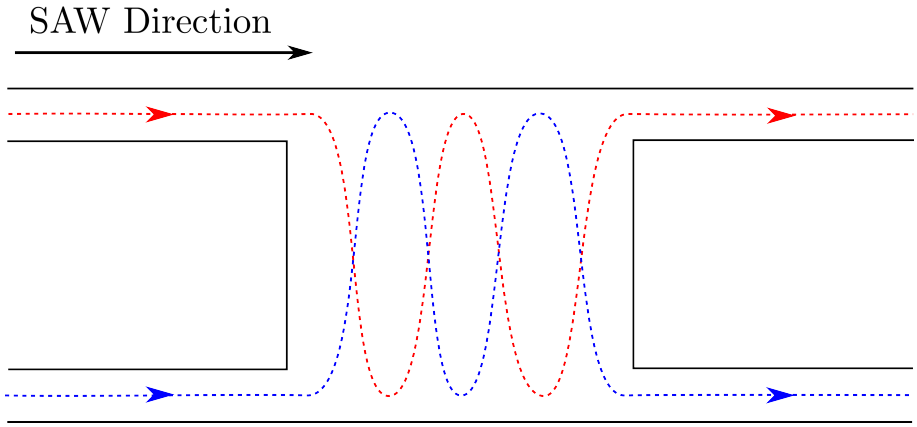

Figure 3.10: An implementation of the entangling operation using electrostatically defined surface gates and SAWs on a doped semiconductor heterostructure. A pair of electrons are confined to a single SAW minimum and two parallel one-dimensional quantum wires. A sudden merging of the wires causes the electrons to oscillate and interact. For this example, we have $n = 4$ interactions and the final qubit state would depend on the strength of the interaction.

reduced if we had stronger longitudinal confinement which could be generated by increasing the amplitude or the frequency of the SAW.

Whilst it is useful to focus on some explicit physical realisations, the entangling method described in this chapter does not depend on any particular physical system. The only requirements are that the system is confined to one-dimension, that the interaction between the particles is local, that the particles can be initialised in coherent states where the initial displacement is significantly longer than the length scale of the oscillator and the particles have an associated two-level system which can be used as a qubit. Harmonic oscillators are ubiquitous to physical systems such as ultra-low temperature atomic gases [80–82], trapped ions [83], superconducting resonators [84], vibrating molecules [85] and optical systems [86]. The robustness of this two-qubit gate to initialisation errors and variations in the system parameters suggests that this technique should be strongly considered when proposing new quantum computational schemes.

3.6 Discussion

Having shown that we can produce high fidelity, maximally entangled states with a method which is robust against variations in the interaction strength, system parameters and the initial state of the wave function, it is worth reflecting on what makes this technique different from the exchange interaction described in Sec. 1.2.3. For the Heisenberg exchange Hamiltonian, Eq. 1.42, the entanglement is generated by an interaction which directly couples the two qubits. This means that any errors in the dynamics, through system control or initial state preparation, directly translates to errors in the output of the entangling two-qubit gate.

In contrast, the method proposed in this chapter has no direct coupling between the qubits. Instead, the qubits are associated with an ancilliary degree of freedom in which the dynamics are realised. Through a simple scattering event, this additional degree of freedom can be entangled easily and with high fidelity. Additionally, the final states can be manipulated so that the scattered and transmitted parts of the spatial wave function are far apart so the two outcomes of the two-qubit gate, namely $|L_{\varsigma_1} R_{\varsigma_2}\rangle$ and $|L_{\varsigma_2} R_{\varsigma_1}\rangle$, are well separated. The entanglement in the ancilliary degrees of freedom is inherited by the qubits which allows us to describe the operation as a two-qubit quantum gate, even though the qubits have not experienced any direct interaction between each other. This form of entanglement process, which we term *inherited entanglement*, has been studied before in quantum wires [87] and interactions between static and dynamic quantum dots [74, 88, 89]. However, these works did not focus on the difference between their methods and direct coupling of the qubits or on why this leads to high fidelity quantum gate operations.

In this chapter, we have presented a method for generating maximally entangled states with arbitrarily high fidelity by associating the qubits with a pair of interacting particles in a one-dimensional harmonic potential. By studying the energy spectrum of the system, we showed that if we assume that the interaction generates a constant parity-dependent shift of the energy levels, then, after a

half-integer number of periods of the oscillator, the spatial wave function is in a parity-swapped superposition of the initial state. If the strength of the interaction is tuned such that the two contributions of this superposition are equal, then the qubits will be maximally entangled. We showed that this approximation is exact in the limit of a contact interaction where the initial displacement of the particles is arbitrarily large. Furthermore, we showed that errors due to deviations from this approximation only resulted in a small reduction of the fidelity. We used numerical simulations to demonstrate this for contact, Gaussian and softened Coulomb interactions. A couple of possible physical realisations of this method in semiconductor heterostructures were discussed. We concluded by discussing how this method differs from direct coupling of the qubits through the exchange interaction.

Chapter 4

Discretising the Spin-Orbit Interaction

4.1 Introduction

In the previous chapter, we focused on how one might implement the two-qubit quantum gate from the DiVincenzo criteria of Sec. 1.2.1. However, a quantum computer also needs to be able to make single-qubit rotations on the Bloch sphere. For semiconductor heterostructures, manipulating the spins of individual electrons can be challenging. External magnetic fields rotate all qubits simultaneously but in order to address single qubits, one needs to create localised magnetic fields. One method for doing this is by fabricating nanomagnets [49] with fields which are only significant for a single qubit. Whilst this fabrication is possible [90, 91], either the qubits must be moved into and out of this local magnetic field or it must be possible to switch the fields on and off which adds an extra layer of complexity to the computational scheme. Additionally, stray magnetic fields could generate unwanted spin rotations on qubits other than the target.

One possible alternative to magnetic fields is the spin-orbit interaction (SOI). The SOI couples the spin of a particle to its orbital angular momentum so the spin qubit can be manipulated by changing the electron's position in a controlled way. Through electrical control, any rotation on the Bloch sphere is possible so this could provide a more robust method for implementing single qubit gates.

In order to investigate new methods of utilising SOI for quantum information processing, we need to understand how it affects the dynamics of our qubits. However, unlike for the magnetic fields in Sec. 2.3.1, there is no generally accepted spatial discretisation of the SOI. Numerical solutions exist for systems with reduced dimensionality [92] and high symmetry [93–95] but they do not exist for particles moving in arbitrary potentials.

In this chapter, we will present a general discretisation for the spin-orbit Hamiltonian. We start by deriving the SOI terms for one and two particle systems. The resulting Hamiltonian takes a similar form to the advection-diffusion equation which has been studied in relation to various fluid dynamical systems [96–98]. We will use a similar substitution to the one developed by Grima and Newman [99] for these systems, which will allow us to discretise the SOI Hamiltonian in a physically reasonable manner. We will show that the resulting model has many similarities to the Peierls substitution of the magnetic field from Sec. 2.3.1. We perform some preliminary simulations of electron dynamics in quantum wires and quantum dots in the presence of the SOI in order to show that this discretisation technique is better than a simple centred finite-differences approach.

4.2 Derivation of the Spin-Orbit Interaction

The SOI can be derived through a low energy expansion of the Dirac equation for a particle of mass m [100]:

$$\hat{E}\Psi = (c\,\vec{\alpha}\cdot\vec{p} + \beta mc^2 + V)\Psi \tag{4.1}$$

where $\vec{\alpha} = (\alpha_x, \alpha_y, \alpha_z)^T$ and β are 4×4 matrices

$$\alpha_i = \begin{pmatrix} 0 & \sigma_i \\ \sigma_i & 0 \end{pmatrix}, \qquad \beta = \begin{pmatrix} \mathbb{1} & 0 \\ 0 & -\mathbb{1} \end{pmatrix} \tag{4.2}$$

$\vec{\sigma} = (\sigma_x, \sigma_y, \sigma_z)^T$ is the vector of Pauli matrices, $\Psi = (\psi, \chi)^T$ is a spinor formed from the two-component spinors ψ and χ, V is some external scalar potential and $\hat{E} = i\hbar\partial_t$ is the energy operator. The spinors are coupled in the Dirac equation

by the off-diagonal elements of the α_i. Solving these coupled equations for one of the spinors ψ gives us the equation of motion

$$(E - mc^2 - V)\psi = c\,\vec{\sigma}\cdot\vec{p}\left(\frac{1}{E + mc^2 - V}\right) c\,\vec{\sigma}\cdot\vec{p}\,\psi. \tag{4.3}$$

The energy in the Dirac equation includes the rest mass of the particle mc^2 so, in order express Eq. 4.1 in Schrödinger equation form, we offset the energy $E \to E' = E - mc^2$. At low energies, $E' - V \sim pc \ll mc^2$, so we can Taylor expand the fraction in Eq. 4.3 to $\mathcal{O}(v^2/c^2)$ where $v \approx p/m$ is the velocity of the particle

$$\frac{1}{E + mc^2 - V} = \frac{1}{2mc^2}\left(1 + \frac{E' - V}{2mc^2}\right)^{-1} \tag{4.4}$$

$$= \frac{1}{2mc^2}\left(1 - \frac{E' - V}{2mc^2} + \mathcal{O}(v^2/c^2)\right). \tag{4.5}$$

Inserting this into Eq. 4.3, we get

$$E'\psi = \left[\frac{(c\,\vec{\sigma}\cdot\vec{p})^2}{2mc^2} + V - (c\,\vec{\sigma}\cdot\vec{p})\left(\frac{1}{2mc^2}\frac{E' - V}{2mc^2}\right)(c\,\vec{\sigma}\cdot\vec{p})\right]\psi \tag{4.6}$$

$$= \left[\frac{(c\,\vec{\sigma}\cdot\vec{p})^2}{2mc^2}\left(1 - \frac{E'}{2mc^2}\right) + V + \frac{1}{(2mc^2)^2}(c\,\vec{\sigma}\cdot\vec{p})V(c\,\vec{\sigma}\cdot\vec{p})\right]\psi. \tag{4.7}$$

The potential V is a function of position so we can use the identities

$$\vec{p}V = -i\hbar\nabla V = -i\hbar[V\nabla + (\nabla V)] = V\vec{p} - i\hbar\nabla V, \tag{4.8}$$

$$(\vec{\sigma}\cdot\vec{A})(\vec{\sigma}\cdot\vec{B}) = \vec{A}\cdot\vec{B} + i\vec{\sigma}\cdot(\vec{A}\times\vec{B}) \tag{4.9}$$

where $\vec{A}$ and $\vec{B}$ are arbitrary operators which commute with the Pauli matrices, to rewrite the last term in Eq. 4.7 as

$$(\vec{\sigma}\cdot\vec{p})V(\vec{\sigma}\cdot\vec{p}) = Vp^2 - i\hbar\nabla V\cdot\vec{p} - \hbar\vec{\sigma}\cdot(\nabla V\times\vec{p}) \tag{4.10}$$

which gives us

$$E'\psi = \left[\frac{p^2}{2m}\left(1 - \frac{E' - V}{2mc^2}\right) + V - \frac{i\hbar}{(2mc)^2}\nabla V \cdot \vec{p} - \frac{\hbar}{(2mc)^2}\vec{\sigma}\cdot(\nabla V \times \vec{p})\right]\psi. \tag{4.11}$$

The final step in the low energy expansion requires us to normalise the wave function Ψ given by

$$\int \Psi^\dagger \Psi \, \mathrm{d}\vec{r} = \int \left(\psi^\dagger\psi + \chi^\dagger\chi\right) \, \mathrm{d}\vec{r} = 1. \tag{4.12}$$

We can substitute in for χ using the low energy form of the Dirac equation, Eq. 4.1, where $E \to mc^2$ and $V \to 0$ so

$$\chi \approx \frac{\vec{\sigma}\cdot\vec{p}}{2mc}\psi \equiv a_\chi \psi. \tag{4.13}$$

This means we can rewrite the Hamiltonian in Eq. 4.11 in terms of the total wave function Ψ using the normalisation $\Psi = \mathcal{N}\psi = \sqrt{1 + a_\chi^2}\psi$ and the identity from Eq. 4.9:

$$\psi = \mathcal{N}^{-1}\Psi = \left(1 + \frac{(\vec{\sigma}\cdot\vec{p})^2}{4m^2c^2}\right)^{-\frac{1}{2}}\Psi \tag{4.14}$$

$$\approx \left(1 - \frac{p^2}{8m^2c^2}\right)\Psi. \tag{4.15}$$

We are expanding the Dirac equation to $\mathcal{O}(v^2/c^2)$, which is the order of the correction in the normalisation, so the only term in Eq. 4.11 at $\mathcal{O}(1)$ which does not commute with $\vec{p}$ is the potential V. The normalisation transforms the potential as

$$\left(1 + \frac{p^2}{8m^2c^2}\right)V\left(1 - \frac{p^2}{8m^2c^2}\right) \approx V + \frac{1}{8m^2c^2}\left(-\hbar^2\nabla^2 V - 2i\hbar(\nabla V \cdot \vec{p})\right) \tag{4.16}$$

which means that the normalised form of the low energy expansion of the Dirac equation is given by

$$E'\Psi = \left[\frac{p^2}{2m}\left(1 - \frac{E' - V}{2mc^2}\right) + V - \frac{\hbar^2}{8m^2c^2}\nabla^2 V \right. \\ \left. - \frac{i\hbar}{2m^2c^2}\nabla V \cdot \vec{p} - \frac{\hbar}{(2mc)^2}\vec{\sigma} \cdot (\nabla V \times \vec{p})\right]\Psi. \quad (4.17)$$

The first term is the kinetic energy which contains an additional relativistic correction, the third term is the Darwin term [101] and the fourth term describes *Zitterbewegung* [102–104]. The final term is the one we are interested in and is the only term which couples the spin and momentum of the particle. It is the spin-orbit interaction and we will define its Hamiltonian as

$$\hat{H}_{\text{SOI}} = \frac{\hbar}{(2mc)^2}\nabla V(\vec{r}) \cdot (\vec{\sigma} \times \vec{p}) \quad (4.18)$$

where we have used the cyclicity of the vector triple product.

Initially, Eq. 4.18 was applied to atomic systems where V is the Coulomb potential of the nucleus [105]. However, for the semiconductor heterostructures described in Sec. 1.3, the SOI can also be an important effect. Firstly, the zincblende structure of the GaAs crystal lattice contains an asymmetry which can generate the so-called Dresselhaus SOI [106]. Additionally, when the dimensionality of the electrons in a semiconductor is constrained, the confinement produces a non-zero ∇V term. The dimensionality of the system is reduced by integrating over the constraining direction and if the confining potential is symmetric then, as Eq. 4.18 is linear in ∇V, the spin-orbit term will integrate to zero and there will be no SOI. However, for asymmetric potentials, the SOI Hamiltonian generates a coupling between the spin and the momentum of the electron, which can cause the spin to precess. This effect, known as the Rashba SOI [107], can be produced through asymmetries in the semiconductor heterostructure or in the electrostatic potentials defined by surface gates. These SOI contibutions can be used to manipulate the spins of the electrons and perform single qubit operations.

4.2.1 The Breit Equation and Spin-Orbit Interaction for Two-Particle Systems

Whilst the SOI can be used to manipulate a single spin, in quantum computers two-qubit interactions are also necessary. A pair of electrons will also interact via Coulomb repulsion and this could produce a two-particle SOI. In order to see the form of this interaction, we need to extend the Dirac equation into its two-particle form. There is no exact relativistic Hamiltonian for two particles but a useful, low energy approximation is the Breit equation [108]

$$\left(E - H_{(1)} - H_{(2)} - \frac{e^2}{r_{12}}\right)\Psi = -\frac{e^2}{2r_{12}}\left(\vec{\alpha}_1 \cdot \vec{\alpha}_2 + \frac{(\vec{\alpha}_1 \cdot \vec{r}_{12})(\vec{\alpha}_2 \cdot \vec{r}_{12})}{r_{12}^2}\right)\Psi \quad (4.19)$$

where $H_{(i)}$ is the Dirac Hamiltonian of Eq. 4.1 for the ith particle, e is the charge on the electron, $\vec{r}_{12}$ is the vector separating the particles, Ψ is the two-particle sixteen-component spinor and $\vec{\alpha}_j$ is the vector of Dirac matrices of Eq. 4.2 for the jth particle spinor. The left-hand side of Eq. 4.19 is the instantaneous form of the Dirac equation for two particles whilst the "Breit operator" on the right-hand side provides an approximation for the effects of quantum electrodynamics [105]. Eq. 4.19 assumes that the particles are moving in a weak external potential, that is $E \ll mc^2, p \ll mc$, which is the same level of approximation used to obtain Eq. 4.17.

Using similar methods as those used in the previous section, the Breit equation can be expanded to give a low energy, two-particle Schrödinger equation with relativistic corrections [105]. This Hamiltonian can be broken into separate parts and the two-particle form of the SOI is identifed as

$$H_{\mathrm{SOI}}^{(2)} = \frac{\hbar}{(2mc)^2}\sum_{\substack{i,j=1,2\\ i\neq j}} \vec{\sigma}_i \cdot \left[-\nabla_i V \times \vec{p}_i + \frac{2e}{r_{ij}^3}(\vec{r}_{ij} \times \vec{p}_j)\right]. \quad (4.20)$$

The first term is the single-particle SOI from Eq. 4.18 whilst the second term represents the SOI generated by the inter-particle Coulomb interaction. The Coulombic SOI depends on the angular momentum of the two particles so if they are constrained to move in one dimension then Eq. 4.20 will reduce to a pair of

single-particle SOI Hamiltonians.

4.3 Discretising the Spin-Orbit Interaction

The single-particle SOI from Eq. 4.18 takes a similar form as the magnetic field Hamiltonian in Eq. 2.21 in that it contains a term which is linear in momentum multiplied by some function of position. We could discretise the momentum term in Eq. 4.18 using a traditional centred finite differences approach:

$$\frac{\partial \Psi}{\partial x} = \frac{\Psi(x + \Delta x) - \Psi(x - \Delta x)}{2\Delta x} + \mathcal{O}(\Delta x^2). \tag{4.21}$$

However, as in Sec. 2.3.1, we would like to develop an improved form for the discretisation in terms of an additional phase factor on the hopping terms. In order to find this form, we will use the substitution of Grima and Newman [99].

In their original paper, Grima and Newman studied the advection-diffusion equation

$$\partial_t \rho = D\nabla^2 \rho - \alpha \nabla(\rho \nabla \phi) \tag{4.22}$$

where D and α are constants and $\phi = \phi(\vec{x}, t)$ is some scalar potential. When D and α are real, Eq. 4.22 describes a variety of classical diffusion problems [96–98]. However, the time-dependent SOI Schrödinger equation takes a similar form to Eq. 4.22 where

$$D = -\frac{i\hbar}{2m}, \tag{4.23}$$

$$\alpha \nabla \phi = -\frac{\hbar}{(2mc)^2}(\vec{\sigma} \times \nabla V) \tag{4.24}$$

and the scalar potential is given by the electrostatic potential $V(\vec{x}, t)$. To recover the Schrödinger equation, we must also subtract $\nabla^2 \phi$ from Eq. 4.22. Grima and Newman presented a substitution which provides a more accurate and physically appealing discretisation of Eq. 4.22. The omission of the $\nabla^2 \phi$ term in the Schrödinger equation means that we must slightly alter the substitution but our method still uses an exponential substitution to recast the SOI in terms of second order derivatives. In Sec. 4.3.2, we will show that when we discretise the expo-

nential terms of this substitution, the resulting Hamiltonian is similar in form to the Peierls substitution for magnetic fields. We will see in Sec. 4.4 that the substitution we present in this section provides higher fidelity numerical solutions than using the centred differences method of Eq. 4.21 for discretising the linear momentum term.

For a single dimension, the modified substitution is given by

$$\begin{aligned}
\partial_x^2\psi + 2(\partial_x\phi)(\partial_x\psi) &= \partial_x^2\psi + 2(\partial_x\phi)(\partial_x\psi) \\
&\quad +(\partial_x\phi)^2\psi + \psi\partial_x^2\phi - (\partial_x\phi)^2\psi - \psi\partial_x^2\phi \qquad (4.25)\\
&= e^{-\phi}\partial_x[e^{\phi}(\partial_x\psi + \psi\partial_x\phi)] - e^{-\phi}\partial_x(e^{\phi}\partial_x\phi)\psi \qquad (4.26)\\
&= e^{-\phi}\partial_x^2(e^{\phi}\psi) - e^{-\phi}(\partial_x^2 e^{\phi})\psi. \qquad (4.27)
\end{aligned}$$

To apply this to the low energy Dirac Hamiltonian from Eq. 4.17, we must expand out all the momentum terms so that the equation is explicitly expressed in terms of p_x, p_y and p_z. Using $p_i = -i\hbar\partial_i$ and gathering terms containing only one combination of p_i and σ_j, repeated application of Eq. 4.27 can be used to write Eq. 4.17 with no first order derivatives. By expressing the SOI Hamiltonian in this form, we can discretise the second order derivatives using Eq. 2.19. This method can also be applied to the two-particle spin-orbit Hamiltonian of Eq. 4.20.

4.3.1 An Explicit Derivation for One-Dimension

Performing the general three-dimensional expansion of the low-energy Dirac equation using the substitution from Eq. 4.27 is messy, tedious and uninformative. However, in order to understand the consequences of this scheme, it will be useful to see exactly what the form of the discretised Hamiltonian is. For simplicity, we will demonstrate the technique for a free particle in one dimension with SOI which is described by the Hamiltonian

$$\hat{H}\psi = -\frac{\hbar^2}{2m}\frac{\partial^2\psi}{\partial x^2} - \frac{i\hbar^2}{(2mc)^2}\frac{\partial\psi}{\partial x}\left[\nabla V(\vec{r})\cdot(\vec{\sigma}\times\vec{n}_x)\right] \qquad (4.28)$$

where $\vec{n}_x$ is a unit vector in the x direction. The term in square brackets is the SOI term which may come from asymmetries in the potential confining the

particle to one dimension. In order to implement the substitution of Eq. 4.27, we factor out $-\hbar^2/2m$, expand the cross product which gives

$$\hat{H}\psi = -\frac{\hbar^2}{4m}\left[2\frac{\partial^2\psi}{\partial x} + \frac{i}{mc^2}\left(\sigma_y\frac{\partial V(\vec{r})}{\partial z} - \sigma_z\frac{\partial V(\vec{r})}{\partial y}\right)\frac{\partial\psi}{\partial x}\right] \tag{4.29}$$

and identifying two scalar fields

$$\partial_x\phi_1 = \frac{i\sigma_y\partial_z V(\vec{r})}{2mc^2}, \qquad \partial_x\phi_2 = -\frac{i\sigma_z\partial_y V(\vec{r})}{2mc^2} \tag{4.30}$$

The Grima-Newman substitution of Eq. 4.27 can then be made for ϕ_1 and ϕ_2 separately. This ensures that for a single substitution of the form Eq. 4.27 all commutation relations are trivial as each term contains only one of the Pauli matrices σ_i and the identity. For simplicity, let us assume that the asymmetry inducing the SOI is in the z direction so $\partial_x\phi_2 = 0$. We can then discretise this form of the Hamiltonian using the discretisation of the second order derivative from Eq. 2.19

$$\begin{aligned}
\hat{H}\psi &= -\frac{\hbar^2}{2m}\left(e^{-\phi_1}\partial_x^2(e^{\phi_1}\psi) - e^{-\phi_1}(\partial_x^2 e^{\phi_1})\psi\right) && (4.31)\\
&\approx -\frac{\hbar^2}{2m\Delta x^2}\Big(e^{-\phi_1(x)}(e^{\phi_1(x+\Delta x)}\psi(x+\Delta x) - 2e^{\phi_1(x)}\psi(x) + e^{\phi_1(x-\Delta x)}\psi(x-\Delta x))\\
&\qquad -e^{-\phi_1(x)}(e^{\phi_1(x+\Delta x)} - 2e^{\phi_1(x)} + e^{\phi_1(x-\Delta x)})\psi(x)\Big) && (4.32)\\
&= -\frac{\hbar^2}{2m\Delta x^2}(e^{\Delta x\partial_x\phi_1(x)}\psi(x+\Delta x) + e^{-\Delta x\partial_x\phi_1(x)}\psi(x-\Delta x)\\
&\qquad +(e^{\Delta x\partial_x\phi_1(x)} + e^{-\Delta x\partial_x\phi_1(x)})\psi(x)) && (4.33)\\
&= -\frac{\hbar^2}{2m\Delta x^2}\Bigg\{\exp\left[\frac{i\Delta x\sigma_y\partial_z V}{4mc^2}\right](\psi(x+\Delta x) - \psi(x))\\
&\qquad +\exp\left[-\frac{i\Delta x\sigma_y\partial_z V}{4mc^2}\right](\psi(x-\Delta x) - \psi(x))\Bigg\} && (4.34)
\end{aligned}$$

where we have Taylor expanded $\phi_1(x \pm \Delta x)$ in the exponentials of Eq. 4.32. For clarity, we have assumed that $\partial_x^2\phi_1 = 0$, which is true for many SOIs, such as uniform Rashba coupling [109]. However, if necessary it is simple to include these higher order terms in the discretisation above.

The exponentiated Pauli matrices of Eq. 4.34 generate rotations around the s_x, s_y and s_z directions on the Bloch sphere, as described in Sec. 1.1.2. For example,

$$R_y(\theta) = e^{i\theta\sigma_y/2} = \mathbb{1}\cos\theta/2 + i\sigma_y \sin\theta/2 \tag{4.35}$$

$$= \begin{pmatrix} \cos\theta/2 & \sin\theta/2 \\ -\sin\theta/2 & \cos\theta/2 \end{pmatrix} \tag{4.36}$$

and similarly for σ_x and σ_z. If we resolve the wave function in terms of spin-up and spin-down components $\psi = (\psi_\uparrow, \psi_\downarrow)^T$ and rewrite the exponentials as rotation matrices, then we have our final discretised form for the SOI Hamiltonian, Eq. 4.28.

4.3.2 Comparison of the Grima-Newman Substitution with Harper's Equation

At this point, it is useful to compare the result from Eq. 4.34 with the magnetic field Hamiltonian of Hofstadter from Eq. 2.24. Firstly, let us draw some comparisons between the non-discretised Hamiltonians. From the low energy Dirac equation, if we only include the non-relativistic momentum, spin-orbit and potential terms, then the low energy Hamiltonian is given by

$$\hat{H} = -\frac{\hbar^2}{2m}\nabla^2 - \frac{i\hbar^2}{(2mc)^2}(\nabla V \times \vec{\sigma}) \cdot \nabla + V. \tag{4.37}$$

We want to combine the terms which are quadratic and linear in ∇ by "completing the square" so, as an ansatz, let us expand

$$(\nabla + i\beta(\nabla V \times \vec{\sigma}))^2 = \nabla^2 + 2i\beta(\nabla V \times \vec{\sigma})\cdot\nabla + i\beta\nabla\cdot(\nabla V \times \vec{\sigma}) - \beta^2(\nabla V \times \vec{\sigma})^2. \tag{4.38}$$

If we set $\beta = (4mc^2)^{-1}$, then the first two terms give the momentum and spin-orbit contributions for Eq. 4.37 up to a factor of $-\hbar^2/2m$. Using the identity $\nabla \cdot (\vec{A} \times \vec{B}) = \vec{B} \cdot \nabla\vec{A} - \vec{A} \cdot \nabla\vec{B}$, we see that the third term vanishes as the Pauli matrices have no spatial dependence and $\nabla \cdot \nabla V = 0$ for any scalar field V. For the final term, we can use the identity $|\vec{A} \times \vec{B}|^2 = |\vec{A}|^2|\vec{B}|^2 - (\vec{A} \cdot \vec{B})^2$ along with

Eq. 4.9 which gives

$$(\nabla V \times \vec{\sigma})^2 = 3(\nabla V)^2 - (\vec{\sigma} \cdot \nabla V)^2 = 2(\nabla V)^2. \tag{4.39}$$

Therefore, we can rewrite Eq. 4.37 using a transformed momentum operator as

$$\hat{H} = -\frac{\hbar^2}{2m}\left(\nabla + \frac{i}{4mc^2}(\nabla V \times \vec{\sigma})\right)^2 + \left(V + \frac{\hbar^2(\nabla V)^2}{16m^3c^4}\right). \tag{4.40}$$

We see that the SOI induces an additional scalar potential and a transformation of the canonical momentum operator

$$\hat{p} \to \hat{p} - \frac{\hbar}{4mc^2}(\nabla V \times \vec{\sigma}) \tag{4.41}$$

similar to the Peierls substitution of Sec. 2.3.1. By directly comparing the Eqs. 2.21 and 4.40, we can compare the magnetic vector potential and the SOI

$$\frac{q\vec{A}}{\hbar} \sim \frac{(\nabla V \times \vec{\sigma})}{4mc^2}. \tag{4.42}$$

The transformation of the canonical momentum due to a magnetic field only affects the spatial dynamics of the electron. Spin dynamics is generated independent of the particle dynamics due to the Zeeman term $\hat{H}_{\mathrm{Z}} = -\mu_B \vec{\sigma} \cdot \vec{B}$ where $\mu_B = q\hbar/2m$ is the Bohr magneton. The SOI affects the dynamics of both the spin and spatial parts of the wave function.

Having compared the continuous forms of the magnetic and SOI Hamiltonians, we will now consider their discretised form. For the off-diagonal (hopping) terms, the Grima-Newman substitution in Eq. 4.34 and the Peierls substitution in Eq. 2.24 are the same if we apply the identity from Eq. 4.42. For the diagonal terms, Eq. 4.34 contains exponential factors multiplying the on-site wave function which do not occur in the Peierls substitution. However, we can express the two

exponentials as a cosine which we can Taylor expand to give us

$$\frac{\hbar^2}{2m\Delta x^2}\left\{\exp\left[\frac{i\Delta x\sigma_y\partial_z V}{4mc^2}\right]\psi(x)+\exp\left[-\frac{i\Delta x\sigma_y\partial_z V}{4mc^2}\right]\psi(x)\right\}$$

$$= \frac{\hbar^2}{m\Delta x^2}\cos\left[\frac{i\Delta x\sigma_y\partial_z V}{4mc^2}\right]\psi(x) \tag{4.43}$$

$$\approx \left(\frac{\hbar^2}{m\Delta x^2}+\frac{\hbar^2(\partial_z V)^2}{16m^3c^4}\right)\psi(x)+\mathcal{O}(\Delta x^2). \tag{4.44}$$

The first term in Eq. 4.44 is the on-site momentum term which is present in the magnetic field version of the Peierls expansion. The second term is the additional scalar potential for the SOI where $(\nabla V)^2 = (\partial_z V)^2$ as we set $\partial_x\phi_2 \propto \partial_y V = 0$ and the particle is free in the x direction.

These comparisons demonstrate the similarities between the discretisation of the SOI and magnetic field Hamiltonians. For this reason, we will call Eq. 4.34 the *spin-orbit interaction Peierls* (SOIP) substitution. The substitution has been recently studied in relation to the Hofstadter problem [110, 111] but only for Rashba-type interactions and not in the general form presented here. The physical nature of the Peierls substitution for the magnetic field in Eq. 2.24 in terms of a two-dimensional Hubbard model increases the accuracy of this discretisation so we expect that the SOIP substitution will have a similar effect for SOI.

4.4 Simulations

Having developed a new discretisation of the SOI Hamiltonian in Eq. 4.18, we must now test it to see whether it provides higher fidelity solutions than the simpler centred finite differences approach. A useful approach would be to calculate the fidelity of the numerical solutions generated by the two methods with the wave functions of analytically solvable systems. The hard wall wire [112] and the hard wall quantum dot [113] with Rashba SOI have both been solved in the position basis but the initial states must be obtained by solving sets of transcendental equations. For these systems, any errors in the simulations cannot be solely attributed to the propagation method as fidelity could be lost due to inaccurately calculated initial states. In this section, we will simulate two analytically soluable

systems with initial states which have a simple functional form. We will show that the SOIP discretisation derived in Sec. 4.3 provides higher fidelity solutions than the centred differences method.

4.4.1 The Moroz-Barnes Wire

The first system we will consider is the pseudo-one-dimensional wire studied by Moroz and Barnes [109, 114]. The wire is constrained by a parabolic potential in the (transverse) x direction whilst the potential is flat in the (longitudinal) y direction. In their paper, Moroz and Barnes separated the wave function into transverse and longitudinal components. The eigenstates of the system must consist of plane waves along the y direction due to the translational invariance of the wire, multiplied by a transverse function which can be obtained by calculating the eigenstates of the transverse Hamiltonian as a function of the longitudinal wave vector k_y. The influence of both the gradient of the harmonic potential and Rashba SOI coupling were studied but inclusion of the Rashba term needed to be solved numerically so we will ignore this term for these simulations. However, the effect of the harmonic potential gradient provides a transverse displacement of the ground state by

$$\Delta = \frac{\hbar\omega a_x k_y}{4mc^2} \tag{4.45}$$

where $a_x = \sqrt{\hbar/m\omega}$. The direction of this displacement depends on the σ_z eigenstate of the particle's spin. Therefore, the lowest energy band of the Moroz-Barnes system consists of eigenstates with the form

$$\psi = N \exp\left[-\frac{(x \pm \Delta)^2}{2a_x^2}\right] e^{ik_y y} \tag{4.46}$$

where N is a normalisation constant. The propagation techniques we are using in this thesis act on finite spatial domains, so to initialise our state we must confine it in the y direction. Therefore, the initial states for our simulations will have the form

$$\psi = N \exp\left[-\frac{(x \pm \Delta)^2}{2a_x^2}\right] \Phi(y) e^{ik_y y}. \tag{4.47}$$

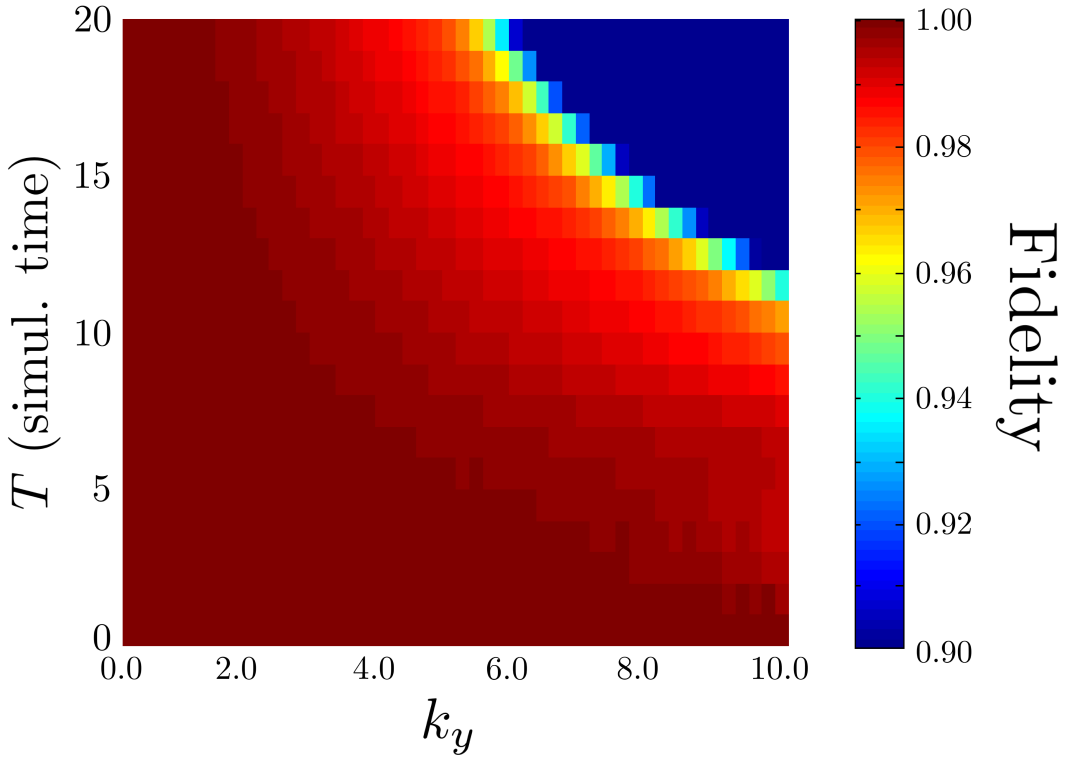

Figure 4.1: Fidelity to a wave packet freely propagating along the longitudinal coordinate of the Moroz-Barnes wire without Rashba SOI using the SOIP substitution for the spatial discretisation. The fidelity remains high ($\mathcal{F} > 0.98$) for a range of wave vectors k_y. For large times and momenta, the wave packet reflects off the simulation's domain boundary and the fidelity rapidly decreases.

However, this is no longer an eigenstate as Heisenberg's uncertainty principle states that the confining function $\Phi(y)$ will broaden the range of k_y in our initial state. We can minimise this spread by using a Gaussian envelope $\Phi(y) = \exp(-y^2/2a_y^2)$ which is a minimal uncertainty state. The Fourier transform of $\Phi(y)$ gives a corresponding spread of wave vectors $\Delta k_y = a_y^{-1}$ so our initial states will behave like eigenfunctions if we only weakly confine the particle in the y direction.

The simulations for the Moroz-Barnes wire were performed in natural units, $\hbar = m = c = 1$, with a propagation time step $\Delta t = 10^{-4}$. We used a wire with transverse frequency $\omega = 1$ with lattice spacing $\Delta x = 0.05$ over a grid of size $N_x = 200$, $N_y = 5000$. The confinement in the y direction was set to $\sigma_y = 20$, which gives a spread in the wave vector of $\Delta k_y = 0.05$. The target

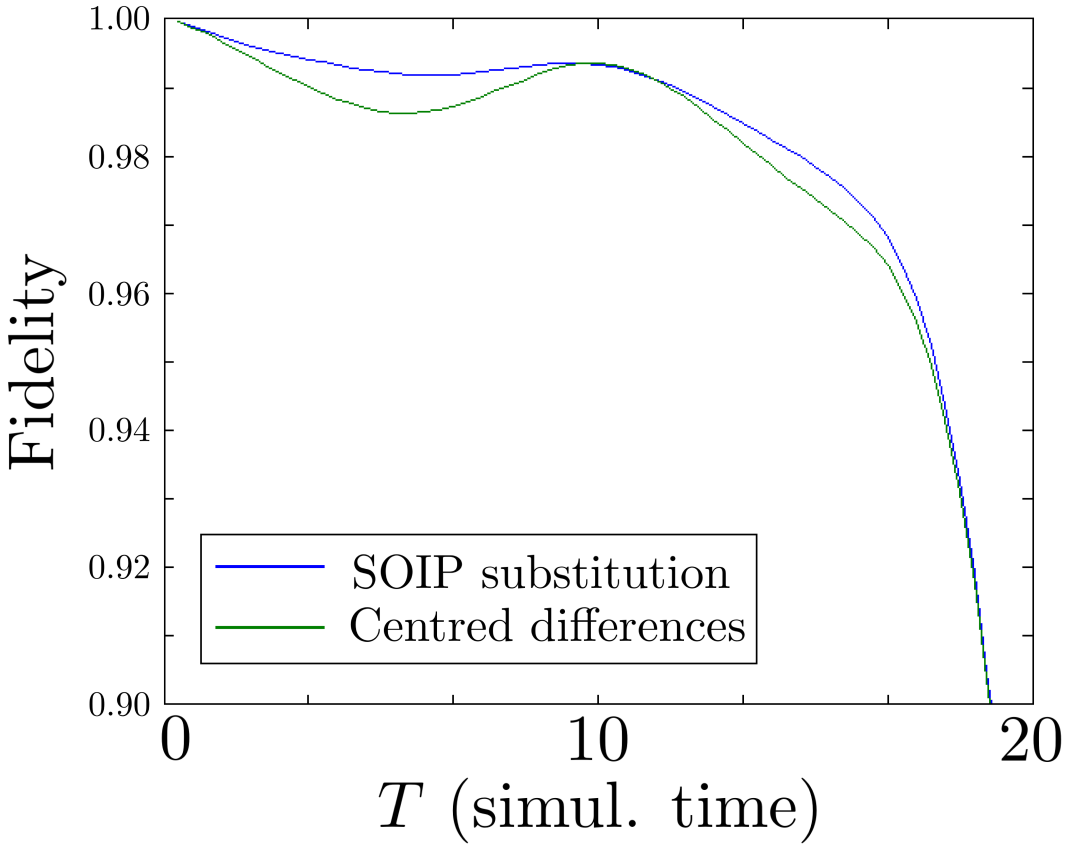

Figure 4.2: A comparison of the fidelity to a freely propagating wave packet for the Moroz-Barnes wire for $k_y = 10.0$. Whilst the SOIP substitution is slightly more accurate, the improvement in fidelity over the centred differences method is not significant for this system.

state which we measure the fidelity with respect to is the initial transverse state multiplied by a freely propagating wave packet with momentum $p_y = \hbar k_y$ in the longitudinal direction. Fig. 4.1 shows this fidelity as a function of time t and wave vector k_y using the SOIP substitution for the spatial discretisation. The fidelity does not decrease substantially below 98% for the majority of the plot. For large t and k_y, the fidelity rapidly drops as the wave packet reflects from the edge of the simulational domain. Unfortunately, for this system, the centred differences approach gives similar fidelity solutions, as seen in Fig. 4.2. The coupling strength for this scheme is proportional to k_y so in order to simulate large SOI, we must have shorter wavelengths. However, as we decrease the wavelength, the plane wave becomes under-sampled and the discretisation will become less accurate. This can be solved by decreasing the lattice spacing but this decreases the difference between the SOIP substitution and the centred differences method. For this reason, it is not possible in this scheme to differentiate between the two methods. However, this is a system specific problem and does not mean that the centred differences method will always be accurate enough.

4.4.2 Ground State of a Harmonic Oscillator with Spin-Orbit Interaction

The Moroz-Barnes wire provides exact analytic solutions with which we can compare our propagated wave functions but we have seen that we cannot extend this to arbitrarily high interaction strengths for a given lattice density as the longitudinal plane waves become undersampled. This can be corrected for by decreasing the lattice spacing but one of the potential advantages of the discretisation proposed in Sec. 4.3 is that it more accurately describes the SOI Hamiltonian in Eq. 4.18 for a sparser grid. Therefore, in order to compare our discretisation with the centred finite-differences approach, we want to be able to change our SOI strength for arbitrary lattice density.

The Rashba SOI provides an ideal system as the Hamiltonian takes the form $\hat{H}_{\mathrm{R}} = -i\alpha\sigma_y\partial_x$ where the coupling strength is parameterised by α. Therefore, the strength of the interaction can be increased without increasing the particle's momentum which requires a denser grid. We will now show that there is a simple,

analytic form which describes the effect of the Rashba SOI on the eigenfunctions of any one-dimensional Hamiltonian. The Hamiltonian for such a general system is given by

$$\hat{H} = -\frac{\hbar^2}{2m}\frac{\partial^2}{\partial x^2} - i\alpha\sigma_y\frac{\partial}{\partial x} + V(x). \tag{4.48}$$

We start by making the ansatz that the wave function can be separated into an overall magnitude ψ and some position-dependent phase θ which mixes the up and down states such that

$$\Psi = \begin{pmatrix} \psi\cos\theta \\ \psi\sin\theta \end{pmatrix}. \tag{4.49}$$

If we insert this into the time-independent Schrödinger equation $\hat{H}\Psi = E\Psi$ with the Hamiltonian from Eq. 4.48, we get two sets of coupled differential equations

$$\begin{aligned} -\frac{\hbar^2}{2m}\left(\cos\theta(\partial_x^2\psi) - 2\sin\theta(\partial_x\theta)(\partial_x\psi) - \cos\theta(\partial_x\theta)^2\psi - \sin\theta(\partial_x^2\theta)\psi\right) \\ +\alpha\left(\sin\theta(\partial_x\psi) + \cos\theta(\partial_x\theta)\psi\right) + \left(V(x) - E\right)\psi\cos\theta = 0, \end{aligned} \tag{4.50}$$

$$\begin{aligned} -\frac{\hbar^2}{2m}\left(\sin\theta(\partial_x^2\psi) + 2\cos\theta(\partial_x\theta)(\partial_x\psi) - \sin\theta(\partial_x\theta)^2\psi + \cos\theta(\partial_x^2\theta)\psi\right) \\ -\alpha\left(\cos\theta(\partial_x\psi) - \sin\theta(\partial_x\theta)\psi\right) + \left(V(x) - E\right)\psi\sin\theta = 0. \end{aligned} \tag{4.51}$$

We would like to remove the θ dependence from Eqs. 4.50 and 4.51 so, examining the $\sin\theta$ coefficients in Eq. 4.50, we get

$$-\frac{\hbar^2}{2m}\left(-2\sin\theta(\partial_x\theta)(\partial_x\psi) - \sin\theta(\partial_x^2\theta)\psi\right) + \alpha\sin\theta(\partial_x\psi) = 0 \tag{4.52}$$

which requires that

$$\theta = -\frac{m\alpha x}{\hbar^2}. \tag{4.53}$$

For Eq. 4.51, we find the same requirement for the $\cos\theta$ terms which shows that this ansatz is consistent. Inputting this value of θ into Eqs. 4.50 and 4.51 also gives consistent equations for ψ, namely

$$-\frac{\hbar^2}{2m}\frac{\partial^2\psi}{\partial x^2} + \left(V(x) - E - \frac{\alpha^2 m}{2\hbar^2}\right)\psi = 0. \tag{4.54}$$

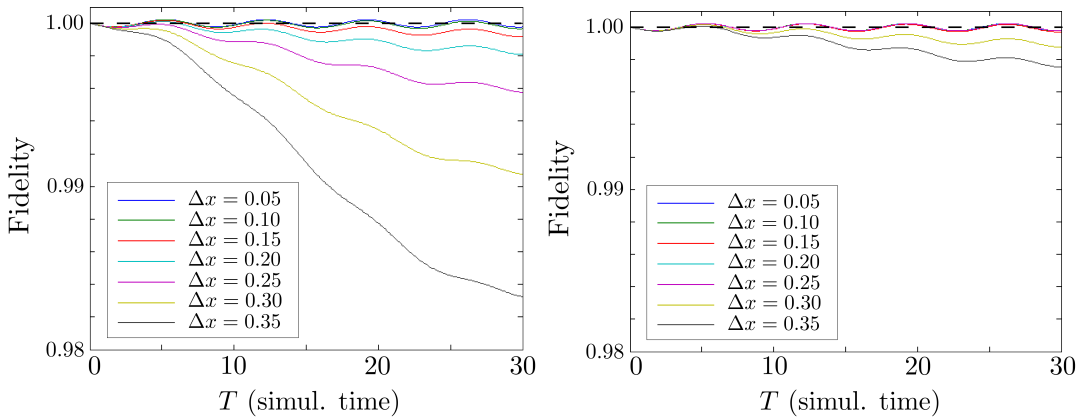

(a) Centred differences

(b) SOIP substitution

Figure 4.3: Fidelity to the ground state of a harmonic oscillator with Rashba SOI strength $\alpha = 1$ for a range of lattice spacings. For small lattice spacings, both methods produce high fidelity results but as we increase Δx the fidelity decreases an order of magnitude faster for the centred differences method compared to the SOIP substitution. The dashed line corresponds to a fidelity of one.

This is the Hamiltonian for the system without SOI with the energy levels shifted up by $\Delta E_{\text{SOI}} = \alpha^2 m/2\hbar^2$. Therefore, if we know the eigenstates of the Hamiltonian in Eq. 4.48 for $\alpha = 0$, then we know the eigenstates for all α, namely, they are the same states but multiplied by a standing wave with wave vector $k = \alpha m/\hbar^2$. As we had a spin doublet in the non-SOI Hamiltonian where spin-up and spin-down were degenerate, there should be an orthogonal state to Ψ. This state is given by $\Psi' = (-\psi \sin\theta, \psi \cos\theta)^T$ where ψ, θ and ΔE_{SOI} are the same as for Ψ. The fact that these states have the same energy is not surprising as the SOI is time-reversal symmetric and therefore should not split the degenerate Kramers doublet [115].

We will test our discretisation using the ground state of a harmonic oscillator with the Rashba SOI. The Hamiltonian of the system is given by:

$$\hat{H} = -\frac{\hbar^2}{2m}\frac{\partial^2}{\partial x^2} - i\alpha\sigma_y\frac{\partial}{\partial x} + \frac{1}{2}m\omega^2 x^2 \tag{4.55}$$

and the eigenstates when $\alpha = 0$ are

$$\psi_n(x) = \frac{1}{\sqrt{2^n n!}} \left(\frac{m\omega}{\pi\hbar}\right)^{\frac{1}{4}} e^{-\frac{m\omega x^2}{2\hbar}} H_n\left(\sqrt{\frac{m\omega}{\hbar}}x\right) \tag{4.56}$$

where $H_n(y)$ are the Hermite polynomials. We initialise the wave function in the ground state, Eq. 4.49, with $\alpha = 1$ and $\omega = 0.1$. We use natural units $\hbar = m = c = 1$ with a propagation time step of $\Delta t = 0.001$ for $N_t = 30000$. The fidelity to the ground state was calculated as a function of the propagation time for a range of Δx using both the centred differences method and the SOIP substitution. The results are shown in Fig. 4.3.

The figures show that the fidelity for both methods is high when the lattice discretisation is sufficiently small as the two methods are the same to $\mathcal{O}(\Delta x)$ in the limit of small Δx. However, as we increase the lattice spacing, we see that the centred differences method quickly loses fidelity whilst the SOIP substitution produces solutions which are an order of magnitude more accurate. The oscillations in the fidelity occur at a frequency proportional to the energy of the dominant frequency component of the initial wave function. This effect may be due to the small non-unitary contribution of the staggered leapfrog method described in Sec. **??** but it was not investigated further as the oscillations appear stable and are smaller than the decreasing drift in the fidelity. As the new method is similar in computational complexity to the centred differences approach, it is sensible to always use the discretisation from Sec. 4.3 as this generates superior numerical solutions.

In this chapter, we have discussed the spin-orbit interaction and demonstrated a new method for simulating continuous systems with the SOI. We derived the SOI Hamiltonian for one- and two-particle systems from the Dirac and Breit equations, respectively. We then discretised the single-particle Hamiltonian using an adapted exponential substitution originally used for the advection-diffusion equation in fluid dynamics. Comparing the discretisation with Harper's equation for magnetic fields, we saw that its form is similar to the Peierls substitution from

Sec. 2.3.1 so we refer to it as the *spin-orbit interaction Peierls* (SOIP) substitution. We performed simulations to demonstrate the accuracy of this method and showed that we can produce numerical solutions with fidelities which decreased an order of magnitude slower than those generated using a simple, centred differences discretisation. We will use the SOIP substitution in the following chapter to study how the SOI affects the proposal of Ch. 3.

Chapter 5

Implementing a $\sqrt{\text{SWAP}}$ Quantum Gate in a One-Dimensional Harmonic Oscillator with Spin-Orbit Coupling

5.1 Introduction

The requirement of scalability is a strong constraint on the possible systems for implementing quantum computation. Whilst single atoms and photons provide relatively simple qubits to manipulate, scaling the control systems up in order to address the numerous qubits which make up a quantum computer's register is challenging. Solid state systems provide a practical alternative as advanced lithographic techniques for fabricating complicated structures on the surface of wafers are already available from the semiconductor industry.

One of the most versatile set of solid state systems involve using the spins of electrons confined within low-dimensional semiconductor heterostructures. We described possible implementations of two-qubit quantum gates in semiconductor systems in Secs. 1.2.3 and 3.5. However, as noted in Ch. 4, the spin-orbit interaction, which couples the spin and momentum degrees of freedom, can be useful for generating single qubit rotations. Other methods can be used to rotate the spins

but whilst the SOI is typically small for conduction band electrons in GaAs [32], its effects on implementations of two-qubit quantum gates can be important. For example, in the exchange interaction scheme of Loss and DiVincenzo described in Sec. 1.2.3, Kavokin pointed out that the SOI can significantly increase the gate error rate [116]. He argued that when one of the electrons tunnels to the adjacent quantum dot, the SOI precesses the spin during the tunnelling event which means that the effective qubit basis of the tunnelled spin rotates. This introduces an anisotropic term to the exchange interaction Hamiltonian which was not accounted for in the Loss and DiVincenzo scheme. These SOI effects on the energy level structure of the double quantum dot system have been observed experimentally by Schreiber *et al.* [117]. In response, Bonesteel *et al.* [118], Burkard and Loss [119] and Stepanenko *et al.* [120] developed protocols based on time-symmetric pulsing of the tunnel coupling which showed that the effect of the SOI on the gate error rates could be reduced.

In this chapter, we will expand upon the proposal of Ch. 3 in a similar fashion. We have proposed a method for generating maximally entangled states with arbitrarily high fidelity using two interacting particles in a one-dimensional harmonic potential. The two particles are displaced from the centre of the well in opposite directions and allowed to fall towards each other. If the interaction strength is tuned correctly, the resulting wave function becomes an equal superposition of scattered and transmitted states. The qubits do not evolve as they are eigenstates of the system so the resulting spatial superposition corresponds to a maximally entangled state in the qubit space.

However, the SOI complicates this method as the dynamics of the spatial degrees of freedom couple to the qubits. As the momentum of the particles are in opposite directions, one of the qubits will precess in a clockwise fashion and the other will rotate counter-clockwise which means that the qubits will not necessarily be in the same eigenbasis when they interact. Therefore, we cannot disregard the symmetric qubit states as we did previously.

In this chapter, we will show that these problems can be mitigated by using appropriate initial conditions. We will develop a simple spin-precession model which allows us to understand how point particles behave in this system and we show that, with an additional constraint on our initial conditions, we can

implement a two-qubit "root-of-SWAP" quantum gate with low error. The discretisation method of Ch. 4 will be used to simulate the system for spatially extended particles and we present numerical results to justify the point-particle model.

5.2 Spin-Orbit Coupling and Qubit Precession

The system we will be considering consists of a pair of spin-1/2 particles in a one-dimensional harmonic potential $V(x) = \frac{1}{2}m\omega^2 x^2$. The qubits are defined by the spins where the computational basis states $\{|0\rangle, |1\rangle\}$ are the eigenstates of σ_z. In order to reduce the dimensionality of the particles to a single spatial degree of freedom x we require a confining potential in the y and z directions which we will assume is asymmetric. This asymmetry induces a Rashba SOI of the form $\hat{H}^R_{\text{SOI}} = i\alpha\sigma_y\partial_x$ as described in Sec. 4.4.2. In this chapter, we will only consider the effects of the Rashba SOI on our system although if this is replaced by the Dresselhaus SOI[1] then we would obtain similar results. The effects of combined Rashba and Dresselhaus SOI on the system are not considered. As we have already studied the effects of different interaction potentials in Sec. 3.4, we will choose the contact interaction as this is the simplest and produces the highest fidelities to maximally entangled states. For clarity, the Hamiltonian of this system is given by:

$$\hat{H} = \sum_{i=1,2}\left[-\frac{\hbar^2}{2m}\frac{\partial^2}{\partial x_i^2} + i\alpha\sigma_y\frac{\partial}{\partial x_i} + \frac{1}{2}m\omega^2 x_i^2\right] + V_0\delta(x_1 - x_2). \tag{5.1}$$

The intent of this chapter is to show that this system can implement a root-of-SWAP quantum gate. As described in Ch. 3, when there is no SOI this gate generates entanglement conditionally dependent on the initial state. Therefore, in order to realise a root-of-SWAP gate, two of the four possible spin combinations must not entangle. This was straightforward when there was no SOI as the system contained no explicit qubit dynamics so the symmetric qubit states $|00\rangle$ and $|11\rangle$ were always in the same qubit basis. The other two input states $|01\rangle$ and $|10\rangle$

[1]For a one-dimensional system, the Dresselhaus Hamiltonian is given by $\hat{H}^D_{\text{SOI}} = i\beta\sigma_x\partial_x$ and all spin rotations described in this section would be around the s_x spin axis rather than s_y.

were entangled due to the dynamics of their spatial wave function. However, for the system described by Eq. 5.1, the SOI couples together the spatial and spin degrees of freedom and we will see that an additional constraint on the initial wave function is necessary in order to make the entanglement conditional.

To gain a basic understanding of how these particles interact, let us first consider the dynamics of a single point particle with initial displacement x_0. The Rashba SOI only couples the spin to the momentum and since there is no preferential spin axis in Eq. 5.1, the SOI term will not change the dynamics of the spatial coordinate. Therefore, a point particle will oscillate sinusoidally with momentum $p_\pm(t) = \pm m\omega x_0 \sin \omega t$ where the sign depends on which side of the well the particle was on at $t = 0$. The spin dynamics is entirely determined by the SOI so we can consider each of the spins to evolve under the time evolution operator $\hat{U}(t) = \exp[-i \int_0^t \hat{H}^R_{\mathrm{SOI}}(\tau)\, \mathrm{d}\tau/\hbar]$. As the particles are both initially stationary, they will both reach the centre of the well at $t = \pi/2\omega$. The two particles interact locally through the contact interaction so we are interested in the spin configuration at this point. For a single spin, the time evolution operator for this process is given by

$$\hat{U}_\pm(x_i, t = \pi/2\omega) = \exp\left[\frac{i}{\hbar^2}\int_0^{\pi/2\omega} \alpha p_\pm(t')\sigma_y \,\mathrm{d}t'\right] \cdot |x_i = 0\rangle \langle x_i = \pm x_0| \quad (5.2)$$

$$= \begin{pmatrix} \cos\theta/2 & \pm\sin\theta/2 \\ \mp\sin\theta/2 & \cos\theta/2 \end{pmatrix} \cdot |x_i = 0\rangle \langle x_i = \pm x_0| \quad (5.3)$$

where $\theta = 2\alpha m x_0/\hbar^2$ is the precession angle of the spins around the s_y axis of the Bloch sphere due to the SOI. There is no interaction between the point particles until $x_1 - x_2 = 0$.

The two particles are given equal and opposite initial displacements $x_1 = x_L = -x_0$, $x_2 = x_R = x_0$. This defines the initial computational basis of the

qubits which we can write in second quantisation notation:

$$|00\rangle = c_\uparrow^\dagger(x_L)c_\uparrow^\dagger(x_R)\,|\emptyset\rangle\,, \tag{5.4}$$
$$|01\rangle = c_\uparrow^\dagger(x_L)c_\downarrow^\dagger(x_R)\,|\emptyset\rangle\,, \tag{5.5}$$
$$|10\rangle = c_\downarrow^\dagger(x_L)c_\uparrow^\dagger(x_R)\,|\emptyset\rangle\,, \tag{5.6}$$
$$|11\rangle = c_\downarrow^\dagger(x_L)c_\downarrow^\dagger(x_R)\,|\emptyset\rangle \tag{5.7}$$

where $c_\varsigma^\dagger(x)$ are anticommuting creation operators for a particle with spin $\varsigma = \{\uparrow, \downarrow\}$ at position x operating on the vacuum state $|\emptyset\rangle$. Note that these states do not necessarily contain definite spatial and spin symmetries: the $S_z = 0$ spin triplet and singlet states would be $(|01\rangle + |10\rangle)/\sqrt{2}$ and $(|01\rangle - |10\rangle)/\sqrt{2}$ respectively. However, the anticommutation relations of the creation operators ensures that the total wave function is antisymmetric.

Using this notation, the single-particle time-evolution operator from Eq. 5.3 transforms the creation operators as

$$\begin{aligned} c_\uparrow^\dagger(x_L) &\xrightarrow{\hat{U}_+} a\,c_\uparrow^\dagger(0) + b\,c_\downarrow^\dagger(0), & c_\uparrow^\dagger(x_R) &\xrightarrow{\hat{U}_-} a\,c_\uparrow^\dagger(0) - b\,c_\downarrow^\dagger(0), \\ c_\downarrow^\dagger(x_L) &\xrightarrow{\hat{U}_+} -b\,c_\uparrow^\dagger(0) + a\,c_\downarrow^\dagger(0), & c_\downarrow^\dagger(x_R) &\xrightarrow{\hat{U}_-} b\,c_\uparrow^\dagger(0) + a\,c_\downarrow^\dagger(0) \end{aligned} \tag{5.8}$$

where $a = \cos\theta/2$ and $b = \sin\theta/2$. We operate on the combined system with $\hat{U}_+(x_1)\hat{U}_-(x_2)$ to evolve the particles so that they are at the centre of the well. As stated above, the evolution of the particles is independent up to this point so $\hat{U}_+(x_1)c_\varsigma^\dagger(x_R) = c_\varsigma^\dagger(x_R)$ and $\hat{U}_-(x_2)c_\varsigma^\dagger(x_L) = c_\varsigma^\dagger(x_L)$. Therefore, the evolution operator transforms the two-qubit computational basis to

$$|00\rangle \rightarrow 2ab\,c_\downarrow^\dagger c_\uparrow^\dagger\,|\emptyset\rangle\,, \tag{5.9}$$
$$|01\rangle \rightarrow -(a^2 - b^2)\,c_\downarrow^\dagger c_\uparrow^\dagger\,|\emptyset\rangle\,, \tag{5.10}$$
$$|10\rangle \rightarrow (a^2 - b^2)\,c_\downarrow^\dagger c_\uparrow^\dagger\,|\emptyset\rangle\,, \tag{5.11}$$
$$|11\rangle \rightarrow 2ab\,c_\downarrow^\dagger c_\uparrow^\dagger\,|\emptyset\rangle \tag{5.12}$$

where we have defined $c_\varsigma^\dagger(0) = c_\varsigma^\dagger$ and $c_\uparrow^\dagger c_\uparrow^\dagger\,|\emptyset\rangle = c_\downarrow^\dagger c_\downarrow^\dagger\,|\emptyset\rangle = 0$ due to the anticommutation relations[1].

[1]It is reasonable to complain that this constraint leads to the transformations $|00\rangle \rightarrow 0$ and

In fact, we cannot propagate the wave functions to the point $x_1 = x_2 = 0$ as the interaction potential diverges at this point. Instead, let us consider evolving the wave function until the particles are infinitesimally close to the centre of the well. The wave function is then given by

$$\Psi\left(x_1 = -\delta x, x_2 = +\delta x; t = \frac{\pi}{2\omega} - \delta t/2\right)|\varsigma_1\varsigma_2\rangle \tag{5.13}$$

where $|\varsigma_1\varsigma_2\rangle$ is one of the two-qubit states from Eqs. 5.9– 5.12 with $\varsigma_1, \varsigma_2 = \{0, 1\}$. We can then propagate the wave function "over" the contact potential[1] using the short time propagator

$$\hat{U}\left(\frac{\pi}{2\omega} - \frac{\delta t}{2}, \frac{\pi}{2\omega} + \frac{\delta t}{2}\right) = 1 - \frac{i\hat{H}(t)\delta t}{\hbar}. \tag{5.14}$$

We do not need to worry about stability criteria from Sec. 2.2 as we are only performing one, infinitesimally small propagation step. The Hamiltonian should be evaluated at the centre of the time step. We want to show that for specific values of a and b, the contact interaction has no effect on this propagation step for two of the computational basis states. Therefore, we want to show that if we express the total Hamiltonian from Eq. 5.1 as $\hat{H} = \hat{H}^0 + V_0\delta(x_1 - x_2)$, then the short time propagation step in Eq. 5.14 is independent of V_0 for two of states $|\varsigma_1\varsigma_2\rangle$. This is equivalent to requiring that the matrix elements of $\hat{U}$ are the same as for $V_0 = 0$ which is equivalent to requiring that the expectation value of the contact potential vanishes. The contact interaction is spin-independent so, for an arbitrary two-qubit state $|\varsigma_1\varsigma_2\rangle$ with $\varsigma_1, \varsigma_2 = \{0, 1\}$, the only non-vanishing values of the expectation are

$$\langle\varsigma_1\varsigma_2|\delta(x_1 - x_2)|\varsigma_1\varsigma_2\rangle = \begin{cases} 4a^2b^2 & \varsigma_1 = \varsigma_2 \\ (a^2 - b^2)^2 & \varsigma_1 \neq \varsigma_2 \end{cases}. \tag{5.15}$$

Therefore, if we set $2ab = \sin\theta = 0$ then the time-evolution operator for the Hamiltonian in Eq. 5.1 is equivalent to a pair of non-interacting harmonic oscil-

$|11\rangle \to 0$ which is unphysical (and similarly for $a^2 - b^2 = 0$). However, this is a consequence of assuming that the particles are point-like and we will see in Sec. 5.3.2 that this constraint does not produce unphysical behavious when the particles are spatially extended.

[1] i. e. $x_1 \to \delta x, x_2 \to -\delta x$.

lators for the states $|00\rangle$ and $|11\rangle$ This means that the qubits cannot interact so the wave function remains in a tensor product state. The other pair of two qubit states do interact and if V_0 is tuned to generate maximally entangled states then we have produced a root-of-SWAP two-qubit quantum gate. Explicitly, under this constraint, the gate operations on the initial basis states $(|00\rangle, |01\rangle, |10\rangle, |11\rangle)^T$ will be

$$U_1 = \begin{pmatrix} 1 & 0 & 0 & 0 \\ 0 & \frac{1+i}{2\sqrt{2}} & \frac{1-i}{2\sqrt{2}} & 0 \\ 0 & \frac{1-i}{2\sqrt{2}} & \frac{1+i}{2\sqrt{2}} & 0 \\ 0 & 0 & 0 & 1 \end{pmatrix}. \tag{5.16}$$

However, unlike for the entanglement scheme of Ch. 3, we can also set $a^2 - b^2 = \cos\theta = 0$ which prevents the $\{|01\rangle, |10\rangle\}$ states from interacting. This gate operation will be given by

$$U_2 = \begin{pmatrix} \frac{1+i}{2\sqrt{2}} & 0 & 0 & \frac{1-i}{2\sqrt{2}} \\ 0 & 1 & 0 & 0 \\ 0 & 0 & 1 & 0 \\ \frac{1-i}{2\sqrt{2}} & 0 & 0 & \frac{1+i}{2\sqrt{2}} \end{pmatrix}. \tag{5.17}$$

The gates U_1 and U_2 are equivalent under the permutation transformation $U_1 = PU_2P^{-1}$ where

$$P = \begin{pmatrix} 0 & 1 & 0 & 0 \\ 1 & 0 & 0 & 0 \\ 0 & 0 & 0 & 1 \\ 0 & 0 & 1 & 0 \end{pmatrix}. \tag{5.18}$$

This corresponds to relabelling the computational basis

$$\begin{pmatrix} |00\rangle \\ |01\rangle \\ |10\rangle \\ |11\rangle \end{pmatrix} \rightarrow \begin{pmatrix} |01\rangle \\ |00\rangle \\ |11\rangle \\ |10\rangle \end{pmatrix}. \tag{5.19}$$

Physically, we can relate the constraints $2ab = 0$ and $a^2 - b^2 = 0$ to a constraint on the initial displacement of the particles. The precession angle $\theta = 2\alpha m x_0/\hbar^2$

so we can generate two-qubit quantum gates when

$$x_0 = n\pi\hbar^2/4\alpha m \tag{5.20}$$

where odd n gives the gate U_1 and even n gives the gate U_2. This model also allows us to approximate how errors in this constraint affect the fidelity of the two-qubit gate. An error in the initial displacement δx_0 is linearly related to the precession angle θ so the resulting error in the expectation value of the interaction potential in Eq. 5.15 will be $\mathcal{O}(\delta x_0^2)$. This means that the non-interacting components of the two-qubit quantum gates in Eqs. 5.16 and 5.17 are robust against initialisation errors at this order.

This derivation has been rather abstract and it is useful to understand how this evolution effects the spin dynamics of the system. Let us first consider the constraint $2ab = 0$ on the dynamics of the $|00\rangle$ state. The spins of this state are initially parallel and they precess around the s_y axis of the Bloch sphere through

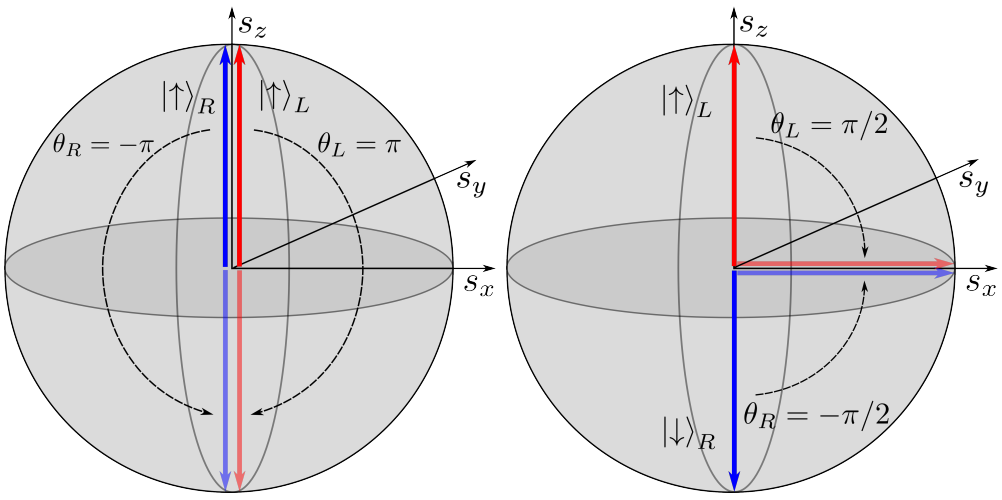

(a) Aligned Spins (b) Anti-aligned Spins

Figure 5.1: For a root-of-SWAP two-qubit quantum gate, a pair of the four possible spin combinations must not entangle. If the interaction between the particles is local, then this can occur if the spin state is symmetric when $x = 0$. The spins precess in opposite directions so there are two possibilities: (a) The spins are initially align and rotate by multiples of π into eigenstates of σ_z and (b) the spins are initially anti-aligned so they are in a symmetric state if they precess into an eigenstate of σ_x.

an angle which is an integer number of π (as shown in Fig. 5.1a). The spins counter-rotate but, as they were originally eigenstates in the σ_z basis, when the particles reach the centre of the well the spins are pointing in the same direction. This means that the total spin state of the wave function is symmetric so the spatial wave function must be antisymmetric. This forces the wave function to vanish at $x_1 = x_2$ so the particles cannot "see" the contact interaction. Therefore, the qubits remain in a tensor product state. However, the $|01\rangle$ and $|10\rangle$ states are not symmetric at the centre of the well so they do interact. By tuning the interaction strength, we can implement the root-of-SWAP gate U_1.

Next, let us consider the dynamics of the $|01\rangle$ state when $(a^2 - b^2) = 0$. For definiteness we will satisfy this constraint by assuming that $\theta = \pi/2$. The spins are initially anti-parallel and they precess so that they are eigenstates of σ_x when they reach the centre of the well (as shown in Fig. 5.1b). As the spins rotate in opposite directions, the overall spin wave function is symmetric for the two anti-parallel states. Using the same arguments as we made above, the states which are spin symmetric at the centre of the well do not interact whilst we can tune the interaction strength so that the other states to become maximally entangled. This leads to an implementation of the root-of-SWAP gate U_2.

5.3 Simulations

Whilst the results of Sec. 5.2 were for point particles, we would also like to understand this system for spatially extended particles. This is also more similar to the problem studied in Ch. 3. However,the system is now more complex and we cannot formulate analytic solutions. Instead, we will generate numerical solutions using the SOIP substitution developed in Ch. 4 with a lattice of $N_x = 1024$ sites and spacing $\Delta x = 0.1$ and a time step of $\Delta t = 0.001$. We use natural units such that $\hbar = m = c = 1$ and the oscillator frequency was set to $\omega = 0.1$.

5.3.1 SOI Coherent States

In order to simulate the system for spatially extended particles with SOI, we would like to use "coherent" states such as those in Eq. 3.33. To recap, these

states are created by displacing the ground state of the harmonic oscillator. The displacement of the centre of the wave function oscillates with the frequency of the well whilst its functional form is invariant. However, if we were to use the coherent states from Ch. 3, when the SOI is introduced there is no guarantee that the particle will retain its Gaussian shape and, furthermore, coupling of the $|\uparrow\rangle$ and $|\downarrow\rangle$ states means that the qubit state may not be well-defined.

As an ansatz, we propose a new set of SOI "coherent" states which are formed by displacing the ground state of Eq. 4.55, which we derived in Sec. 4.4.2, by d. To demonstrate that these states have the desired behaviour, Fig. 5.2 shows the probability density for the spin-up, spin-down and total forms of the wave function for a SOI coherent state where $d = 3\pi$ and $\alpha = 0.5$ at $t = 0, \pi/2\omega, \pi/\omega$. We use the "up" state, of the form given in Eq. 4.49. For these parameters, after a quarter-period of the oscillator, when the particle is in the centre of the well we expect the spin to have precessed by $\theta = 2\alpha md/\hbar^2 = 3\pi$. Fig 5.2b shows that the spin-up and spin-down components have switched whilst the overall form of the wave function is unchanged. After a half-period of the oscillator, the spin has precessed by a further $\theta = 3\pi$ and we see in Fig. 5.2c that the probability densities are the same as for the initial state in Fig. 5.2a. The slight asymmetry in Fig. 5.2c is due to the finite spacing of the lattice. Fig. 5.2 verifies that these states have the same behaviour as the non-SOI coherent states and that the spins behave similarly to the simple point-particle model we proposed in Sec. 5.2. The two particle wave function was constructed by antisymmetrising the tensor product of these single particle "coherent" states.

5.3.2 Two-Qubit Gate Implementation with SOI

We define the error of the two-qubit quantum gate as one minus the average of the fidelity to the ideal states from the root-of-SWAP operation:

$$\epsilon = 1 - \frac{1}{4}\sum_{i=1}^{4} |\langle \alpha_i | \psi_i \rangle| \tag{5.21}$$

where $|\alpha_i\rangle$ are the ideal states and $|\psi_i\rangle$ are the simulated states. As described in Sec. 5.2, there are two possible root-of-SWAP gates that this system can im-

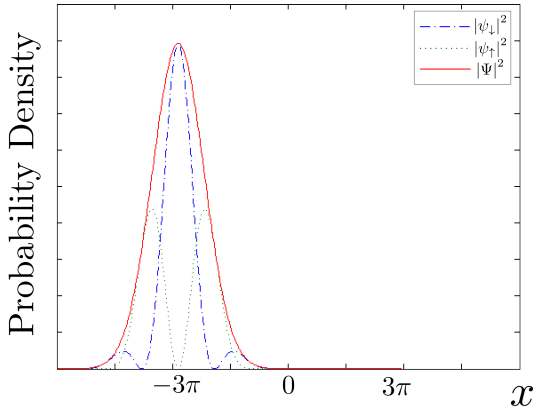

(a) $t = 0$

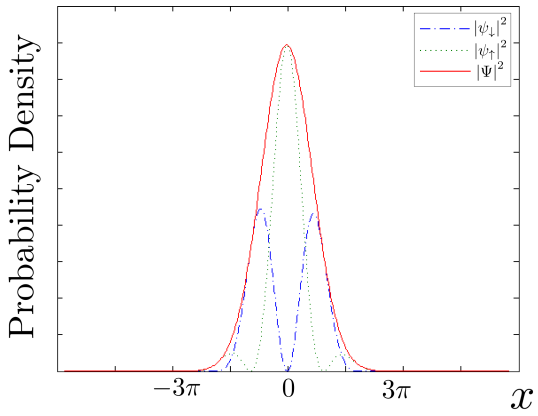

(b) $t = \pi/2\omega$

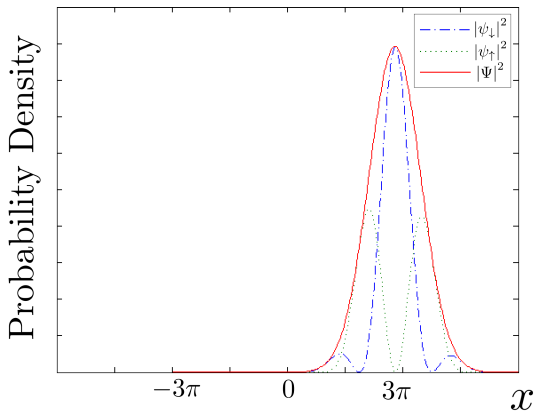

(c) $t = \pi/\omega$

Figure 5.2: SOI coherent type state constructed by displacing the ground state of the SOI system by an initial displacement $d = 3\pi$. The shape of the total probability density remains the same as the particle oscillates across the potential. However, the SOI causes the spin to precess so the particle has swapped from an "up" state to a "down" state by the time it reaches the middle of the well. After a single half-oscillation, the particle returns to its initial state as it has precessed through an angle $\theta = 4\alpha md/\hbar^2 = 6\pi$.

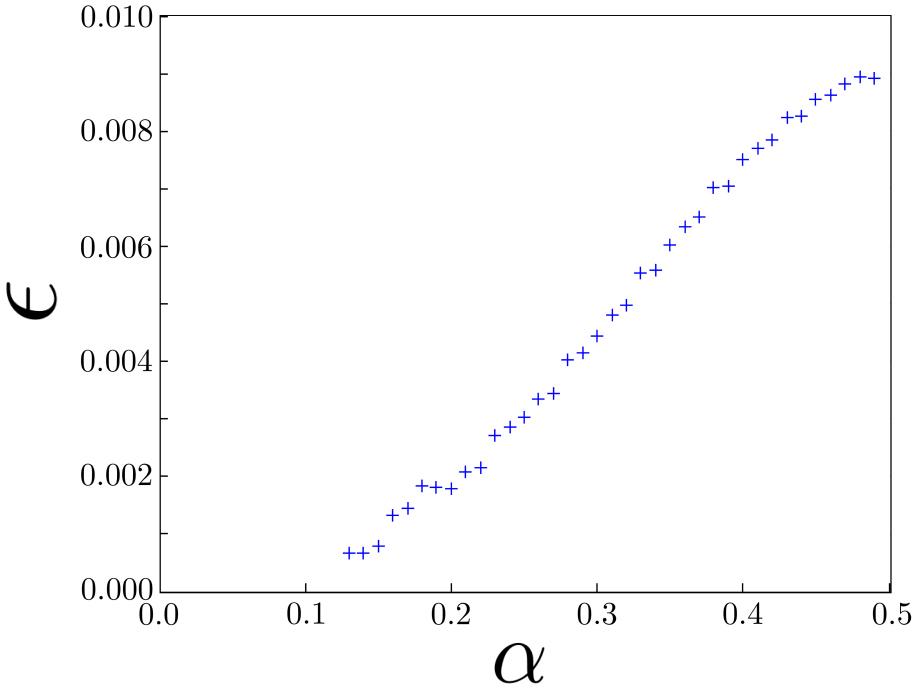

Figure 5.3: A cross section of the gate error for U_2 at $\theta = 3\,\pi$. As the initial condition constraint of Eq. 5.20 is fulfilled, the error is lower than 1% for all α. Decreasing α corresponds to increasing x_0 which decreases the error as the PDHA from Ch. 3 is more accurate. Irregularities in the plot are due to lattice discretisation errors.

plement and therefore there are two sets of ideal states $|\alpha_i\rangle$. Note that if the simulated states are replaced with the ideal states for the opposite gate then $\epsilon = 1 - 1/2\sqrt{2} \approx 0.3$ as the entangled target states partially overlap with the non-interacting product states. This is not an upper bound on the error as the overlap decreases if the spatial form of the wave function is strongly perturbed by the interaction. However, as we saw in Sec. 3.4.1, the fidelity to maximally entangled states is high when a contact interaction is used so we expect this to be a typical maximum gate error.

The simulations were run for one half-period of the oscillator and the error was calculated for both of the gates defined in Eqs. 5.16 and 5.17. The interaction strength V_0 was optimised empirically such that the interacting spin combinations produced states with the maximum entanglement possible. Fig. 5.4 shows the error as a function of both precession angle θ and SOI strength α. The initial displacement of the particles is determined by both θ and α, as shown in Eq. 5.3.

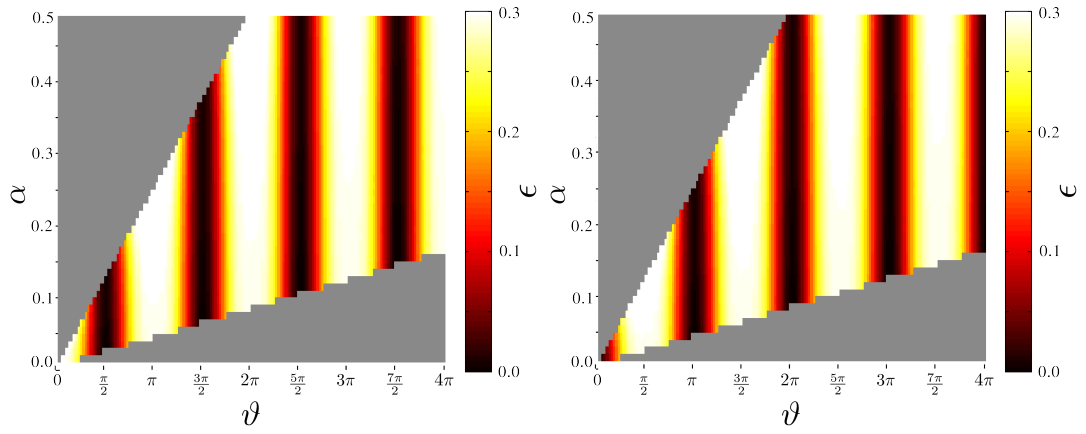

(a) n odd (b) n even

Figure 5.4: Gate error as a function of the SOI strength α and the precession angle θ for the two root-of-SWAP gates U_1 and U_2. The gate error is minimised when the constraint given in Eq. 5.20 is satisfied. ϵ varies sinusoidally as a function of θ which demonstrates robustness against perturbations in the initial displacement of the single particle wave functions.

However, as in Ch. 3, the initial single particle states must be well separated. For a given θ, as α gets larger x_0 must get smaller and at some point the wave functions of the particles overlap significantly. Therefore, we constrained the initial displacement such that $x_0 > \sigma_0$, where $\sigma_0 = \sqrt{\hbar/m\omega}$ is the width of the ground state when $\alpha = 0$. Also, to prevent reflections from the edge of the simulation domain, we limit $x_0 < 10\,\sigma_0$ which, for these simulation parameters, is equivalent to the centre of the particles being approximately $6\,\sigma_0$ from the boundary. We did not run the simulations in these regimes which corresponds to the grey regions in Fig. 5.4.

The comparative strength of the SOI is given by the shift in energy of the ground state ΔE_{SOI} relative to the level spacing of the harmonic oscillator $\hbar\omega$. The maximum value of α used in the simulations for Fig. 5.4 was $\alpha = 0.5$ which, using the results of Sec. 4.4.2, corresponds to $\Delta E_{\mathrm{SOI}} \sim 10\,\hbar\omega$. This shows that the SOI simulated is well beyond the perturbative regime.

The gate error is minimal when the precession angle obeys the constraint in Eq. 5.20. The error remains low for the range of α included in the simulation domain. Fig. 5.3 shows a cross section of the error for the gate U_2 when n is even

for a precession angle of $\theta = 3\,\pi$. We see that the gate error remains below 1% over the entire range of α with a minimum of $\epsilon \approx 10^{-3}$. The noise in Fig. 5.3 is due to the lattice discretisation. Although it appears that the error decreases to zero for a critical value of α, this is because we have introduced a cutoff for large x_0. Decreasing α means that we have to increase x_0 which results in the error quickly approaching zero asymptotically, as shown in Ch. 3. Fig. 5.4 also shows that ϵ varies sinusoidally as a function of θ, as we predicted in Sec. 5.2, so the error remains low under small perturbations in the initial displacement. Finally, note that the maximum error in these Fig. 5.4 is $\epsilon_{\text{max}} \approx 0.3$ which occurs for values of θ which have a minimal error for the opposite gate which indicates that the combination of the SOI and the contact interaction is not significantly perturbing the spatial wave function.

5.3.3 Coulomb interaction

Up to this point, we have only focused on the contact interaction potential. In this section, we will discuss how replacing this interaction with a Coulomb potential affects these results. As discussed in Sec. 3.4.3, in one-dimension we must add a softening parameter γ to the Coulomb interaction. This gives a characteristic length to the entire system, and we can scale the coordinates to express the interaction as

$$V_{\text{Coul}}(x_1 - x_2) = \frac{q^2}{4\pi\epsilon\alpha} \frac{1}{\sqrt{(x_1 - x_2)^2 + \gamma'^{\,2}}} \tag{5.22}$$

as shown in Eq. 3.52 from Sec. 3.4.3. The particles will interact before they approach the centre of the well which is contrary to the arguments made in this chapter. Fortunately, the results of Secs. 5.2 and 5.3.2 show that gate errors are not significantly affected if the precession angle θ is slightly misaligned. Therefore, we would expect that if θ varies slowly over the characteristic length scale of the potential, that is, if

$$\int_{-\gamma}^{\gamma} \left.\frac{\partial\theta}{\partial x_1}\right|_{x_1=0} \left.\frac{\partial\theta}{\partial x_2}\right|_{x_2=0} \cdot V_{\text{Coul}}(x_1 - x_2)\,\mathrm{d}x \approx 0 \tag{5.23}$$

then the misalignment of the qubits over the length of the interaction should not be important and the gate error should remain low. It is possible to satisfy Eq. 5.23 either by decreasing the characteristic length scale γ or by decreasing the SOI strength α so that the rate $\partial_x\theta$ at which the spins precess is reduced. However, to demonstrate low gate errors, we would need to perform simulations where the contact interaction in Eq. 5.1 was replaced with V_{Coul}. These simulations were not performed and constitute further work which should be done in order to determine whether the entangling scheme described in this chapter is feasible.

In this chapter, we have proposed a method for extending the entanglement method from Ch. 3 to systems with spin-orbit interaction. By developing a simple spin-precession model for point particles, we found a general form for the time-evolved computational basis states when they reach the centre of the potential. By adding an additional constraint on the initial displacement of the particles, we can prevent two of the four computational basis states from entangling. A root-of-SWAP quantum gate can then be created by tuning the strength of the inter-particle interaction so that the other pair of states are maximally entangled. We performed numerical simulations for this method using spatially extended particles and showed that gate errors of $\epsilon \approx 0.1\%$ can be acheived. The simulations also showed that the system is robust against perturbations in this additional constraint on the initial displacement. We concluded by arguing that these results should be applicable for softened Coulomb interactions with short characteristic length scales.

Chapter 6

Conclusions

The aim of this work has been to demonstrate the possibility for robust entanglement generation between a pair of qubits associated with two interacting particles confined to a one-dimensional harmonic potential. We have investigated this system using a combination of theoretical and numerical techniques. In this chapter, we will summarise the results of this thesis and describe possible future directions of research for this system.

6.1 Summary

In Ch. 1, we introduced the phenomenon of entanglement and how it can be used in quantum information processing. We showed that it is not possible to describe entangled states using classical theories as Bell's theorem shows that any local, deterministic hidden-variables theory is incompatible with experiment. This means that the correlations present in entangled systems represent a new type of resource which can be used for new technologies. We introduced various representations for entangled states and showed that, for a pair of qubits, there exists a set of four maximally entangled states. These states are one of the most important resources in quantum information processing and we demonstrated two protocols — quantum key distribution and teleportation — which consume these states as a resource. This provided one of the motivations for developing methods for generating maximally entangled states.

We also introduced the field of quantum computing where a register of qubits is manipulated and measured in order to perform calculations which are impractical using classical computation. We explained the DiVincenzo criteria for implememting a quantum computer with particular emphasis on the requirement for two-qubit quantum gates which DiVincenzo declared to be "the heart of quantum computing" [10]. These gates are required to generate entanglement within the computer's qubit register. We described one form of two-qubit gate called the root-of-SWAP gate which, when we input a tensor product of two qubits in the computational basis, conditionally outputs maximally entangled states. This provided another motivation for studying processes which generate maximally entangled states but in this case conditionally on the input states. We introduced the exchange interaction proposal of Loss and DiVincenzo which can implement the root-of-SWAP gate. We gave a brief description of how this gate is realised in low-dimensional semiconductor systems and we mentioned how the sensitivity of this system to errors in the spatial and temporal control limited its applicability as a component for scalable quantum computing. One of the main themes of the thesis was to propose new methods for implementing a root-of-SWAP gate in a more robust manner.

In Ch. 2, we presented the numerical methods which we used to generate the simulations in this thesis. One of the most important equations we needed to solve was the time-dependent Schrödinger equation. However, many of the systems we considered were too complicated to solve analytically so we needed to derive numerical solutions to the TDSE. To do this, we used propagation methods to discretise the temporal coordinate of the wave function and propagate it from one time step to the next. We studied the stability properties of three possible short-time propagators: the Euler, Crank-Nicolson and staggered leapfrog methods. We also considered the spatial discretisation of the Hamiltonian in real space, with and without magnetic fields. As well as describing methods for generating stable and accurate numerical solutions, we considered how using graphics processing technology (GPUs) could increase the efficiency of the propagation method. We finished the chapter by showing that the staggered leapfrog propagation methods was ideal for GPU acceleration.

In Ch. 3, we proposed a method for entangling a pair of qubits by associat-

ing them with two interacting particles confined to a one-dimensional harmonic potential. The particles were initialised on either side of the well and were allowed to evolve freely according to the TDSE. They fell into the centre of the well where the interaction, which was assumed to be local, generated a scattering event which resulted in the final state consisting of a superposition of scattered and transmitted states. By tuning the interaction strength, we were able to make this an equal superposition such that if we identified the particle on the left side of the well as "qubit 1" and the qubit on the right side of the well as "qubit 2" then we generated a maximally entangled state. Additionally, as the system contains no direct coupling between the qubits, this entanglement was generated conditionally as the computational basis states with two qubits in the same state was unchanged. Therefore, in the qubit space, this process is equivalent to a root-of-SWAP two-qubit quantum gate.

We use a spectral decomposition of the spatial wave function to investigate this proposal in a more rigourous manner. We noted that if the energy spectrum receives a constant, parity-dependent shift of the eigenstates due to the interaction potential, then, with the correct interaction strength, maximally entangled states were produced with 100% fidelity. We called this energy level structure the parity-dependent harmonic approximation and we showed that for a contact potential interaction and with large initial displacement of the particles from the centre of the well, the fidelity to the maximally entangled states can be made arbitrarily high. We also demonstrated that the fidelity to these states is robust against variations in the approximation.

To verify these results for non-idealised systems, we provided numerical solutions to the TDSE for a variety of interaction potentials. We described the dynamics of the spatial wave function and demonstrated numerically that the fidelity was robust against perturbations in the interaction. We also proposed two possible physical implementations of this entangling scheme using electrons in low-dimensional semiconductor systems. We concluded the chapter by discussing how our proposal differs from the exchange interaction gate described in Ch. 1.

In low-dimensional semiconductor heterostructures, the spin-orbit interaction can be an important effect. We wanted to be able to introduce the SOI into our simulations but, unlike for magnetic fields, the interaction has no generally

accepted discretisation. In Ch. 4, we presented a novel method for discretising the SOI Hamiltonian which produces high fidelity solutions to the TDSE. After having derived the SOI Hamiltonian using a low energy expansion of the Dirac equation, we considered an adaptation of the exponential substitution used by Grima and Newman for studying the advection-diffusion equation in fluid dynamical systems. We showed that the discretised form of the Hamiltonian was similar to the Peierl's substitution for the magnetic field. Using analytically soluable systems, we compared this subsitution with a standard centred finite-differences approach discretisation. We concluded the chapter by demonstrating that, for certain systems, the fidelity of simulated results to analytic solutions decreased an order of magnitude slower for the new substitution.

In Ch. 5, we investigated the effects of SOI on the entangling scheme of Ch. 3. Without SOI, a root-of-SWAP gate was automatically generated because the Hamiltonian was independent of the qubit degree of freedom. However, for electrons in low-dimensional semiconductor systems, when the electron spin is used as the qubit, the SOI will couple the qubit dynamics to the spatial degree of freedom. We started by considering the dynamics when the particles were point-like. We used a contact interaction, which is local, so the dynamics of the particles was decoupled until the particles reached the centre of the well. We found an analytic expression for how the spin of a single particle precesses through the influence of the SOI. Using this to describe the dynamics of two point particles up to the time when they interact we could analysing the infinitesimal propagation step when the two particles reach the centre of the well to show that an additional constraint on the initial displacement of the particles will prevent them from interacting. We were able to relate this constraint to the symmetry of the wave function and the spin dynamics of the particles. If the interaction strength is tuned, we can conditionally generate maximally entangled states which demonstrates that this system can also be used to implement a root-of-SWAP two-qubit quantum gate. We argued that the gate error should be robust against perturbations in the constraint on the initial displacement. We concluded the chapter by providing numerical solutions for the system using the numerical discretisation from Ch. 4 with two spatially extended particles which demonstrated low gate error and robustness against the additional constraint.

6.2 Further Work

We finish this thesis with a summary of possible future directions of research suggested by the results we have obtained. One of the most promising directions for this work is in the field of open quantum systems. We will begin by summarising what open quantum systems are and how they can be simulated by introducing a stochastic term to the TDSE. We will then argue that the numerical techniques used in this thesis could efficiently implement this scheme and we will finish by demonstrating why we expect the entanglement schemes proposed in this thesis to be robust against decoherence from the environment.

In quantum mechanics, and in this entire thesis, we normally only consider systems consisting of one or two particles. It is incredibly difficult to simulate larger systems because the size of the Hilbert space, and therefore the information stored in the wave function, increases exponentially with the number of particles. Indeed, the ability to isolate single quantum systems is one of the great acheivements of modern physics. However, there will always be some coupling to other systems or to the environment and it is impossible to simulate the dynamics of the combined wave function of the system and the environment. Coupling to the environment can strongly affect the dynamics of the system and is described by the phenomenon known as decoherence [121–127]. The most important implication of this effect in the context of this work is that when entangled systems decohere, they lose the quantum correlations necessary for quantum information processing.

For the systems we described in this work, there are two possible modes of decoherence. The first is decoherence of the qubits and their entanglement. Direct coupling of the environment to the qubits will always decohere the entangled states and the decoherence rate will limit how useful the system is for quantum computation. For example, when the qubits are defined by the spins of electrons in a GaAs substrate, the nuclear spins of the lattice will cause the qubits to decohere through the hyperfine interaction [46, 128]. Whilst feedback mechanisms can be developed to recover the qubit information from the bath [129], this interaction will act as a constant decohereing mechanism. In fact, long qubit decoherence times was the third DiVincenzo criterion outlined in Sec. 1.2.1. How-

ever, decoherence can also occur due to the quantum processes which the qubits undergo. Manipulating a quantum system requires the control apparatus to couple to the qubit and this can decohere the system. The ideal entangling process is one which minimises the effect of this coupling on the decoherence rate of the entangled qubit state.

As we mentioned earlier in this section, it is impossible to accurately describe the combined wave function of the system and the environment. Instead, a common approach is to use a master equation for the density matrix of the system [130–132]. The most general form of the master equation can be written in terms of the (non-Hermitian) Linblad operators [133]:

$$\frac{\partial \rho_S}{\partial t} = -\frac{i}{\hbar}\left[\hat{H}_S, \rho_S\right] + \sum_i \hat{A}_i \rho_S \hat{A}_i^\dagger - \frac{1}{2}\left(\rho_S \hat{A}_i \hat{A}_i^\dagger + \hat{A}_i^\dagger \hat{A}_i \rho_S\right) \tag{6.1}$$

where $\hat{H}_S$ is the system Hamiltonian and $\hat{A}_i$ are the Linblad operators. However, using this approach, we must propagate the density matrix ρ_S rather than the wave function ψ. For a system described by a wave function of size N, then the density matrix of this system is of size N^2 which makes iterating Eq. 6.1 computationally challenging when N is large.

One method for simplifying this problem is provided by the stochastic Schrödinger equation [134–136]. Typically, we can express the coupling between the system and the environment as $\hat{H}_{\text{int}} = \lambda \sum_\alpha \hat{B}_\alpha \hat{S}_\alpha$ where $\hat{B}_\alpha$ are operators on the environment, $\hat{S}_\alpha$ are operators on the system and λ is some coupling constant which is typically small. By treating the environment as a thermodynamic bath, we can integrate over the degrees of freedom of the environment such that the evolution of the system is determined by

$$\frac{\partial \psi(t)}{\partial t} = \left(\hat{H}_S + \lambda \sum_\alpha \gamma_\alpha(t)\hat{S}_\alpha - i\lambda^2 \left[\sum_{\alpha,\beta} \hat{S}_\alpha \int_0^t C_{\alpha,\beta}(\tau) e^{-i\hat{H}_S\tau} \hat{S}_\beta e^{i\hat{H}_S\tau}\, \mathrm{d}\tau\right]\right)\psi(t) \tag{6.2}$$

where the noise terms $\gamma_\alpha(t)$ are stochastic variables, $C_{\alpha,\beta}(t-t') = \langle \gamma_\alpha^*(t)\gamma_\beta(t')\rangle$ are the bath correlation function and, for clarity, we have set $\hbar = 1$. It can be shown that if we propagate Eq. 6.2 for multiple realisations of the noise $\gamma_\alpha(t)$

then the the true density matrix of the system is given by

$$\rho_S(t) = \lim_{N\to\infty} \frac{1}{N} \sum_i |\phi_i(t)\rangle \langle\phi_i(t)| \tag{6.3}$$

where each $|\phi_i(t)\rangle$ are solutions to Eq. 6.2 for a different realisation of the noise $\gamma_\alpha^{(i)}(t)$. We can calculate the observables $\hat{O}$ for the open quantum system using $\hat{O}(t) = \mathrm{Tr}(\rho_S(t)\hat{O})$. In order to have a good approximation to Eq. 6.3, we must propagate Eq. 6.2 many times. The numerical methods developed in Ch. 2 could do this very efficiently but the GPU-accelerated staggered leapfrog method have not yet been adapted to solve Eq. 6.2. At present, only systems with a limited Hilbert space have been simulated such as a two-level atom compromising the system coupled to an optical cavity which represents the bath [137]. With the acceleration provided by the techniques used in this thesis, we should be able to simulate larger open quantum systems.

Ideally, we could simulate the effects of decoherence on the root-of-SWAP gates proposed in Chs. 3 and 5. If decoherence due to direct coupling with the qubits occurs faster than the entangling process, then DiVincenzo's third criterion is not satisfied and the system cannot be used as a quantum computer. Therefore, we would be able to assume that there was no direct coupling of the environment to the qubits. However, the environment can transfer momentum into the system which would decohere the spatial wave function. It would be useful to investigate the robustness of these schemes against such momentum kicks. For the proposal of Ch. 3, we would not expect this form of decoherence to strongly affect the fidelity of the two-qubit quantum gate. We showed that the fidelity only weakly depends on the initial momenta of the particles so small changes in the momentum during the evolution should not have much of an effect on the resulting qubit state. Therefore, we would expect that this proposal would be robust against decoherence effects. The proposal of Ch. 5 would be more interesting as the qubits couple to the momentum so decoherence in the spatial degree of freedom might decohere the qubits due to indirect coupling through the SOI to the environment. Simulations would need to be produced to determine whether this is a strong effect and, therefore, whether this technique would be a viable two-qubit quantum gate when there was significant coupling to the environment.

References

[1] A. Einstein, B. Podolsky & N. Rosen. "Can Quantum-Mechanical Description of Physical Reality Be Considered Complete?" *Phys. Rev.* **47**, 777 (1935) 1

[2] C. H. Bennett & S. J. Wiesner. "Communication via one- and two-particle operators on Einstein-Podolsky-Rosen states". *Phys. Rev. Lett.* **69**, 2881 (1992) 2, 11

[3] A. K. Ekert. "Quantum cryptography based on Bell's theorem". *Phys. Rev. Lett.* **67**, 661 (1991) 2, 11

[4] D. Deutsch. "Quantum Theory, the Church-Turing Principle and the Universal Quantum Computer". *Proc. R. Soc. A* **400**, 97 (1985) 2

[5] P. W. Shor. "Algorithms for quantum computation: discrete logarithms and factoring". *Proceedings of the 35th Annual Symposium on Fundamentals of Computer Science* pages 124 – 134 (1994) 13

[6] L. K. Grover. "A fast quantum mechanical algorithm for database search". *Proceedings of the 28th Annual ACM Symposium on the Theory of Computing* pages 212 – 219 (1996)

[7] M. Neilsen & I. Chuang. *Quantum Computation and Quantum Information.* Cambridge University Press (2000) 2, 13, 15

[8] C. H. Bennett, G. Brassard & J.-M. Robert. "Privacy Amplification by Public Discussion". *SIAM J. Comp.* **17**, 210 (1988) 2

[9] C. H. Bennett, G. Brassard, C. Crepeau, R. Jozsa, A. Peres & W. K. Wootters. "Teleporting an unknown quantum state via dual classical and Einstein-Podolsky-Rosen channels". *Phys. Rev. Lett.* **70**, 1895 (1993) 2, 12

[10] D. P. DiVincenzo. "The Physical Implementation of Quantum Computation". *arXiv* (2000) 3, 14, 15, 108

[11] A. Pais. "Einstein and the quantum theory". *Rev. Mod. Phys.* **51**, 863 (1979) 3

[12] J. S. Bell. "On the Einstein-Podolsky-Rosen Paradox". *Physics* **1**, 195 (1964) 3

[13] F. Laloë. "Do we really understand quantum mechanics? Strange correlations, paradoxes, and theorems". *Am. J. Phys.* **69**, 655 (2001) 5

[14] A. Aspect, P. Grangier & G. Roger. "Experimental Tests of Realistic Local Theories via Bell's Theorem". *Phys. Rev. Lett.* **47**, 460 (1981) 5

[15] M. A. Rowe, D. Kielpinski, V. Meyer, C. A. Sackett, W. M. Itano, C. Monroe & D. J. Wineland. "Experimental violation of a Bell's inequality with efficient detection". *Nature* **409**, 791 (2001) 5

[16] R. M. Stevenson, R. J. Young, P. Atkinson, K. Cooper, D. A. Ritchie & A. J. Shields. "A semiconductor source of triggered entangled photon pairs". *Nature* **439**, 179 (2006)

[17] M. Ansmann, H. Wang, R. C. Bialczak, M. Hofheinz, E. Lucero, M. Neeley, A. D. O'Connell, D. Sank, M. Weides, J. Wenner, A. N. Cleland & J. M. Martinis. "Violation of Bell's inequality in Josephson phase qubits". *Nature* **461**, 504 (2009) 5

[18] A. Ekert & P. L. Knight. "Entangled quantum systems and the Schmidt decomposition". *Am. J. Phys.* **63**, 415 (1995) 9

[19] K. F. Riley, M. P. Hobson & S. J. Bence. *Mathematical Methods for Physics and Engineering.* Cambridge University Press, 3rd edition (2006) 9

[20] M. B. Plenio & S. Virmani. "An introduction to entanglement measures". *Quant. Inf. Comp.* **7**, 1 (2007) 9

[21] W. K. Wooters & W. H. Zurek. "A single quantum cannot be cloned". *Nature* **299**, 802 (1982) 11

[22] V. Buzek & M. Hillery. "Quantum copying: Beyond the no-cloning theorem". *Phys. Rev. A* **54**, 1844 (1996) 11

[23] D. Bruss, D. P. DiVincenzo, A. Ekert, C. A. Fuchs, C. Macchiavello & J. A. Smolin. "Optimal universal and state-dependent quantum cloning". *Phys. Rev. A* **57**, 2368 (1998) 11

[24] C. H. Bennett, H. J. Bernstein, S. Popescu & B. Schumacher. "Concentrating partial entanglement by local operations". *Phys. Rev. A* **53**, 2046 (1996) 13

[25] B. Kraus. "Topics in Quantum Information". In D. P. DiVincenzo (Editor) *Quantum Information Processing*, IFF Spring School Lecture Notes, chapter C3. Forschungszentrum Jülich GmbH (2013) 13

[26] W. H. Zurek. "Pointer basis of quantum apparatus: Into what mixture does the wave packet collapse?" *Phys. Rev. D* **24**, 1516 (1981) 14

[27] W. H. Zurek. "Environment-induced superselection rules". *Phys. Rev. D* **26**, 1862 (1982) 14

[28] J. Preskill. "Fault-Tolerant Quantum Computation". In H.-K. Lo, S. Popescu & T. Spiller (Editors) *Introduction to Quantum Computation and Information*, pages 213 – 269. World Scientific Publishing (1998) 14

[29] A. Barenco, C. H. Bennett, R. Cleve, D. P. DiVincenzo, N. Margolus, P. Shor, T. Sleator, J. A. Smolin & H. Weinfurter. "Elementary gates for quantum computation". *Phys. Rev. A* **52**, 3457 (1995) 14, 15

[30] P. O. Boykin, T. Mor, M. Pulver, V. Roychowdhury & F. Vatan. "On universal and fault-taulerant quantum computing". *arXiv preprint quant-ph/9906054* (1999) 15

[31] D. Loss & D. P. DiVincenzo. "Quantum computation with quantum dots". *Phys. Rev. A* **57**, 120 (1998) 16, 17, 20

[32] G. Burkard, D. Loss & D. P. DiVincenzo. "Coupled quantum dots as quantum gates". *Phys. Rev. B* **59**, 2070 (1999) 17, 92

[33] E. Koch. "Entanglement and Exchange in Correlated Electron Systems". In D. P. DiVincenzo (Editor) *Quantum Information Processing*, IFF Spring School Lecture Notes, chapter C3. Forschungszentrum Jülich GmbH (2013) 17

[34] A. Imamoglu, D. D. Awschalom, G. Burkard, D. P. DiVincenzo, D. Loss, M. Sherwin & A. Small. "Quantum Information Processing Using Quantum Dot Spins and Cavity QED". *Phys. Rev. Lett.* **83**, 4204 (1999) 18

[35] E. Knill, R. Laflamme & G. J. Milburn. "A scheme for efficient quantum computation with linear optics". *Nature* **409**, 46 (2001) 18

[36] G. K. Brennen, C. M. Caves, P. S. Jessen & I. H. Deutsch. "Quantum Logic Gates in Optical Lattices". *Phys. Rev. Lett.* **82**, 1060 (1999) 18

[37] D. G. Cory, A. F. Fahmy & T. F. Havel. "Ensemble quantum computing by NMR spectroscopy". *Proc. Natl. Acad. Sci. USA* **94**, 1634 (1997) 18

[38] B. E. Kane. "A silicon-based nuclear spin quantum computer". *Nature* **393**, 133 (1998) 18

[39] C. J. Wellard, L. C. L. Hollenberg, F. Parisoli, L. M. Kettle, H.-S. Goan, J. A. L. McIntosh & D. N. Jamieson. "Electron exchange coupling for single-donor solid-state spin qubits". *Phys. Rev. B* **68**, 195209 (2003)

[40] J. J. Pla, K. Y. Tan, J. P. Dehollain, W. H. Lim, J. J. L. Morton, D. N. Jamieson, A. S. Dzurak & A. Morello. "A single-atom electron spin qubit in silicon". *Nature* **489**, 541 (2012) 18

[41] M. H. Devoret & J. M. Martinis. "Implementing Qubits with Superconducting Integrated Circuits". *Quant. Inf. Proc.* **3**, 163 (2004) 18

[42] A. J. Berkley, H. Xu, R. C. Ramos, M. A. Gubrud, F. W. Strauch, P. R. Johnson, J. R. Anderson, A. J. Dragt, C. J. Lobb & F. C. Wellstood. "Entangled Macroscopic Quantum States in Two Superconducting Qubits". *Science* **300**, 1548 (2003)

[43] D. P. DiVincenzo. "Fault-tolerant architectures for superconducting qubits". *Phys. Scr.* **2009**, 014020 (2009)

[44] M. D. Reed, L. DiCarlo, S. E. Nigg, L. Sun, L. Frunzio, S. M. Girvin & R. J. Schoelkopf. "Realization of three-qubit quantum error correction with superconducting circuits". *Nature* **482**, 382 (2012)

[45] E. Lucero, R. Barends, Y. Chen, J. Kelly, M. Mariantoni, A. Megrant, P. OMalley, D. Sank, A. Vainsencher, J. Wenner, T. White, Y. Yin, A. N. Cleland & J. M. Martinis. "Computing prime factors with a Josephson phase qubit quantum processor". *Nat. Phys.* **8**, 719 (2012) 18

[46] J. R. Petta, A. C. Johnson, J. M. Taylor, E. A. Laird, A. Yacoby, M. D. Lukin, C. M. Marcus, M. P. Hanson & A. C. Gossard. "Coherent Manipulation of Coupled Electron Spins in Semiconductor Quantum Dots". *Science* **309**, 2180 (2005) 20, 111

[47] S. D. Barrett & C. H. W. Barnes. "Double-occupation errors induced by orbital dephasing in exchange-interaction quantum gates". *Phys. Rev. B* **66**, 125318 (2002) 20

[48] S. Rahman, T. M. Stace, H. P. Langtangen, M. Kataoka & C. H. W. Barnes. "Pulse-induced acoustoelectric vibrations in surface-gated GaAs-based quantum devices". *Phys. Rev. B* **75**, 205303 (2007) 20, 67

[49] C. H. W. Barnes, J. M. Shilton & A. M. Robinson. "Quantum computation using electrons trapped by surface acoustic waves". *Phys. Rev. B* **62**, 8410 (2000) 20, 71

[50] H. F. Trotter. "On the product of semi-groups of operators". *Proc. Am. Math. Soc.* **10**, 545 (1959) 27

[51] C. Moler & C. Van Loan. "Nineteen Dubious Ways to Compute the Exponential of a Matrix, Twenty-Five Years Later". *SIAM Rev.* **45**, 3 (2003) 27, 29

[52] J. Von Neumann & H. H. Goldstine. "Numerical inverting of matrices of high order". *Bull. Amer. Math. Soc* **53**, 1021 (1947) 28

[53] W. H. Press, S. A. Teukolsky, W. T. Vetterling & B. P. Flannery. *Numerical Recipes in C++*. Cambridge University Press, Cambridge, U. K. (1992) 28, 29, 30

[54] J. Crank & P. Nicolson. "A practical method for numerical evaluation of solutions of partial differential equations of the heat-conduction type". *Math. Proc. Cam. Phil. Soc.* **43**, 50 (1947) 29

[55] A. Askar & A. S. Cakmak. "Explicit integration method for the time-dependent Schrödinger equation for collision problems". *J. Chem. Phys.* **68**, 2794 (1978) 30

[56] C. Leforestier, R. H. Bisseling, C. Cerjan, M. D. Feit, R. Friesner, A. Guldberg, A. Hammerich, G. Jolicard, W. Karrlein, H.-D. Meyer, N. Lipkin, O. Roncero & R. Kosloff. "A comparison of different propagation schemes for the time dependent Schrödinger equation". *J. Comp. Phys.* **94**, 59 (1991) 31, 35, 36

[57] N. Watanabe & M. Tsukada. "Finite Element Approach for Simulating Quantum Electron Dynamics in a Magnetic Field". *J. Phys. Soc. Jap.* **69**, 2962 (2000) 32

[58] C. Kittel & P. McEuen. *Introduction to Solid State Physics*, volume 7. Wiley, New York (1996) 32

[59] D. R. Hofstadter. "Energy levels and wave functions of Bloch electrons in rational and irrational magnetic fields". *Phys. Rev. B* **14**, 2239 (1976) 33

[60] E. Merzbacher. *Quantum Mechanics*. Wiley, 3rd edition (1997) 34

[61] C. Zhidong, Z. Jinyu & Y. Zhiping. "Solution of the time-dependent Schrodinger equation with absorbing boundary conditions". *J. Semicon.* **30**, 012001 (2009) 35

[62] M. Feit, J. F. Jr. & A. Steiger. "Solution of the Schrodinger equation by a spectral method". *J. Comp. Phys.* **47**, 412 (1982) 35

[63] H. Bauke & C. H. Keitel. "Accelerating the Fourier split operator method via graphics processing units". *Comp. Phys. Comm.* **182**, 2454 (2011) 36

[64] *CUDA C Programming Guide*. NVIDIA Corporation, 5.0 edition (2012) 37, 38

[65] E. T. Owen, M. C. Dean & C. H. W. Barnes. "Generation of entanglement between qubits in a one-dimensional harmonic oscillator". *Phys. Rev. A* **85**, 022319 (2012) 42

[66] W. Janke & B. K. Cheng. "Statistical properties of a harmonic plus a delta-potential". *Phys. Lett. A* **129**, 140 (1988) 48

[67] F. W. J. Olver, D. W. Lozier, R. F. Boisvert & C. W. Clark. *NIST Handbook of Mathematical Functions*. Cambridge University Press, 1st edition (2010) 48

[68] D. J. Tannor. *Introduction to Quantum Mechanics: A Time-Dependent Perspective*. University Science Books (2006) 49

[69] E. Schrödinger. "Der stetige Übergang von der Mikro-zur Makromechanik". *Naturwissenschaften* **14**, 664 (1926) 49

[70] T. Busch, B.-G. Englert, K. Rzazewski & M. Wilkens. "Two Cold Atoms in a Harmonic Trap". *Found. Phys.* **28**, 549 (1998) 61

[71] E. Gasiorowicz. *Quantum Physics*. Wiley, 3rd edition (2003) 62

[72] E. Moore, B. Gherman & D. Yaron. "Coulomb screening and exciton binding energies in conjugated polymers". *J. Chem. Phys.* **106**, 4216 (1997) 63

[73] V. Perebeinos, J. Tersoff & P. Avouris. "Scaling of Excitons in Carbon Nanotubes". *Phys. Rev. Lett.* **92**, 257402 (2004)

[74] G. Giavaras, J. H. Jefferson, M. Fearn & C. J. Lambert. "Generation of Einstein-Podolsky-Rosen pairs and interconversion of static and flying electron spin qubits". *Phys. Rev. B* **76**, 245328 (2007) 63, 69

[75] R. P. Feynman. "Forces in Molecules". *Phys. Rev.* **56**, 340 (1939) 65

[76] M. Kataoka, M. R. Astley, A. L. Thorn, D. K. L. Oi, C. H. W. Barnes, C. J. B. Ford, D. Anderson, G. A. C. Jones, I. Farrer, D. A. Ritchie & M. Pepper. "Coherent Time Evolution of a Single-Electron Wave Function". *Phys. Rev. Lett.* **102**, 156801 (2009) 66

[77] A. T. Johnson, L. P. Kouwenhoven, W. de Jong, N. C. van der Vaart, C. J. P. M. Harmans & C. T. Foxon. "Zero-dimensional states and single electron charging in quantum dots". *Phys. Rev. Lett.* **69**, 1592 (1992) 66

[78] J. S. Blakemore. "Semiconducting and other major properties of gallium arsenide". *J. Appl. Phys.* **53**, R123 (1982) 67

[79] M. R. Astley, M. Kataoka, C. J. B. Ford, C. H. W. Barnes, D. Anderson, G. A. C. Jones, I. Farrer, D. A. Ritchie & M. Pepper. "Energy-Dependent Tunneling from Few-Electron Dynamic Quantum Dots". *Phys. Rev. Lett.* **99**, 156802 (2007) 67

[80] D. Blume & C. H. Greene. "Fermi pseudopotential approximation: Two particles under external confinement". *Phys. Rev. A* **65**, 043613 (2002) 68

[81] E. L. Bolda, E. Tiesinga & P. S. Julienne. "Effective-scattering-length model of ultracold atomic collisions and Feshbach resonances in tight harmonic traps". *Phys. Rev. A* **66**, 013403 (2002)

[82] P. Shea, B. P. van Zyl & R. K. Bhaduri. "The two-body problem of ultracold atoms in a harmonic trap". *Am. J. Phys.* **77**, 511 (2009) 68

[83] D. M. Meekhof, C. Monroe, B. E. King, W. M. Itano & D. J. Wineland. "Generation of Nonclassical Motional States of a Trapped Atom". *Phys. Rev. Lett.* **76**, 1796 (1996) 68

[84] X.-L. He, Y.-x. Liu, J. Q. You & F. Nori. "Variable-frequency-controlled coupling in charge qubit circuits: Effects of microwave field on qubit-state readout". *Phys. Rev. A* **76**, 022317 (2007) 68

[85] J. Janszky, A. V. Vinogradov, T. Kobayashi & Z. Kis. "Vibrational Schrödinger-cat states". *Phys. Rev. A* **50**, 1777 (1994) 68

[86] R. J. Glauber. "Coherent and Incoherent States of the Radiation Field". *Phys. Rev.* **131**, 2766 (1963) 68

[87] F. Buscemi, P. Bordone & A. Bertoni. "Entanglement dynamics of electron-electron scattering in low-dimensional semiconductor systems". *Phys. Rev. A* **73**, 052312 (2006) 69

[88] G. Giavaras, J. H. Jefferson, A. Ramšak, T. P. Spiller & C. J. Lambert. "Quantum entanglement generation with surface acoustic waves". *Phys. Rev. B* **74**, 195341 (2006) 69

[89] P. Bordone, A. Bertoni & C. Jacoboni. "Simulation of Entanglement Dynamics for Scattering Between a Free and a Bound Carrier in a Quantum Wire". *J. Comp. Elec.* **3**, 407 (2004) 69

[90] F. H. L. Koppens, C. Buizert, K. J. Tielrooij, I. T. Vink, K. C. Nowack, T. Meunier, L. P. Kouwenhoven & L. M. K. Vandersypen. "Driven coherent oscillations of a single electron spin in a quantum dot". *Nature* **442**, 766 (2006) 71

[91] R. P. G. McNeil, R. J. Schneble, M. Kataoka, C. J. B. Ford, T. Kasama, R. E. Dunin-Borkowski, J. M. Feinberg, R. J. Harrison, C. H. W. Barnes, D. H. Y. Tse, T. Trypiniotis, J. A. C. Bland, D. Anderson, G. A. C. Jones & M. Pepper. "Localized Magnetic Fields in Arbitrary Directions Using Patterned Nanomagnets". *Nano Lett.* **10**, 1549 (2010) 71

[92] K. Shakouri, B. Szafran, M. Esmaeilzadeh & F. M. Peeters. "Effective spin-orbit interaction Hamiltonian for quasi-one-dimensional quantum rings". *Phys. Rev. B* **85**, 165314 (2012) 72

[93] B. H. Wu & J. C. Cao. "Magnetotransport through a ring conductor with Rashba spin-orbit interaction". *Phys. Rev. B* **74**, 115313 (2006) 72

[94] B. C. Hsu & J.-F. S. Van Huele. "Spin dynamics for wave packets in Rashba systems". *Phys. Rev. B* **80**, 235309 (2009)

[95] M. P. Nowak, B. Szafran & F. M. Peeters. "Fano resonances and electron spin transport through a two-dimensional spin-orbit-coupled quantum ring". *Phys. Rev. B* **84**, 235319 (2011) 72

[96] G. Gonnella & M. Ruggieri. "Rheological behavior of microemulsions". *Phys. Rev. E* **66**, 031506 (2002) 72, 77

[97] J. Lega & T. Passot. "Hydrodynamics of bacterial colonies: A model". *Phys. Rev. E* **67**, 031906 (2003)

[98] S. Bottin-Rousseau & A. Pocheau. "Self-Organized Dynamics on a Curved Growth Interface". *Phys. Rev. Lett.* **87**, 076101 (2001) 72, 77

[99] R. Grima & T. J. Newman. "Accurate discretization of advection-diffusion equations". *Phys. Rev. E* **70**, 036703 (2004) 72, 77

[100] V. K. Thankappan. *Quantum Mechanics*. Wiley Eastern Ltd. (1985) 72

[101] C. G. Darwin. "The wave equations of the electron". *Proc. R. Soc. A* **118**, 654 (1928) 75

[102] E. Schrödinger. "Über die kräftefreie Bewegung in der relativistischen Quantenmechanik". *Sitz. Preuss. Akad. Wiss. Phys.-Math. Kl.* **24**, 418 (1930) 75

[103] P. Krekora, Q. Su & R. Grobe. "Relativistic Electron Localization and the Lack of *Zitterbewegung*". *Phys. Rev. Lett.* **93**, 043004 (2004)

[104] R. Gerritsma, G. Kirchmair, F. Zahringer, E. Solano, R. Blatt & C. F. Roos. "Quantum simulation of the Dirac equation". *Nature* **463**, 68 (2010) 75

[105] H. A. Bethe & E. E. Salpeter. *Quantum Mechanics of One- and Two-Electron Atoms*. Springer-Verlag, Berlin, Germany (1957) 75, 76

[106] G. Dresselhaus. "Spin-Orbit Coupling Effects in Zinc Blende Structures". *Phys. Rev.* **100**, 580 (1955) 75

[107] E. I. Rashba. *Sov. Phys. Solid State* **2**, 1109 (1960) 75

[108] G. Breit. "The Effect of Retardation on the Interaction of Two Electrons". *Phys. Rev.* **34**, 553 (1929) 76

[109] A. V. Moroz & C. H. W. Barnes. "Effect of the spin-orbit interaction on the band structure and conductance of quasi-one-dimensional systems". *Phys. Rev. B* **60**, 14272 (1999) 79, 83

[110] S. Sosa y Silva & F. Rojas. "Effects of the Rashba spin-orbit coupling on Hofstadter's butterfly". *J. Phys.: Cond. Matt.* **24**, 135502 (2012) 82

[111] D. Cocks, P. P. Orth, S. Rachel, M. Buchhold, K. Le Hur & W. Hofstetter. "Time-Reversal-Invariant Hofstadter-Hubbard Model with Ultracold Fermions". *Phys. Rev. Lett.* **109**, 205303 (2012) 82

[112] C. A. Perroni, D. Bercioux, V. M. Ramaglia & V. Cataudella. "Rashba quantum wire: exact solution and ballistic transport". *J. Phys.: Cond. Matt.* **19**, 186227 (2007) 82

[113] E. Tsitsishvili, G. S. Lozano & A. O. Gogolin. "Rashba coupling in quantum dots: An exact solution". *Phys. Rev. B* **70**, 115316 (2004) 82

[114] A. V. Moroz & C. H. W. Barnes. "Spin-orbit interaction as a source of spectral and transport properties in quasi-one-dimensional systems". *Phys. Rev. B* **61**, R2464 (2000) 83

[115] E. P. Wigner. "The operation of time reversal in quantum mechanics". *Nachr. Ges. Wiss. G. Math.-Phys. Kl.* **1**, 32 (1932) 88

[116] K. V. Kavokin. "Anisotropic exchange interaction of localized conduction-band electrons in semiconductors". *Phys. Rev. B* **64**, 075305 (2001) 92

[117] L. Schreiber, F. Braakman, T. Meunier, V. Calado, J. Danon, J. Taylor, W. Wegscheider & L. Vandersypen. "Coupling artificial molecular spin states by photon-assisted tunnelling". *Nat. Comm.* **2**, 556 (2011) 92

[118] N. E. Bonesteel, D. Stepanenko & D. P. DiVincenzo. "Anisotropic Spin Exchange in Pulsed Quantum Gates". *Phys. Rev. Lett.* **87**, 207901 (2001) 92

[119] G. Burkard & D. Loss. "Cancellation of Spin-Orbit Effects in Quantum Gates Based on the Exchange Coupling in Quantum Dots". *Phys. Rev. Lett.* **88**, 047903 (2002) 92

[120] D. Stepanenko, N. E. Bonesteel, D. P. DiVincenzo, G. Burkard & D. Loss. "Spin-orbit coupling and time-reversal symmetry in quantum gates". *Phys. Rev. B* **68**, 115306 (2003) 92

[121] E. Joos & H. Zeh. "The emergence of classical properties through interaction with the environment". *Z. Phys. B Cond. Matt.* **59**, 223 (1985) 111

[122] W. H. Zurek. "Decoherence and the Transition from Quantum to Classical". *Physics Today* **44**, 36 (1991)

[123] W. H. Zurek. "Decoherence, einselection, and the quantum origins of the classical". *Rev. Mod. Phys.* **75**, 715 (2003)

[124] E. Joos, H. D. Zeh, C. Kiefer, D. J. W. Giulini, J. Kupsch & I.-O. Stamatescu. *Decoherence and the Appearance of a Classical World in Quantum Theory*. Springer, 2nd edition (2003)

[125] M. A. Schlosshauer. *Decoherence and the Quantum-to-Classical Transition*. Springer (2008)

[126] M. Brune, E. Hagley, J. Dreyer, X. Maitre, A. Maali, C. Wunderlich, J. M. Raimond & S. Haroche. "Observing the Progressive Decoherence of the "Meter" in a Quantum Measurement". *Phys. Rev. Lett.* **77**, 4887 (1996)

[127] C. J. Myatt, B. E. King, Q. A. Turchette, C. A. Sackett, D. Kielpinski, W. M. Itano, C. Monroe & D. J. Wineland. "Decoherence of quantum superpositions through coupling to engineered reservoirs". *Nature* **403**, 269 (2000) 111

[128] A. V. Khaetskii, D. Loss & L. Glazman. "Electron Spin Decoherence in Quantum Dots due to Interaction with Nuclei". *Phys. Rev. Lett.* **88**, 186802 (2002) 111

[129] H. Bluhm, S. Foletti, D. Mahalu, V. Umansky & A. Yacoby. "Enhancing the Coherence of a Spin Qubit by Operating it as a Feedback Loop That Controls its Nuclear Spin Bath". *Phys. Rev. Lett.* **105**, 216803 (2010) 111

[130] C. Gardiner & P. Zoller. *Quantum Noise: A Handbook of Markovian and Non-Markovian Quantum Stochastic Methods with Applications to Quantum Optics*. Springer, 3rd edition (2004) 112

[131] H.-P. Breuer & F. Petruccione. *The Theory of Open Quantum Systems*. Oxford University Press, USA (2007)

[132] W. C. Schieve & L. P. Horwitz. *Quantum Statistical Mechanics*. Cambridge University Press, 1st edition (2009) 112

[133] G. Lindblad. "On the generators of quantum dynamical semigroups". *Comm. Math. Phys.* **48**, 119 (1976) 112

[134] H.-P. Breuer, B. Kappler & F. Petruccione. "Stochastic wave-function method for non-Markovian quantum master equations". *Phys. Rev. A* **59**, 1633 (1999) 112

[135] P. Gaspard & M. Nagaoka. "Non-Markovian stochastic Schrödinger equation". *J. Chem. Phys.* **111**, 5676 (1999)

[136] R. Biele & R. D'Agosta. "A stochastic approach to open quantum systems". *J. Phys.: Cond. Matt.* **24**, 273201 (2012) 112

[137] I. de Vega, D. Alonso & P. Gaspard. "Two-level system immersed in a photonic band-gap material: A non-Markovian stochastic Schrödinger-equation approach". *Phys. Rev. A* **71**, 023812 (2005) 113